PREPARATION AND CHARACTERIZATION OF POLY(LACTIC ACID)/ETHYLENE VINYL ACETATE/GRAPHENE OXIDE POLYMER COMPOSITES FOR WATER PURIFICATION

By

LESIA SYDNEY MOKOENA (B.Sc. Hons)

2013200718

Submitted in accordance with the requirements for the degree

MASTER OF SCIENCE (M.Sc.)

Department of Chemistry

Faculty of Natural and Agricultural Sciences

at

UNIVERSITY OF THE FREE STATE (QWAQWA CAMPUS)

SUPERVISOR: MR K. MPITSO

CO-SUPERVISOR: DR J.P. MOFOKENG

October 2020

DECLARATION

I, the undersigned, hereby declare that the research in this thesis is my own original work and has not been previously submitted to any other university for degree purposes. I further cede copyright of the thesis in favour of the University of the Free State.

_____

Mokoena L.S.

DEDICATION

This work is dedicated to anyone and everyone struggling to make ends meet. To everyone feeling as if they have hit a dead end, lost hope and are struggling to see the light at the end of the tunnel. This is for you, better days are coming.

Manners maketh man!!!!

ABSTRACT

Water contamination by heavy metals, due to most industries is a global problem. The released heavy metals are in the form of ions, which do not naturally degrade, but rather form part of water that is consumed. This has numerous negative effects on humans, animals, plants as well as the environment. The purpose of this study was to synthesize graphene oxide (GO) from expandable graphite powder (EG) and prepare environmentally friendly poly(lactic acid) (PLA)/ethylene vinyl acetate (EVA)/graphene oxide (GO) composites through melt mixing to be used to remove lead ions from solution. The GO was synthesized following the modified Hummer's method and verified with FTIR, XRD and SEM-EDS. FTIR spectra showed numerous peaks denoting the successful attachment of oxygen containing functional groups to EG. XRD analysis for GO resulted in a peak at 7.5˚, with an increased interlayer spacing (0.347 nm for EG and 1.18 nm for GO), which validated the presence of oxygen containing functional groups. SEM images showed GO layers as well as their exfoliated surfaces and in EDS the oxygen content was proven to be higher in GO (39.4%) as compared to EG (12.3%). The PLA/EVA/GO blend (70/30, 50/50, and 30/70) composites, with different amounts of GO (1, 3, and 5 wt.%), were prepared by melt mixing. The morphology, surface, flow, and thermal properties as well as water studies (Water absorption and Pb (II) adsorption), were performed using Scanning electron microscopy (SEM), Surface energy evaluation system (SEES), Melt flow indexer (MFI), Differential scanning calorimetry (DSC), Thermogravimetric analyser (TGA), water intake experiments and Atomic absorption spectroscopy (AAS), respectively.

The morphology of the blends showed that PLA and EVA were immiscible. In the blend composites, it illustrated that GO was mostly situated on the interface between PLA and EVA, although it could also settle in either of the polymer phases. The highest PLA containing blend composites showed cracks on the polymers and gaps on the interface, while in the other composites there were no visible cracks and gaps. GO sheets were present in the blend composites, and it brought about partial miscibility to the polymer matrices. The interfacial tensions, through SEES analysis, calculated for PLA/GO and EVA/GO pairs were similar, indicating an equal chance of GO to disperse in either one of the polymers, or even the interface. The wetting coefficient value of 0.523 suggested GO to be on the interface of the two polymers. Thermal analysis (melting and crystallization by DSC runs) showed that PLA and EVA are immiscible, as two melting peaks were observed for these polymers, 149 ℃ and 97.9 ℃, respectively. EVA was seen to have a hindering effect on the re-crystallization and melting

process of PLA, this was because the cold crystallization temperature peak of PLA disappeared leading to no melting of PLA. While PLA had a semi-catalytic effect on the crystallization process of EVA, as the crystallization temperature of EVA was observed earlier, for all blends, though there was a decrease in degree of crystallinity. With the introduction of GO to the polymer matrices, the glass transition temperature of PLA moved to lower values, and in the 50/50 w/w PLA/EVA composites (with 1, 3 and 5 wt.% GO loadings) the individual melting peaks approached one another. This meant that GO brought partial miscibility to the polymer matrices. GO seemed to have a hindering effect on the crystallization of EVA, and a nucleating effect on the chains of PLA. This was observed through the drastic reduction in the degree of crystallinity of EVA, and the reappearance of the cold crystallization temperature peak of PLA, resulting in the re-definition of melting, for all the blend composites. In terms of thermal degradation studies through TGA analyses, the polymers degraded separately in the blends, proving their immiscibility. The introduction of GO to the blends showed the autocatalytic effect on the thermal degradation of the polymers (early degradation at lower temperatures, and delayed degradation with polymer char at higher temperatures). There was a presence of char in all the blend composites, which showed the presence of polymer (either PLA or EVA) as well as GO. This suggested that the polymers masked GO and in turn, the GO improved their thermal stability to some extent. Water absorption studies showed that the 66.5/28.5/5 PLA/EVA/GO composite had the highest water absorption degree, which was because of the cracks and spaces observed on it. The 50/50 w/w PLA/EVA composites also showed a high-water intake, and the exposed GO layers observed on their morphology was the attribution made to these observations. Then in Pb(II) intake studies through AAS, all the analysed samples had very high metal adsorption capacities, and the 66.5/28.5/5 PLA/EVA/GO composite adsorbed more metal ions under a basic medium and 5 hours contact time. Adsorption kinetic modelling showed a favourable heterogeneous and homogeneous adsorption as both the Langmuir and Freundlich isotherms gave linear fits. However, the Langmuir fit was more precise and therefore the conclusion was that adsorption took place mostly on a homogenous surface.

TABLE OF CONTENTS

LIST OF TABLES

LIST OF FIGURES

LIST OF ABBREVIATIONS AND SYMBOLS

AFM	Atomic force microscopy
AAS	Atomic absorption spectroscopy
C_a	Concentration of lead ions adsorbed
C_0	Initial adsorbate concentration
C_e	Equilibrium adsorbate concentration
d	Interlayer spacing
ΔH^o_m	Melting enthalpy of 100% crystalline polymers
ΔH_m	Specific melting enthalpy for a polymer
ΔH_{cc}	Cold crystallization enthalpy
DSC	Differential scanning calorimetry
EDS	Energy dispersive spectroscopy
EG	Expandable graphite
EVA	Ethylene vinyl acetate
FTIR	Fourier transform infrared spectroscopy
γ	Surface energy
GO	Graphene oxide
HCl	Hydrochloric acid
H_2O_2	Hydrogen peroxide
HPMC	Hydroxypropylmethylcellulose
H_3PO_4	Phosphoric acid
H_2SO_4	Sulfuric acid
IR	Infrared Spectroscopy
K_L	Distribution coefficient

$KMnO_4$	Potassium permanganate
λ	Wavelength
LDPE	Low density polyethylene
m_b	Mass when material absorbs water to saturation
MFI	Melt flow index
m_g	Mass when material is dry
MPa	Mega Pascal
n	Adsorption favourability constant
NRF	National Research Foundation
ω_a	Wetting coefficient
PCL	Poly(ε-caprolactone)
PHBV	Poly(3-hydroxybutyrate-co-3-hydroxyvalerate)
PLA	Poly(lactic acid)
PP	Polypropylene
PVA	Poly(vinyl alcohol)
PVC	Poly(vinyl chloride)
ρ_w	Density of water
q_e	Adsorption capacity
R	Degree of water absorption
R^2	Correlation coefficient
ρ	Density
R_L	Separation factor
ROP	Ring opening polymerization
TGA	Thermogravimetric analysis

SAIF	Sasol Inzalo Foundation
SEM	Scanning electron microscopy
TEM	Transmission electron microscopy
SEES	Surface energy evaluation system
θ	Contact angle
T_g	Glass transition temperature
T_m	Melting temperature
T_{cc}	Cold crystallization temperature
WHO	World health organization
wt.%	Weight percentage
XPS	X – ray photoelectron spectroscopy
XRD	X – ray diffraction
V_0	Volume of dry material in natural state
VA	Vinyl Acetate
W_m (%)	Specific absorption quality
W_v	Specific absorption of volume
X_c	Degree of crystallinity
XPS	X-ray photoelectron spectroscopy

CHAPTER 1

INTRODUCTION

1.1 GENERAL INTRODUCTION

Water contamination by heavy metals has become an increasing crisis on a global scale, and with this came a vast amount of research to combat this contamination. Heavy metals have no clear definition and density is used as a distinguishing factor amongst the different metals, for instance, heavy metals are those considered to be having a specific density of more than 5 g/cm^3. A report was issued out by the World Health Organization (WHO) in 2007 which stated that about 1,1 billion people lack access to a clean water supply across the globe and this has been proven to have dire health consequences [1]. Further research shows that the metals, in the form of ions, mainly responsible for the contamination of water are copper, zinc, lead, chromium, cadmium and nickel. These metals, although found in small concentrations as water contaminants, have been proven to have very bad health implications which include: liver, nerve bone damage and may also interfere with the normal functioning of various metalloenzymes (enzyme proteins which contain metal ions) upon consumption of water contaminated by these heavy metal ions [2].

According to the International Lead and Zinc Study Group (ILZSG), the production and consumption of lead increases every year, and statistics show that in 2010 about 8,757 million tons of lead were excessively produced and consumed across the globe. The lead released to the environment comes mainly from industries, specifically manufacturing, acid metal plating and finishing, ammunition, ceramic and glass industries, painting, dying, and other industries [3]. The residues from these industrial processes are released into the environment through transporting agents like wind, surface run off and gravity, which end up contaminating water. Lead containing and water-transporting pipes may release lead into the water, which will form part of drinking and irrigation. Lead is not biodegradable, as a result consumption of water containing it results in its accumulation on the living cells, leading to fatal damages to the kidneys, liver, reproductive system and the brain [3,4]. As a public health and safety issue, it is thus critical to investigate and implement methods to remove lead ions from water.

The past years have seen a variety of methods formulated and tested for their effectiveness in removing heavy metal ions from solution. These methods, amongst others, include ion exchange, membrane filtration, coagulation and precipitation, and adsorption. Most of these

methods, however, have not yet been accepted on a commercial basis due to their failures in the execution and/or financial implications [5-7]. The membrane filtration method has been proven effective in removing low concentration, heavy metal ions from solutions. The problem with this method is that the membrane does not have enough lifetime before it is subjected to fouling which results in its deterioration [8]. This fouling is due to the organic matter contaminants present in most wastewater, which become deposited in the membrane pores [9]. In the coagulation and precipitation method, the contaminants are transferred to the insoluble solids and removed from the liquid phase water by filtration and sedimentation [10-12]. This method has also been proven effective in removing heavy metal ions from solution. The downside is that there is no suitable, cost effective way to dispose the waste generated from this method [13]. The ion exchange method has a limited pH tolerance, a high regeneration and does not have a waste disposal problem as in the coagulation and precipitation method. This method's problem is high maintenance and execution costs [14]. As a result, the adsorption method has been shown to be the most effective of the other mentioned methods for removal of heavy metal ions.

The process of adsorption is one whereby a gas or a liquid accumulates on the surface of a solid or a liquid [15]. The phase that adsorbs is termed the adsorbent whereas the material that is adsorbed is termed the adsorbate. The adsorption process has been proven to remove various contaminants in high capacities. Fast kinetics (Optimal rate of metal ion removal) and the ability to selectively remove contaminants have also been reported. There is also flexibility in terms of the environments in which adsorption can take place, the environments can be liquid-liquid, liquid-gas, solid-liquid, and solid-gas. All these are easily attainable environments, which add on the effectiveness of this method [16,17]. The adsorption process, unlike the previously mentioned methods, also has low running costs, making it ideal and advantageous in removing heavy metal ions from solution [17]. The choice of the adsorbent is very crucial with this method. Research shows that there are many materials that have been previously and currently used as adsorbents. These materials, amongst others, are zeolites, activated carbon, modified silica gel, natural fibers and recently graphene oxide [18-20]. The first three (zeolites, activated carbon and modified silica gel) have been proven to be very expensive and hazardous to the environment when used as adsorbents. Natural fibers have been proven very effective in adsorbing heavy metal ions, but the fiber has a short life span before it is subjected to fouling and thus degradation [21]. This leaves the latter option, graphene oxide, as a choice for a suitable adsorbent to remove heavy metal ions from solution.

Graphene oxide is a derivative of graphene, whereby the graphene sheets become functionalized with hydroxyl, epoxy and carboxylic acid groups on the planes and edges [22]. Literature suggests that the oxygen-containing functional groups on graphene oxide make it a good adsorbent, with better mechanical, electrical properties and a higher surface area onto which adsorption will take place [23]. However, aggregation / agglomeration has been proven to be the major problem encountered when graphene oxide is used as an adsorbent on its own. This is the case for most micro/nanoscale inorganic materials. It is prevented through forming polymer nanocomposites with graphene oxide whereby the polymer matrix would play the role of masking the graphene oxide. This masking usually results in improved mechanical properties, reduced aggregation and improved adsorption capacity of GO. The masking can be done using a single or more polymers as matrices.

Using a single polymer masking system limits the overall resultant properties to that of the single polymer. This is mostly the case if a biodegradable polymer is to be used, as most of them are either too flexible or too brittle. This encourages the use of two or more polymers to mask, which have different properties. The process is called polymer blending, and it results in averaged properties, whereby there is a balance between flexibility and brittleness whilst involving biodegradability [24]. This process refers to the physical mixing of two or more polymers to develop a polymeric material with improved properties depending on the area of focus. Polymer blends have been proven to be good masking agents for different purposes [24]. This masking proceeds via blending to form composites with different fillers and an overall improvement in properties becomes apparent. Biodegradable polymers are amongst the different types of polymers we have. These are specialized type of polymers that are degraded down by microbes after their intended usage. This degradation results in natural by-products like gases, biomass, inorganic salts, and water. They infiltrate into the ground and fertilize the soil [25]. As much as we want to purify the water, we also do not desire to harm the environment. Therefore, the choice of these polymers is very much good as non-biodegradable/petroleum based polymers might end up in landfills, thereby contributing to the ongoing pollution problem.

1.1.1 Biodegradable polymers

Biodegradation refers to a process whereby a material disintegrates due to the action of enzymes or living organisms like bacteria, fungi amongst others [25]. This property is very

important in materials as it helps in reducing pollution and overall harm to the environment, caused by the non-biodegradable plastics. Some polymers possess biodegradability and biocompatibility. These polymers have found great usage across the globe in line with the idea and goal to ensure a sustainable environment that is free of harm from chemical processes. Biodegradable polymers are divided into two types namely, the natural biodegradable polymers and the synthetic biodegradable polymers [26]. Research suggests that synthetic biodegradable polymers are more advantageous compared to natural ones, and this is because they can be tailored for specific properties in line with what is required, they are easily processed and do not run the risk of running out.

Research shows that the usage of biodegradable polymers increased from 14 million kg in 1996 to about 68 million kg in 2001 [27]. Moreover, the global production of biodegradable polymers was 870 million kg in 2017, and is expected to be about 2.4 billion kg in 2022 [28]. The target markets for biodegradable polymers are mainly packaging materials, hygiene products, consumer goods and agricultural tools [29]. The current, but improving disadvantage of biodegradable polymers is their close competitor, common plastics. These inexpensive polymer materials hamper the commercialization of these biodegradable polymers. This is due to their familiarity and prolonged usage over the years [29-31]. However, biodegradable polymers have slowly gained popular usage subject to ongoing research on their properties. Poly (lactic acid) (PLA), poly(ε-caprolactone) (PCL) and poly(3-hydroxybutyrate-co-3-hydroxyvalerate) (PHBV) are some of the examples of biodegradable polymers, PLA being one of the most common biodegradable polymers having versatile usage.

1.1.2 Poly (lactic acid) (PLA)

PLA belongs to the family of aliphatic polyesters that are derived from α-hydroxy acids. The monomer responsible for synthesizing PLA is lactic acid. This monomer can be synthesized chemically or biologically, however, the biological route is the more preferred and accounts for the majority of the world's lactic acid synthesis. This monomer is synthesized biologically, through fermenting starch and other polysaccharides like sugar beet, corn, sugar cane, potatoes and other biomasses. The monomer, lactic acid, has two isomeric structures, which are L-lactide and D-lactide [32,33]. Figure 1.1 shows a typical PLA structure. The structure consists of a chain of lactide monomers, which can have two isomeric states (L- isomer and D- isomer). The structure clearly shows that the monomer consists of a three-carbon organic chain, which

has carbonyl, ester as well as methyl substituents [33]. The presence of these oxygen containing functional groups are very crucial in attracting heavy metals from solution.

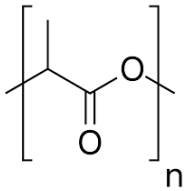

Figure 1.1: Typical PLA structure displaying the lactic acid monomer and the overall atomic interactions [34].

The polymerization of PLA proceeds via one of two ways, which are direct polymerization or the ring opening polymerization (ROP). In the direct method, polycondensation is used, whereby the monomer, lactic acid, is polymerized, at a low pressure, and in the presence of a catalyst. This polymerization yields a low molecular weight polymer, as it is difficult to remove water from the viscous reaction mixture. The ring opening polymerization of PLA, on the other hand, results in a polymer having a high molecular weight and the synthesized polymer can be stereo-regulated for specific and desired properties. This means that the ring opening polymerization process can be tailored to yield PLA that is either L-lactide or D-lactide configured. These two stereoisomers of PLA differ slightly in their properties, hence the ROP of PLA is useful in property control. In this method, PLA is synthesized by the polymerization of its cyclic monomer, lactide [35]. Homopolymers of PLA typically have a glass transition temperature in the range 55-65 ℃, a melting point in the range 150-170 ℃. They undergo thermal degradation at 200 ℃ and have a tensile strength of about 32.22 MPa [35,36].

PLA is a brittle polymer, with a certain degree of hydrophobicity, and as a result, its usage in polymer blending should be done with care, in order to attain compatibility by choosing a polymer with complementary properties to blend it. In most cases, a polymer with a high flexibility and lower crystallinity would be used. Examples of these flexible polymers include ethylene vinyl acetate (EVA), polyethylene, low-density polyethylene (LDPE), amongst others [37].

1.1.3 Ethylene vinyl acetate (EVA)

EVA is a copolymer derived from the ethylene and vinyl acetate monomers. The polymer exists commercially in a state that has different vinyl acetate contents. These contents are 16, 18 and 28 % by weight vinyl acetate. The reactivity ratio between vinyl acetate and ethylene is close to 1, which in turn results in the random distribution of vinyl acetate monomers in the polymer backbone. This random distribution affects the melting temperature, degree of crystallinity and the optical properties of the polymer. The addition and distribution of the vinyl acetate monomer also increases the polarity of the ethylene backbone, and as a result affects the solubility of small molecules within EVA as well as the compatibility of EVA with other polymeric material [38]. This property of EVA allows for its tailoring for versatile usage like blending with other polymers to improve properties.

The Figure 1.2 shows the typical structure of EVA, whereby the ethylene and vinyl acetate monomer parts are clearly depicted. The vinyl acetate component of this copolymer consists of carbonyl and ester [38,39]. These groups have been proven to be very crucial in adsorbing heavy metals from solution. The chemical structure of EVA, although it is not biodegradable, allows for its usages in heavy metal ion removal [23].

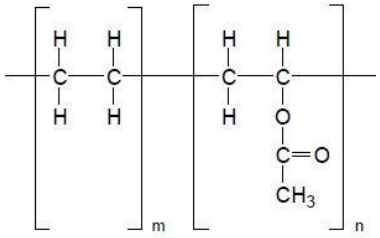

Figure 1.2: Typical EVA structure showing its vinyl acetate and ethylene monomer parts [39].

The glass transition temperature of EVA varies according to the content of vinyl acetate in the polymer. As the vinyl acetate content increases, it has been found that the glass transition temperature shifts to higher temperatures with the value ranges of -23 to 19℃ [38,39]. Literature also suggest that the opposite holds for the melting temperature of EVA, whereby the melting peak weakens and broadens with an increase in the vinyl acetate content, thus implying that the vinyl acetate monomer is responsible for the amorphous properties in EVA [39]. The melt flow index of the polymer has been reported to be 2.5 g/10 min at 190 ℃ and a density of 0.941 g/cm^3 [38,39].

The above-mentioned examples of polymers (PLA and EVA) might be effective in forming a composite with graphene oxide. This is due to their properties complementing each other. That

is, the biodegradability of PLA and its environmental friendliness, and the flexibility of EVA to increase elasticity in the composite. These stated properties might result in composites that are flexible enough to bend, and strong enough to withstand impact. In addition, composites from these two polymers might be disposed with ease due to the biodegradability of PLA. In addition, the oxygen-containing functional groups on the polymers could work to improve the adsorption efficiency in their matrix with graphene oxide and strengthen the graphene oxide mechanically. The water absorption capacity of GO might also be improved with the introduction of these polymers which have their own absorbing capabilities.

1.1.4 Water absorption (Intake)

Water absorption or intake is very important when assessing the heavy ion removal properties ρof materials. Briefly, water absorption refers to the process of absorbing water when a material is exposed to water. It is expressed by the water absorption ratio and there are two types of expressions namely: (i) the specific absorption of quality and (ii). The specific absorption of volume [40].The specific absorption of quality refers to the percentage of the absorbed water to the dry mass when the material absorbs water to saturation, and it is defined by. Equation 1.1.

$$W_m(\%) = m_b - m_g m_g \times 100\% \quad (1.1)$$

Whereby W_m (%) is the specific absorption quality, m_b is the mass when the material absorbs water to saturation (g) and m_g is the mass when the material is dry [40,41].

The specific absorption of volume refers to the percentage of the absorbed water's volume to the natural volume of the material when the material has absorbed water to saturation. It is expressed by the Equation 1.2, which reads:

$$W_V\ (\%) = m_b - m_g V_0 \rho_w \times 100 \quad (1.2)$$

Where W_v (%) is the specific absorption of volume, V_0 (cm^3) is the volume of dry material in natural state and ρ_w the density of water (g/cm^3) [40,41]. The specific absorption of quality and the specific absorption of volume are related through the Equation 1.3:

$$W_V = W_m \times \rho_0 \quad (1.3)$$

Where ρ_0 is the apparent density of the material in dry state (g/cm^3) [40,41].

Apart from water absorption being dependent on hydrophilicity and hydrophobicity of a material, it is also dependent on the porosity and characteristics of a material's pores. In normal materials, a higher porosity results in a stronger water absorption. The more open and connected tiny pores are, then the water absorption also goes up. If the porosity lacks then the degree to which the material absorbs water will also decrease [40,41]. Water absorption, however, affects a material's properties in that a high absorbing material has its volume expanding, thermal conductivity increasing and its overall mechanical properties decreasing, like tensile strength and durability. Some of the downfalls, like mechanical strength, could be counteracted by introducing another material of known good mechanical properties to form composites and thus maintain the mechanical strength.

Water absorption analysis is very important if we desire to remove heavy metals from solution. A materials ability to pass water is important as it also influences its ability to leave heavy metals attached on it while water is passed. As such, water absorption is a necessary procedure in order for metal intake (adsorption) to occur.

1.1.5 Adsorption

Adsorption refers to the physical accumulation of gaseous or liquid material on the surface of a solid. It is regarded as a surface phenomenon and the substance to which it occurs is called the absorbent whilst the phase getting adsorbed is the adsorbate. There are two types of adsorption processes which are chemisorption and physisorption. Chemisorption, or chemical adsorption is adsorption in which the forces involved are valence forces similar to those involved in chemical compound formation. Chemisorption is characterized by: chemical specificity, changes in electronic state, enthalpy changes and activation energy as the first step

amongst others. Physisorption, or physical adsorption, is an adsorption in which the forces involved are intermolecular forces (van der Waals forces) similar to those involved in the imperfection of real gases and the condensation of vapours. It is characterized by the chemical nature of the adsorbent being the same as the solution which held it. The energy of interaction between adsorbent and adsorbate is in the same order of magnitude, but greater than, the energy of the adsorptive and it can happen in any solid/fluid system. The adsorption process proceeds by creating a film of the adsorbate on the surface of the adsorbent which distinguishes it from the absorption process whereby the adsorbate is dissolved in a liquid or permeates the adsorbent. Therefore, adsorption is a surface-based process whilst absorption involves the whole volume of the material [42].

The process of adsorption is very handy in industries as it is used to remove certain components from a mobile phase (gas phase or liquid phase) and to separate mixtures. The applications of this process can be production-related or reduction-related. These may include the removal of water from natural gas, or the removal of organic constituents from flue gas (Gas escaping to the atmosphere from a fireplace) which occurs mostly in refinery processes, natural gas processing operations and coal processing operations. Preferred adsorbents are those with a wide distribution of large different sized pores. This enables the adsorbents to accommodate the various types and sizes of different molecular species occurring in gas or liquid streams. The adsorption process is reversible through a counter process termed desorption. This process occurs when an adsorbed substance (adsorbate) is detached from the surface of the adsorbent. This process is very important, more especially if the adsorbent is in the form of a membrane which will have to be reused in water purification processes [43,44].

1.1.5.1 Adsorption isotherms

Generally, adsorption give equilibrium studies based on the amount of adsorbate that has been adsorbed by a certain mass of solid adsorbent and the amount of adsorbate remaining in solution. Two adsorption isotherms are mostly used for the purpose of removing heavy metal ions from solution, and these are the Freundlich isotherm as well as the Langmuir isotherm. Generally, the adsorption capacity of adsorbates on adsorbents is given by the Equation 1.4.

$$q_e = \frac{(C_0 - C_e)V}{m} \qquad (1.4)$$

Where V is the solution's volume, m the mass of the adsorbent and C_o and C_e are the initial and equilibrium concentrations of the adsorbate respectively [45].

Langmuir isotherm

This model was initially used and designed to describe gas-solid phase adsorption. However, it eventually found usage in quantifying the adsorption capacities of different adsorbents in solution. It describes adsorption processes whereby the extent of adsorbate coverage is limited to one molecular layer. The model operates under the assumption that each adsorbate molecule occupies only one site, the surface at which adsorption occurs is homogeneous and that the adsorption surface is localized. The model also describes the balancing of adsorption and desorption to achieve dynamic equilibrium, and assumes that adsorption is proportional to the surface of the adsorbent which is open while desorption is proportional to the adsorbent's surface which is covered. The Langmuir isotherm has a linear form given by the Equation 1.5.

$$\frac{C_e}{q_e} = \frac{1}{q_m K_L} + \frac{C_e}{q_m} \qquad (1.5)$$

Where C_e (mg/L) is the equilibrium concentration of the adsorbate, K_L and q_m are constants relating to the energy of adsorption and the maximum adsorption capacity, respectively. The plot of Ce / q_e against C_e gives a straight-line graph and the values of q_m and K_L are obtained from the gradient and the y-intercept respectively. The important traits of the Langmuir isotherm can be determined using the dimensionless constant called the separation factor, R_L, given by the Equation 1.6, which reads:

$$R_L = \frac{1}{1+K_L C_0} \qquad (1.6)$$

Where K_L is an adsorption constant and C_o is the initial concentration of the adsorbate. From this constant the following conclusions are drawn:

If R_L is greater than 1 there's unfavourable adsorption, if R_L is greater than zero (0) but less than 1 there is linear adsorption and if R_L is less than one there is favourable adsorption [46-48].

Freundlich isotherm

The Freundlich isotherm applies to adsorption processes that take place on heterogeneous surfaces. It gives an expression defining surface heterogeneity and the distribution of active sites exponentially as well as their energies. This isotherm is mainly used in adsorption of organic material from aqueous solution and onto organic surfaces. The isotherm has an exponential form given by the Equation 1.7.

$$q_e = K_f C_e^{1/n} \quad (1.7)$$

Where q_e (mg/g) represents the amount adsorbed to the amount of adsorbent (capacity) at equilibrium, C_e the equilibrium concentration (mg/L), K_f (mg/g) the distribution coefficient representing the quantity of adsorbed material into adsorbent, and n is a constant indicating the favourability, or lack thereof, of the adsorption process. The equation is linearized for analysis purpose to take the logarithmic form which is Equation 1.8.

$$\log q_e = \log K_f + \frac{1}{n} C_e \quad (1.8)$$

Whereby $\log q_e$ is plotted against C_e to give a straight line and the parameters n and K_f are determined from the gradient and y-intercept of the graph respectively [46-48].

1.2 AIMS AND OBJECTIVES

- The main aim of this study was to successfully synthesize Graphene oxide from expandable graphite in order to use it for water purification studies.
- To formulate and prepare effective and environmentally friendly PLA/EVA/GO composites in order to mask the GO and elongate its lifespan.

- To assess the morphologies and interfacial adhesion between the blends and the GO using the scanning electron microscopy (SEM), melt flow index tester (MFI) and surface energy evaluation system (SEES).
- To study the effect of blending (PLA/EVA) and GO on the thermal properties (glass transition, melting, crystallization, enthalpies, miscibility, thermal degradation and stabilities) of the prepared composites using differential scanning calorimetry (DSC) and thermogravimetric analysis (TGA)
- To assess the water intake properties of the composites through the water absorption test, in order to select the optimal absorbing composites for adsorption studies.
- To assess the effectiveness of neat GO as well as the composites in lead ion removal through atomic absorption spectroscopy (AAS), with the help of water absorption studies. Investigation of the impact of contact time, pH level and initial concentration on the composites. Usage of the Langmuir and Freundlich adsorption isotherms to mathematically model and interpret the adsorption effectiveness.

1.3 THESIS OUTLINE

This thesis is outlined as follows:

Chapter 1: Introduction

Chapter 2: Literature review

Chapter 3: Materials and methods

Chapter 4: Results and discussions

Chapter 5: Conclusions

REFERENCES

1. T. A. Makhetha, K. Mpitso, A. S. Luyt: Preparation and characterization of EVA/PLA/Sugarcane bagasse composites for water purification. Journal of Composite Materials 2016; 51:1169-1186.
   DOI: 10.1177/0021998316675399

2. V. K. Gupta, S. Agarnal, T. A. Saleh. Synthesis and characterization of alumina-coated carbon nanotubes and their application for lead removal. Journal of Hazardous Materials 2011; 185:17-23.
DOI:10.1016/J.Jhazmat.2010.08.053
3. E. Pehlivan, T. Altun, S. Cetin, M. I. Bhanger. Lead sorption by waste biomass of hazelnut and almond shell. Journal of Hazardous Materials 2009; 167:1203-1208
DOI: 10.1016/j.jhazmat.2009.01.126
4. L. Fang, L. Li, Z. Qu, H. Xu, J. Xu, N. Yan. A novel method for the sequential removal and separation of multiple heavy metals from waste water. Journal of Hazardous Materials 2017; 342:617-624.
DOI:10.1016/j.jhazmat.2014.08.072
5. E. Tahmasebi, M. Y. Masomi, Y. Yamimi, A. Marsali. Application of mechanosynthesized azine-decorated zinc (ii) metal-organic frameworks for highly efficient removal and extraction of some heavy-metal ions from aqueous samples: A comparative study. Inorganic Chemistry 2015; 54:425-433.
DOI: 10.1021/ic5015384
6. J. M. Luo, X. B. Luo, J. L. Crittenden, J. H. Qu, Y. H. Bai, Y. Peng, J. H. Li. Removal of antimonite (SbC(iii)) an antimonite (Sb(U)) from aqueous solution using carbon nanotubes that are decorated with zirconium oxide Z_rO_2. Environmental Science and Technology 2015; 49:11115-11124.
DOI:10.1021/aCS.est.5b02903
7. T. A. Kurniawan, G. Chan, W. Lo, S. Babel. Physio-chemical treatment techniques for waste water laden with heavy metals. Chemical Engineering Journal 2006; 118:83-98.
DOI:10.1016/j.cej.2006.01.015
8. M. Beyer, B. Lohrengel, L. D. Nghrem. Membrane fouling and chemical cleaning in water recycling applications. Desalination 2010; 250:977-981.
DOI: 10.1016/J.DESAL.2009.09.088
9. J. Wu, M. A. Eliteman, S. E. Law. Evaluation of membrane filtration and ozonation process for treatment of reactive-dye wastewater. Journal of Environmental Engineering 1998; 124:272-277.
DOI: 10.1061/(asce)0733-9372(1988)124:3(272)
10. S. Madaeni. The application of membrane technology for water disinfection. Water Research 1999; 33:301-368.
DOI: 10.1016/S0043-1354(98)00212-7

11. J. Jiang, B. Lloyd. Progress in the development and use of ferrate (iv) salt as an oxidant and coagulant for water and waste water treatment. Water Research 2002; 36:1397-1408. DOI: 10.1016/S0043-1354(01)00358-X
12. V. Golob, A. Vinder, M. Simonie. Efficiency of the coagulation/flocculation method for the treatment of dyebath effluents. Dyes and Pigments 2005; 67:93-97. DOI:10.1016/j.dyepig.2004.11.003
13. M. A. Sabui, A. A. Khan, S. Saliullah. Treatment of textile wastewater by coagulation precipitation method. Journal of Scientific Research 2012; 4:623-633. DOI: 10.3329/jsr.j4i3.10777
14. A. Dabronski, Z. Hubski, P. Podkoscielny, E. Robens. Selective removal of the heavy metal ions from waters and industrial waste waters by ion-exchange method. Chemosphere 2004; 56:91-100. DOI: 10.1016/j.chemosphere.2004.03.006
15. I. Ali, V. K. Gupta. Advances in water treatment by adsorption technology. Nature Protocols 2007; 1:21661-2667. DOI:10.1038/nprot.2006.370
16. P. C. Vandevivere, R. Branchi, W. Verstraete. Review: Treatment and reuse of wastewater from the textile wet-processing industry. Review of emerging technologies. Journal of Chemical Technology and Biotechnology 1998; 72:289-302.
17. S. M. Shaheen, A. S. Derbalah, F. S. Moghann. Removal of heavy metals from aqueous solution by zeolite in competitive sorption system. International Journal of Environmental Science and Development 2012; 3:362-367. DOI: 10.7763/IJESD.2012.V3.248
18. S. Mehdizadeh, S. Sadjadi, S. J. Ahmadi, M. Outokesh. Removal of heavy metals from aqueous solution using platinum nanoparticles/Zeolite-4A. Journal of Environmental Health Science and Engineering 2014; 12:1-7. DOI: 10.1186/2052-336X-12-7
19. M. Li, C. Feng, Q. Zeng. Preparation and Characterization of multi carboxyl-functionalized silica gel for removal of Cu (II), Cd (II), Ni (II) and Zn (II) from aqueous solution. Applied Surface Science 2014; 314:1063-1069. DOI: 10.16/J.apsusc.2014.06.038
20. E. Repo, J. K. Warchol, A. Bhatnagar, M. Sillianpaa. Heavy metals adsorption by novel EDTA-modified chitosan-silica hybrid materials. Journal of Colloid and Interface Science 2011; 358:261-267.

DOI: 10.1016/J.JCIS.2011.02.059

21. M. Anjum, R. Milardad, M. Waqas, F. Gehany. M.A. Barakat. Remediation of wastewater using various nano-materials. Arabian Journal of Chemistry 2016; 12:4897-4919.
    DOI: 10.1016/J.arabjc.2016.10.004
22. S. Kashyap, S. K. Pratihar, S. K Behera. Strong and ductile graphene oxide reinforced PVA composites. Journal of Alloys and Compounds 2016; 684:254-260.
    DOI: 10.1016/j.jallcom.2016.05.162
23. G. Zhao, J. Li, X. Ren, C. Chen, X. Wang. Few-layered graphene oxide nanosheets as superior sorbents for heavy metal ion pollution management. Environmental Science and Technology 2011; 45:10454-10462.
    DOI: 10.1021/es203439V
24. J-B. Zeng, K-A. Li, A-K. Du. Compatibilization strategies in poly (lactic acid)-based blends. Royal Society of Chemistry 2015; 5:32546-32565.
    DOI: 10.1039/CSRA01655J
25. R. Premraj, D. Mukesh. Biodegradation of polymers. Indian Journal of Biotechnology 2005; 4:186-193
26. L. S. Nair, C. T. Laurencin. Biodegradable polymers as biomaterials. Progress in Polymer Science 2007; 32:763-798.
    DOI: 10.1016/j.progpolymsci.2007.05.017
27. A. Richard. Biodegradable polymers for the environment. Science 2002; 297:803-807.
    DOI: 10.1126/science.297.5582.803
28. T. P. Haider, C. Volker, J. Kramm, K. Landfester, F. R. Wurm. Plastics of the future? The impact of biodegradable polymers on the environment and on society. A Journal of the German Chemical Society 2018; 58:50-62.
    DOI: 10.1002/anie.201805766
29. S. S. Ray, M. Bousmina. Biodegradable polymers and their layered silicate nanocomposites: In greening the 21st century materials world. Progress in Materials Science 2005; 50:962-1079.
    DOI: 10.1016/J.PMATSCI.2005.05.002
30. J. C Middleton, A. J. Tipton. Synthetic biodegradable polymers as orthopaedic devices. Biomaterials 2000; 21:2335-2346.
    DOI: 10.1016/S0142-9612 (00) 00101-0
31. M. Vert, G. Schwarch, J. Coutane. Present and future PLA polymers. Journal of Macromolecular Science 2006; 32:787-796.

DOI: 10.1080/1060/329508010289

32. A. Garlotta. A literature review of Poly (Lactic Acid). Journal of Polymer Science and the Environment 2001; 9:63-84.
DOI: 10.1023/A.102020082
33. K. M. Nampoothiri, N. R. Nair, R. P. John. An overview of the recent developments in Polyactide (PLA) research. Bioresource Technology 2010; 101:8493-8501.
DOI: 10.1016/j.biortech.2010.05.092
34. O. Martin, L. Averous. Poly (Lactic acid): Plasticization and properties of biodegradable multiphase systems. Polymer 2001; 43:6209-6219.
DOI: 10.1016/50032-3861(01)000866-6
35. D. Garlotta. A literature review of Poly (Lactic Acid). Journal of Polymers and the Environment 2001; 9:63-84.
DOI: 10.1023/A: 102020082
36. M. Jamshidian, E. A. Tehrany, M. Imran, M. Jacquot, S. Desobry. Poly-lactic acid: production, applications, nanocomposites and release studies. Comprehensive Reviews in Food Science and Food Society 2010; 9:552-571.
DOI: 10.1111/j.1541-4337.2010.00126.x
37. S. Pilla. Engineering of bioplastics and biocomposites. An overview. In: S. Pilla. Handbook of Bioplastics and Biocomposites Engineering applications. John Wiley & Sons 2011; 1:1-15.
DOI: 10.1002/9781118203699
Online ISBN: 9781118203699
38. S. H. El-Taweel, B. Stoll, C. Schick. Crystallization kinetics and miscibility of blends of polyhydroxybutyrate (PHB) with ethylene vinyl acetate copolymers (EVA). E-Polymers 2011; 18:1-16.
ISSN: 1618-7229
39. R. B. e Dias, N. P. Coto, G. F. Batalha, L. Driemeier. Systematic study of ethylene – vinyl acetate (EVA) in the manufacturing of protector devices for the orofacial system. Biomaterials in Regenerative Medicine 2018; 14:320-340.
DOI: 10.5772/intechopen.69969
40. S. Sreeremya. Adsorption-Review. International Journal of Advance Research and Development 2017; 2:15-18.

41. N. Venkateshwaran, A. Elayaperumal, A. Alavudeen, M. Thiruchitrambalam. Mechanical and water absorption behaviour of banana/sisal reinforced hybrid composites. Materials and Design 2011; 32:4017-4021.
DOI: 10.1016/j.matdes.2011.03.002
42. D. L. Sparks. Sorption phenomena on soils. Environmental Soil Chemistry 2002; 2:133-186.
DOI: 10.1016/B978-012656446-4/50005-0
43. J. G. Speight. Chemical transformations in the environment. Environmental Organic Chemistry for Engineers 2017; 1:305-353.
DOI: 10.1016/B978-0-12-804492-6.00007-1
44. M. B. Desta. Batch sorption experiments: Langmuir and Freundlich isotherm studies for the adsorption of textile metal ions onto teff straw (Erayrostistif) agricultural water. Journal of Thermodynamics 2013; 298:1-6.
DOI: 10.1155/2013/375830
45. A. S. Thajeel. Isotherm, kinetic and thermodynamics of adsorption of heavy metal ions onto local activated carbon. Aquatic Science and Technology 2013; 1:53-77.
DOI: 10.5296/ast.vli2.3763
46. M. Karnib, A. Kabhani, H. Holail, Z. Olama. Heavy metals removal using activated carbon, silica and silica activated carbon composite. Energy Proceedia 2014; 50:113-120.
DOI: 10.1016/j.egypro.2014.06.014
47. N. Ayawei, A.N. Ebelegi, D. Wankasi. Modelling and interpretation of adsorption isotherms. Journal of Chemistry 2017; 2017:1-11.
DOI: 10.1155/2017/3039817
48. J. Meyer, A. K. Germ, M. I. Katsneslson, K. S. Novoselov, J. J. Booth, S. Roth. The structure of suspended graphene sheets. Nature 2007; 446:60-63.
DOI 10.1038/nature05545

CHAPTER 2

LITERATURE REVIEW

The study of using graphene oxide as an adsorbent for heavy metals in water is one that is currently widely explored. The researchers are currently using different approaches to using GO to remove metal ions. Most researchers have used GO on its own to assess its effectiveness in heavy metal removal. However, very little research has been done in utilizing GO/polymer composites in removing heavy metals, and this is where the gap lies.

The following section gives a detailed overview of graphene oxide, outlining its origin as well as its thermal and morphological properties. It also outlines the findings on GO's effectiveness in removing heavy metal ions in solution as well as its water uptake capacities when used on its own. The section further reports on GO/polymer composites previously studied and the composite's morphological, thermal and mechanical properties. Then the absorption and adsorption capabilities of GO/polymer composites are explored lastly in the section.

2.1 GRAPHENE AND GRAPHENE OXIDE

Graphene is a form of carbon which has a single layer of carbon atoms which are arranged in a hexagonal lattice. It is the structural unit for most of the carbon allotropes like graphite, carbon nanotubes, diamond, charcoal and derivatives like graphene oxide amongst others [1]. Graphene consists of a one atom thick planar sheet, which has an sp^2 bonded carbon structure with very high crystal and electronic quality. It gained interest in the field of material science due to its good physiochemical properties. These include a high specific surface area (theoretically 2630 m^2/g for single-layer graphene), good electronic properties and electron transport capabilities. Furthermore, pliability and impermeability, strong mechanical strength as well as good thermal and electrical conductivity [2,3].

One derivative of graphene is graphene oxide (GO). GO has been proven to consist of a single layer of graphite oxide, and its production proceeds via the chemical treatment of graphite by oxidation with subsequent dispersion or exfoliation in water or suitable organic solvents [4]. There have been many models proposed in describing the structure of GO, and each of these models assume GO to be having oxygen-containing functional groups [5,6]. These oxygen-containing functional groups have been identified to be hydroxyl and ester groups on the basal

plane, and little amounts of carboxy, phenol, carbonyl, lactone and quinone at the edges of the sheet. These were observations made by Kim *et al* [7] in analysing graphene oxide. However, the precise structure of GO is still uncertain and under continuous debate. This is primarily due to the uncertainty in the distribution and identity of the oxygen-containing functional groups, the non-stoichiometric atomic quantities and the lack of efficient and successful methods to characterize GO [8].

2.1.1 The morphology of GO

Morphology refers to the study of form through shape, size and structure. It is very important in materials studies as for nanostructured materials morphology gives an indication of chemical and physical properties [9]. Studies of morphology are thus very crucial in identifying materials through verifying their chemical and/or physical structures. A number of these studies have been conducted on GO as a means of verification of its structure and/or success in its synthesis. Different researchers utilized different morphology techniques, amongst these are Atomic force microscopy (AFM), X-ray photoelectron spectroscopy (XPS) and Fourier transform infrared spectroscopy (FTIR). These three techniques were used by one researcher, Shang *et al* [10], in investigating the morphology of GO. The author was successful in synthesizing GO, and this was validated by: the AFM images indicating GO sheets having a height (length) of about 0,9 nm proving the sheets to be monolayers. The average lateral size (thickness) of the nanosheets being found to be 1 µm in AFM. The XPS analysis resulting in a C1 spectrum with four different peaks: C=C (284.3 eV), C-O (286.3 eV), C=O (287.6 eV), and COOH (289.0 eV), proving the existence of the oxygen-containing functional groups in GO. The FTIR analysis resulting in a spectrum with peaks illustrating the presence of C-O (alkoxy) at 1045 cm^{-1} C-O-C (ester) at 1226 cm^{-1}, and C=O in carboxylic acid and carbonyl moieties (carbonyl) at 1719 cm^{-1}. Then bands at 3330 and 1396 cm^{-1} were observed which could have been due to the O-H stretching mode and deformation vibration of intercalated water, respectively. FTIR and XPS results meant that GO is amphiphilic, with a hydrophobic basal plane and hydrophilic edges. Similarly, the FTIR results obtained by Ghosh *et al* [11], in morphology and property analysis, yielded more or less the same outcome, whereby an O-H stretching peak at 3441 cm^{-1} which was prominent indicating the presence of many OH groups in the backbone of GO was observed. A band at 1760 cm^{-1} due to C=O stretching and one at 1403 cm^{-1} owing to the carboxy groups present in GO were observed. Ghosh also used X-ray diffraction (XRD) as well

as Raman spectroscopy and the results were positive in each case. A Raman spectrum was obtained which had two main features: The G band, which describes the first-order scattering of phonons by sp^2 carbon atoms, and the D band, which describes the breathing mode of photons. The G band appeared to have shifted to 1591 cm^{-1} and broadened whilst the D band shifted to a lower region (1341 cm^{-1}) and became more apparent. This observation was because of the destruction of sp^2 character and the formation of defects in the GO sheets due the extensive oxidation of graphite to graphene oxide. In XRD, the diffraction peak of GO was observed at 11.41˚, which was due to the interlayer spacing of 0.741 nm, and this indicated the intercalation of water molecules in the graphite layers as well as the formation of oxygen containing functional groups between the layers of graphite. Several authors obtained similar results in investigating the morphology of GO [12-14]. Figure 1.3 shows the typical structure for graphene oxide. The structure shows the different oxygen – containing functional groups that have previously been validated by researchers reported here. These functional groups will later on in the study prove to be the sites on which metal adsorption takes place.

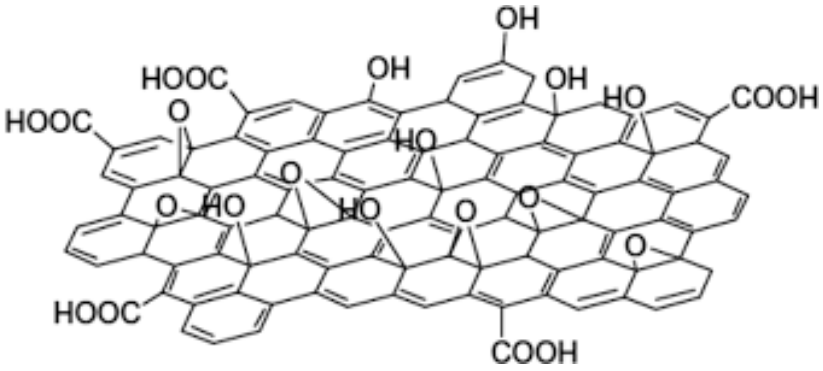

Figure 2.1: Typical graphene oxide structure showing various oxygen-containing functional groups [15].

2.1.2 Thermal properties of GO

Thermal properties are a part of physical properties related to the heat conductivity in materials. In other words, these are properties exhibited by a material when it is subjected to a fluctuating heat. There are four major components of thermal analysis namely: heat capacity, thermal expansion, thermal conductivity and thermal stress [16]. Various methods of analysis are used in assessing the thermal properties of materials. A limited number of researchers have reported on the thermal properties of GO [17,18]. In one study of thermal analysis of GO by Alhassan *et al* [17], Differential Scanning Calorimetry (DSC) and Thermogravimetric analysis (TGA)

were used to investigate the thermal properties of GO. In DSC the authors observed an endothermic peak at about 135 ℃ which they said to be because of the detachment of water molecules from the GO surface. The same transition was observed in TGA at the same temperature, thus showing the detachment of water molecules from GO. Another exothermic peak was observed by the authors in DSC at about 185 ℃, which they attributed to the thermal decomposition of oxygen containing functional groups. The TGA curves showed mass losses for the evolution of carbon dioxide and carbon monoxide from the molecule around 200 ℃. Bhawal *et al* [18] in synthesizing and characterizing GO, observed that generally GO has a very low thermal stability. Its hydrophilicity contributes to its early onset of thermal degradation, which in most cases is below 100 ℃ whereby water molecules are detached. Then between 176 and 201 ℃ is where we get the decomposition of oxygen containing functional groups in GO. From there the main chain decomposition (carbon) occurs.

The current and past work on graphene oxide has indeed been progressive. Apart from analysing the properties of graphene oxide alone, some researchers have also opted to use graphene oxide in polymer composites. This has been done for various purposes, which include but are not limited to improving the properties of GO, improving polymer/polymer interfaces, and-materials strength for various applications, amongst others [19-31]. It is clear that there is a need to look into polymer/GO composites studied in the past, as well as the findings thereof.

2.2 GO/POLYMER COMPOSITES

GO based composites have received great attention over the years, and this is as a result of the reactive sites present in GO which see its structure tailored and improved for different requirements. The common usages for these GO composites are for electrical conductivity, adsorption purposes and improvement of properties. Although little research has been done on GO composites with biodegradable polymers, there has been a variety of papers reporting on the polymer/GO composites with respect to testing the improvement, or lack thereof, of properties afterwards. [19-31]

2.2.1 The morphology of GO/Polymer composites

A few number of researchers have investigated the morphology of polymer/GO composites [19-21]. SEM and TEM were the most common used methods of analysis in this case. SEM

analysis has been shown to not give clear images at high magnifications for PLA/GO composites. This behaviour was attributed to the heat sensitivity of PLA, and thus thermal instability at high magnifications. This resulted in the dispersion of GO in a PLA matrix not being clear with the use of SEM and the need for using TEM for clearer images arises [19]. In TEM the dispersion of GO in the PLA matrix was quite uniform and visible. Pinto *et al* [19], in investigating PLA/GO composites, validated this with a clear identification of GO single sheets and some small aggregates in the polymer matrix. Spectrochemical analysis (Field emission spectrum) showed the transparency of PLA/GO composites to reduce with an increase in GO content. Other polymers like poly (vinyl alcohol) had the GO being visible on their surfaces when their composites were analysed with SEM. This was because of smaller interlayer distances and smaller defects making it hard for it to be broken down, as was reported by Theophile *et al* [20], in analysing electrochemical properties of PVA/GO composites. In the EDS part of this specific polymer/GO composite, it was observed that carbon has a higher percentage (60%) than oxygen (40%). The authors also analysed the morphology of GO using X – Ray Diffraction (XRD). For a typical poly (vinyl alcohol) / GO composite the polymer peaks in XRD became more intense with an increasing GO content. This was interpreted as the crystallinity of the composites increasing with an increase in GO [20].

Ultrahigh molecular weight polymers like polyethylene have also been used in GO composites to assess their morphologies. Chen *et al* [21], in analysing ultrahigh molecular weight polymers with GO, found the resulting SEM images to show the fractured surfaces of the polymer alone to be flat before introducing GO. The authors found out that with the addition of 0.3 wt.% GO, the fractured surfaces became uneven, with a random distribution of GO in the polymer matrix. Further addition of GO to 0.5 wt.% and above changed its distribution from random to homogenous in the polymer matrix. The authors explained that this suggested that GO at loadings of 0.5 wt.% and above worked as a compatibilizer to the composite system. The affinity of GO to the matrix in this case was quite strong because further zooming into the images in SEM showed the GO sheets being deeply embedded into the matrix. When the GO content was increased to 1 wt.% the GO bound more compactly to the matrix, thereby increasing the visible layer size, as the authors reported [21].

2.2.2 Thermal properties of GO/Polymer composites

Thermal analysis is very important in analysing polymer/GO composites. This is mostly done through the differential scanning calorimetry (DSC) and thermogravimetric analysis (TGA). DSC helps in understanding the melting and crystallization behaviour, whereas TGA assesses the thermal stability. Very limited studies have been published that look at the thermal properties of GO/polymer composites [22-24].

2.2.2.1 Melting and crystallization

For thermal transitions, DSC is usually used. Here the general consensus is that the introduction of GO into a matrix increases the crystallinity of the polymer composite. One such observation was made by Xu *et al* [22], in looking at poly (vinyl alcohol)/GO films, wherein the melting temperature of PVA/GO with 3 wt.% GO was 2 ℃ higher than that of the polymer alone. These observations were attributed to homogenous dispersion, alignment of GO sheets in the polymer matrix and strong interfacial interactions between both components. Zhou *et al* [23], in assessing the thermal and properties of resin/GO composites found that the glass transition temperature in DSC, for PVA/GO composites shifted to the right upon 0.5 wt.% GO content. This was explained as GO delaying the transition to the rubbery state for PVA as it increases its crystallinity. The thermal properties of polymer/GO composites are well reliant on the content of GO mostly and in most cases GO improves thermal properties.

While, Mindivan *et al* [24], in studying properties of PVC/GO composites, found out that the glass transition of PVC dropped as GO loadings were increased. This, according to the authors, implied that GO caused an easier relaxation of the molecular chain. The authors went further to observe that the addition of 0.1 wt.% GO increased the melting enthalpy from 58.66 to 62.9 J/g. This was attributed to the reinforcing effect that GO had on PVC, according to the authors. However, increasing GO loadings to above 0.1 wt.% resulted in the melting enthalpy dropping, with the lowest enthalpy observed when GO loading was 1 wt.%. This was explained as due to the weak interaction between GO and the polymer as the GO loading increases, with the possibility of agglomerates. The melting temperature of PVC seemed to not have been influenced by the addition of GO.

2.2.2.2 Thermal degradation/stability

Thermal degradation studies give information about a polymeric material's thermal stability. It is very important to know the thermal degradation/stability of materials to deduce its possible applications. Xu *et al* [22] investigated the thermal stability of PVA/GO composites in TGA. The results showed the thermal stability of the polymer improved with GO addition. For PVA, the peak degradation temperature of its composite with 3 wt. % GO was about 37 ℃ higher than that of the neat polymer. The degradation rate of the composite was slower than that of the polymer alone and became slower as more GO was added. This indicated that the mobility of the polymer segments at the interfaces of the polymer and GO was suppressed by strong interactions, causing an increase in thermal stability. Zhou *et al* [23] investigated the thermal and mechanical properties of phenolic resin/GO composites, and they also obtained the same thermal degradation analysis results for these composites. The authors observed that the thermal stability of phenolic resin/GO composites increased with an increase in GO content. The more GO was added, the slower the degradation rate and the higher the degradation temperatures were observed by the authors. This implied that the thermal stability of the composites improved, and the authors attributed this to a strong interaction between the polymer and GO. This interaction would go on to delay thermal degradation of the components, according to the authors. Mindivian *et al* [24], studied thermal and structural characterization of polyvinylchloride/graphene oxide (PVC/GO) composites. On their thermal degradation analysis by TGA they found that PVC had showed two degradation steps. The first one occurred around 292 ℃ and was said to be the escaping of chlorine gas. The second degradation step of PVC was found at 452 ℃, and was the main chain degradation, with a char of 16%. The addition of GO shifted the first thermal mass loss to lower temperatures (276 ℃). This was attributed to GO losing its initially absorbed moisture, and that GO had a poor interaction with PVC and thus lowered the polymer's thermal stability. The second degradation step shifted to higher temperatures (470 ℃ for 1 wt.% GO). Furthermore, the authors found out that as GO loading increased the residue dropped to 12%. All these were attributed to the dispersion of GO layers, partially preventing the formation of volatile aromatic compounds.

2.3 WATER ABSORPTION

2.3.1 Water absorption of GO

Quite a few researchers have studied the water intake of graphene oxide [25,26]. Graphene alone is believed to have very poor absorption capabilities; however the introduction of

oxygen-containing functional groups provides a solution for this trait, hence graphene oxide has gained popularity in water absorption studies. Liu *et al* [25], in studying the effectiveness of GO in absorbing water under different humidity conditions, observed that generally the water intake capacity increases with an increase in the mass of GO powder (grams) used. This was attributed to GO having oxygen containing functional groups, that act as intercalation sites for water to be diffused through while solid substances are adsorbed. The effect of humidity resulted in the equilibrium absorption being reached faster. This increased rate of absorption was attributed to the hydrophilic nature of GO.

Lian *et al* [26], in investigating the kinetics of GO absorption of water, observed that the rate of absorption increased with an increase in the GO powder mass used (grams). A comparison was also made between flaky GO and grinded GO. Here the authors observed that grinded GO reached absorption equilibrium faster than the flaky GO. They attributed this to ease of penetration of water with reduced particle size. However, the absorption capacity was found to drop when the GO was grinded. This was attributed to the capillary transportation being tempered with when GO is grinded, and the grinding reducing the durability of GO.

The above discussions clearly show that the water intake of GO alone has proven it to be very water loving, or hydrophilic. This was validated by the fact that as the mass used for GO increased, the degree to which it absorbed water also increased. As such, it would only be fair to want to preserve the GO used as much as possible, ergo mask it to some extent. This has been previously done using polymers, amongst others. The water absorption of GO/polymer composites has been and continues to be an area of great concern [27,28].

2.3.2 Water absorption of GO/Polymer composites

Quite a limited number of studies [27,28] have investigated the water intake of polymer/GO composites. Generally, it was found that oxygen containing functional groups in polymers contribute a great deal to the absorption rate of the composites with GO. Biodegradable polymers with oxygen containing functional groups like hydroxypropyl methylcellulose (HPMC) and poly lactic acid (PLA) thus have a high-water absorption rate. Ghosh *et al* [27], in assessing morphology and properties of HPMC/GO composites, have reported water absorption rates (by percentage) of about 10.5% absorption for the polymer alone without GO. Then adding 0.9 wt.% GO to the matrix resulted in the absorption capacity of that composite being lower than that of the neat polymer. This was attributed to the formation of hydrogen

bonds between GO and the polymer, which inhibited the interaction of water molecules with the polymer. Further increasing the GO content to 1.1 wt.% resulted in the rate of water absorbed increasing to even exceed that of the pure polymer. The authors explained that this was because the hydrogen bonds formed at 0.9 wt.% GO loading were now saturated as GO loadings increased to 1.1 wt.%. This resulted in the polymer leaving free running hydroxyl groups that interacted with the water molecules, thereby accounting for the increased absorption capacity at 1.1 wt.% GO loading. It followed further from this that GO was indeed hydrophilic, according to the authors. The water uptake of polymer/GO composites has also previously been assessed in terms of three parameters. These are firstly the water absorption rate, which is the slope obtained at the initial stages of the curve. Secondly, the moisture absorption at saturation, which is the absorption when the curves are steady. Lastly, the coefficient of diffusion (D). This study was performed by Gavin *et al* [28] in assessing the barrier properties of GO/vinyl ester composites. The findings were still that at low GO compositions (0.5 wt.%) the absorption rate of the composites dropped to below that of the polymer alone. This was further attributed to the interaction of GO with the polymer as well as the presence of hydrophobic material in the polymer. The coefficient of diffusion followed the same trend: small GO amounts resulted in lower D values and increasing GO loading increased the value of D. The conclusion from this was that GO increased permeability of water but only if it is in large amounts in the polymer matrix.

2.4 ADSORPTION

2.4.1 GO as an adsorbent for heavy metals in water

A limited number of published papers investigate the effectiveness GO alone in adsorbing heavy metals from solution [29,30]. In one such study by Sitka *et al* [29], the effectiveness of GO alone in removing Cd(II), Cu(II), Zn(II) and Pb(II) from solution was investigated. Here the oxygen containing functional groups were the ones mostly responsible for adsorption of heavy metal ions from solution. Pb (II) was found to be the most adsorbed metal ion amongst the other investigated, and high adsorption capabilities were achieved in the pH range 4-8 for all the metal ions. From this it was further established that the dominant manner in which the metal ions are adsorbed is by chemisorption. This is a type of adsorption which occurs chemically and could result in a reaction between the adsorbent and the adsorbate being an irreversible process. These observations were somewhat common amongst different

researchers. One such researcher is Zhao *et al* [30] where XRD, Raman spectroscopy and AFM were used first to verify GO synthesis. The results obtained from analysing GO prepared by Hummer's method also indicated adsorption of lead ions to be dependent on the oxygen containing functional groups. Further analysis of adsorption in terms of pH, ionic strength and concentration showed that adsorption was more dependent on pH than it was on the latter mentioned. The use of Langmuir isotherms for lead ions were reported to be 842, 1150 and 1850 mg/g at 293, 313 and 333 K, respectively.

The usage of GO alone in adsorbing heavy metals from solution surely arose then need for it to be masked. This has been one scarce route for researchers, as it is practically difficult to mix GO with other materials. However, one particular way to mask GO would be through mixing it in a polymer matrix. This could be an efficient process as some polymers have oxygen containing functional groups which could also aid the adsorption process.

2.4.2 GO / polymer composites as adsorbents for heavy metals in water

There has been a limited number of papers indicating the usage of graphene oxide and its composites as adsorbents for water treatment [29-31]. Many materials have been used to form composites with GO which include metal oxides, sand, and polymers. However, there has not been a lot of research going to polymer/GO composites, especially one which utilizes biodegradable polymers. In one study, Graphene oxide had been synthesized, chemically reduced and functionalized with polypyrrole (GO/polypyrrole composite), chitosan, aromatic diazonium salt and ethylene diamine amongst others. The study was done by Peng *et al* [31], and it followed that the different functional groups had an effect in adsorption. The authors prepared GO/polypyrrole composites, and deduced that adsorption capacities were greater when GO was mixed with materials that already had oxygen containing functional groups. As such, it was concluded that in masking GO for adsorption of heavy metals, the materials used to mix with it should be those that also have oxygen containing functional groups. Desorption were also conducted using hydrochloric acid whereby it was found that the GO/polypyrrole composites had a 95% reusability effectiveness after 4 cycles and a 90% after 8 cycles. This showed that GO/polymer composites could be used commercially for water decontamination purposes. The limited reporting on GO/polymer composites being used as adsorbents was really due to the fact that there has not been a lot of work around this. As such, the usage of

GO/polymer composites has been identified as a knowledge gap, especially using biodegradable polymers.

2.5 REFERENCES.

1. D. Chen, H. Feng, J. Li. Graphene oxide: Preparation, functionalization and electrochemical applications. Chemical Reviews 2012; 112:6027-6053.
   DOI: 10.1021/cr300115g
2. R. Ruoff. Graphene: Calling all chemists. Nature Technology 2008; 3:10-11.
   DOI: 10.1038/nnao 2007.432
3. D. R. Dreyer, S. Park, C. W. Brelawski, R. S. Ruoff. The chemistry of graphene oxide. Chemical Society Reviews 2010; 39:228-240.
   DOI: 10.1039/B917103G
4. A. Lerf, H. He, M. Forster, J. Klinowski. Structure of graphite oxide revisited. The Journal of Physical Chemistry 1998; 23:4477-4482.
   DOI: 10.102//jp9731821
5. G. Eda, M. Chhowalla. Chemically derived graphene oxides towards large-area thin-film electronics and optoelectronics. Advanced Materials 2010; 22:2392-2415.
   DOI: 10.1002/adma.200903689
6. X. Li, G. Zhang, X. Bai, X. Siun, X. Wang, E. Wang, H. Dui. High conductivity graphene sheets and Langmuir-blodget film. Nature Nanotechnology 2008; 9:538-542.
   DOI: 10.1038/nnano.2008.210
7. F. Kim, L. J. Lote, J. Huang. Graphene oxide: surface activity and two-dimensional assembly. Advanced Materials 2010; 22:1954-1958.
   DOI: 10.1002/ADMA.200903932
8. O. C. Compton, S. T. Nguyen. Graphene oxide, highly reduced graphene oxide and graphene. Versatile Building Blocks for Carbon-based Materials 2010; 22:711-723.
   DOI: 10.002/SMLL.200901934
9. M. K. Sanyal, A. Datta, S. Hazra. Morphology of nanostructured materials. Pure and Applied Chemistry 2009; 74:1553-1570.
   DOI: 10.1351/pac200274091553

10. Y. Shang, D. Zhang. Preparation and thermal properties of graphene-oxide-microencapsulated phase change materials. Nanoscale and Microscale Thermophysical Engineering 2016; 2:147-157.
DOI: 10.1080/15567265.2016.1236865.
11. T. K. Ghosh, S. Gope, D. Mondal, B. Bhowmik, M. R. Mollick, D. Maity, I. Roy, G. Sarkar, S. Sadhukhan, D. Rana, M. Chakraborty, D. Chattopadhyguy. Assessment of morphology and property of graphene-hydroxypropylmethylcellulose nanocomposite films. International Journal of Biological Macromolecules 2014; 66:338-345.
DOI: 10.1016/j.ijbiomac 2014.02.054
12. Z. Xia, G. Maccaferri, C. Zanardi, M. Christian, L. Ortolani, V. Morandi, V. Bellani, A. Kovtun, S. Dell'Elce, A. Candini, A. Liscio, V. Palermo. Dispersion stability and surface morphology study of electrochemically exfoliated bilayer grapheme oxide. The Journal of Physical Chemistry 2019; 123:15122-15130.
DOI: 10.1021/acs.jpcc.9bo3395
13. E. Jaafar, M. Kashif, S. Sahari, Z. Ngaini. Study on morphological, optical and electrical properties of graphene oxide (GO) and reduced grapehene oxide (rGO). Materials Science Forum 2018; 917:112-116.
DOI: 10.4028/www.scientific.net/MSF.917.112
14. I. Castilla-Cortaza, A. Vidaurre, B. Mari, A. Campillo-Fernandez. Morphology, crystallinity and molecular weight of poly (ε-caprolactone)/grapheme oxide hybrids. Polymers 2019; 11:1-19.
DOI: 10.3390/polym11071099
15. M. Nasrollahzadeh, F. Babaei, P. Fakhri, B. Jaleh. Synthesis, characterization, structural, optical properties ad catalytic activity of reduced graphene oxide/copper nanocomposites. Royal Society of Chemistry 2015; 5; 10782-10789
DOI: 10.1039/c4ra12552e
16. M. F. Ashby. Overview no. 80: On the engineering properties of materials. Acta Metallurgica 1989; 37:1273-1293.
DOI: 10.1016/0001-6160/89/90158-2
17. S. M. Alhassan, S. Qutubuddin, D. A Schiraldi, T. Agag, H. Ishida. Preparation and thermal properties of graphene oxide/main chain benzoxazine polymer. European Polymer Journal 2013; 49:3825-3833.
DOI: 10.1016/j.europolymj.2013.09.005

18. P. Bhawal, S. Ganguly, T. K. Chaki, N. C. Das. Synthesis and characterization of graphene oxide filled ethylene acrylate hybrid nanocomposites. Royal Society of Chemistry 2016; 6:20781-20790.
DOI: 10.1039/C5RA24914G
19. A. M. Pinto, J. Cabral, D. A. Tanaka, A. M. Mendes, F. D Magalhaes. Effect of incorporation of graphene oxide and graphene nanoplatelets on mechanical and gas permeability properties of poly (lactic acid) films. Polymer International 2012; 62:33-40.
DOI: 10.1002/pi.4290
20. N. Theophile, H. K. Jeong. Electrochemical properties of poly (vinylalcohol) and graphene oxide composite for supercapacitor applications. Chemical Physics 2017; 669:235-129.
DOI: 1016/j.cplett.2016.12.029
21. Y. Chen, Y. Qi, Z. Tai, X. Yan, F. Zhu, Q. Xue. Preparation, mechanical properties and biocompatibility of graphene oxide/ultrahigh molecular weight polyethylene composites. European Polymer Journal 2012; 48:1026-1033.
DOI: 10.1016/j.europolymj.2012103.011
22. Y. Xu, W. Hong, H. Bai, C. Hi, G. Shi. Strong and ductile poly (vinyl alcohol)/graphene oxide composite films with a layered structure. Carbon 2009; 47:3538-3543.
DOI: 10.1016/j.carbon.2009.08.022
23. J. Zhou, Z. Yao, Y. Chen, D. Wei, Y. Wu, T. Xu. Mechanical and thermal properties of graphene oxide/phenolic resin composite. Polymer Composites 2013; 34:125-1249.
DOI: 10.1002/Pc.22533
24. F. Mindivian. The synthesis, thermal and structural characterization of polyvinylchloride/grapheme oxide (PVC/GO) composites. Mterials Science. Non-Equilibrium Phase Transformations 2015; 1:33-36.
ISSN: 2534-8477
25. R. Liu, T. Gong, K. Zhong, C. Lee. Graphene oxide papers with high water adsorption capacity for air dehumidification. Scientific Reports 2017; 7:1-9.
DOI: 10.1038/541598-017-09777-y
26. B. Lian, S. De Luca, Y. You, S. Alwarappan, M. Yoshimura, V. Sahajwalla, S. Smith, G. Leslie, R. Joshi. Extraordinary water adsorption characteristics of graphene oxide. Chemical Science 2018; 9:5106-5111.
DOI: 10.1039/C8SC00545A
27. T. K. Ghosh, S. Gope, B. Bhowmik, M. D. Masud, R. Mollick, D. Marty, I. Roy, G. Sarkar, S. Sadhukhan, D. Rana, M. Chakraborty, D. Chattopadhyay. Assessment of morphology

and property of graphene oxide-hydroxypropylmethylcellulose nanocomposite films. International Journal of Biological Macromolecules 2014; 66:338-345.
DOI: 10.1016/ijbiomac.2014.02.054.

28. F. Gavin, P. Cousin, M. Robert, Effect of modified graphene oxide on the mechanical, thermal and barrier properties of vinylester. Journal of Composite Materials 2018; 52(28):3853-3864.
DOI: 10.1177/0021998318770730
29. R. Sitko, E. Turek, B. Zawisza, E. Malicka, E.Talik, J. Heiman, A. Gagor, B. Feist, R. Wizalik. Adsorption of divalent metal ions from aqueous solutions using graphene oxide. Dalton Transactions 2013; 42:5682-5689.
DOI: 10.1039/C3DT53097d
30. G. Zhao, X. Ren, X. Ghao, X. Tan, J. Li, C. Chen, Y. Huang, X. Wang. Removal of Pb(II) ions from solutions on few-layered graphene oxide nanosheets. Dalton Transactions 2011; 40:10945-10952.
DOI: 10.1039/c1dt1100se
31. W. Peng, H. Li, X. Liu, S. Song. A review on heavy metal ions adsorption from water by graphene oxide and its composites. Journal of Molecular Liquids 2017; 230:496-504.
DOI: 10.1016/j.moll.iq2017.01.064

CHAPTER 3

MATERIALS AND METHODS

In this chapter, the materials used in functionalizing EG to GO, polymers used to form blends and blend composites with different rations by mass, and the techniques used to characterize the above mentioned samples are presented.

3.1 MATERIALS

3.1.1 Poly (L-Lactic acid) (PLA)

Poly (L-Lactic acid) (PLA 4043D) was supplied by Nature Works LLC in USA. It has a melt temperature in the range 145 – 160 ℃, a glass transition temperature in the range 55 – 65 ℃, a density (ρ) of 1.248 g/cm^3, tensile strength at yield 48 MPa and tensile elongation at yield of 2.5%

3.1.2 Ethylene vinyl acetate (EVA)

Ethylene vinyl acetate (EVA-460) used in this study was manufactured and supplied in granule form by DuPont Packaging & Industrial Polymers in South Africa. This EVA contains 18% by weight vinyl acetate content and has a butylated hydroxyl toluene antioxidant thermal stabilizer. The melt flow index (MFI) of this polymer is 2.5 g/10 min, it melts at 88 ℃, has a softening point of 64 ℃ and a density (ρ) of 0.941 g/cm^3.

3.1.3 Expandable graphite (EG)

The expandable graphite used (EG) was commercial grade ES250 B5 which has a 90-95% carbon content, an expansion rate of 250-500 cm^3/g at a starting range temperature range between 180-300 ℃ and with more than 80% of its contents having a particle size greater than 300 µm. It was supplied, in flake form, by Qingdao Kropfmuehl Graphite, China.

3.1.4 Functionalizing chemicals

Sulphuric acid (H_2SO_4), M_w = 98.1 g/mol, ρ = 1.84 g/cm^3, Assay = 95-99 %, Phosphoric acid (H_3PO_4), M_w = 98.0 g/mol, ρ = 1.71 g/cm^3, Assay = 85 %, Potassium permanganate ($KMnO_4$),

M_w = 158.0 g/mol, Appearance: Dark purple needle like crystals, Assay = 99.0 %, Hydrogen peroxide (H_2O_2), M_w = 34.0 g/mol, ρ = 1.11 g/cm^3, Assay = 30 %, Hydrochloric acid (HCl), M_w = 36.5 g/mol, ρ = 1.16 g/cm^3, Assay = 32 %, all supplied by Sigma-Aldrich, South Africa.

3.2 METHODS

3.2.1 Functionalization of EG to form GO

Expandable graphite was functionalized using a modified Hummers method, to form graphene oxide. Briefly this proceeded by first mixing H_2SO_4 (27 ml) with H_3PO_4 (3 ml) and stirring the mixture for 10 minutes. Thereafter, EG (0.225g) was added to this mixture whilst stirring, and the mixture was stirred for another 10 minutes. This was followed by the slow addition of $KMnO_4$ (1.32g) and the solution was stirred for 6 hours (at room temperature and 1200 rpm speed) until it turned green. H_2O_2 (0.675 ml) was added (dropwise) to the green solution and the mixture was stirred for 10 minutes and cooled to room temperature. Following this, a mixture of HCl (10 ml) and deionized water (30 ml) was added to the reaction solution, after which the whole mixture was centrifuged at 5000 rpm for 7 minutes. The supernatant was decanted, and residuals washed with the HCl/water mixture for three times. The product was oven dried for 3 days at 50℃. The functionalization process was repeated a number of times for a higher product yield and what was the highest percentage yield obtained [1].

3.2.2 Sample preparation

Different ratios, by mass, were used to prepare all polymeric blends and composites as shown in Table 2.1. PLA, EVA and GO were dried at - 40 ℃ for 24 hours before mixing, and this was done in order to remove any moisture that might have been trapped in them. Melt mixing was used to prepare all the samples using the Brabender Plastograph. Mixing was done at a temperature of 180 ℃, a rotational speed of 50 rpm for 16 minutes. This was to ensure that crystals are fully melted and to avoid degradation and high torque levels [2]. The polymers (PLA/EVA) were first physically mixed and fed into the Brabender for 3 minutes, after which, the graphene oxide was added for the remaining 13 minutes into the mixer. The composites were melt pressed using the hydraulic melt press for 10 minutes, at 180 ℃ temperature and 50 kPa pressure. They were then cooled for 5 minutes between the steel bars, and then cut and taken for different characterizations.

Table 3.1 Compositions (w/w) for the blends and composites preparation.

Neat polymers and blends	Blend composites
Neat PLA	-
70/30 w/w PLA/EVA	69.3/29.7/1 w/w PLA/EVA/GO
-	67.9/29.1/3 w/w PLA/EVA/GO
-	66.5/28.5/5 w/w PLA/EVA/GO
50/50 w/w PLA/EVA	49.5/49.5/1 w/w PLA/EVA/GO
-	48.5/48.5/3 w/w PLA/EVA/GO
-	47.5/47.5/5 w/w PLA/EVA/GO
30/70 w/w PLA/EVA	29.7/69.3/1 w/w PLA/EVA/GO
-	29.1/67.9/3 w/w PLA/EVA/GO
-	28.5/66.5/5 w/w PLA/EVA/GO
Neat EVA	-

3.3 CHARACTERIZATION OF SAMPLES

3.3.1 Attenuated Total Reflectance Fourier Transform Infrared spectroscopy (ATR-FTIR)

Fourier transform infrared spectroscopy is a characterization method which is used to obtain the infrared spectrum of solids, liquids and gases for absorption and emission. It works by measuring the range of wavelengths in the infrared region that are absorbed by a material. This is achieved through the application of infrared radiation to samples of a material. The sample's absorbance of the infrared light's energy at various wavelengths is measured to determine the molecular composition as well as the structure of the material under analysis. FTIR can be used in identifying unknown materials, additives within polymers, surface contamination on a material amongst others. A device called an interferometer is used in identifying samples. This device produces an optical signal with all the infrared frequencies encoded into it. Then the signal becomes decoded through the application of a mathematical technique known as Fourier

transformation. This is a computer-generated process, which then produces a mapping of the spectral information. Then the resultant graph is a spectrum which is searched against reference libraries for identification [3].

Attenuated total reflectance spectroscopy is a technique of analysis for material surfaces. It is effective in analysing the surfaces of materials that are too thick or too absorbing to be analysed by the transmission infrared spectroscopy alone. Materials of all phases (Solids, gasses and liquids) can be effectively analysed in ATR. The IR spectrum here is obtained by allowing an IR beam to travel from a high reflective index medium to that of a low reflective index, which is the sample. This results in some of the light being reflected to the sample, thereby resulting in the IR spectra of the sample [4].

The confirmation of expandable graphite functionalization to graphene oxide was analysed using the Perkin Elmer Spectrum 100 series spectrometer fitted with a PIKE MiracleTM ATR, equipped with a diamond crystal. In this machine the wavenumber for analysis was set over the range: 650 – 4000 cm^{-1}, using a resolution of 4 cm^{-1} and running a total of 8 scans.

3.3.2 X – Ray diffraction (XRD)

XRD analysis has its basis on constructive interference of monochromatic X-rays and a crystalline. The X-rays are generated by a cathode ray tube and filtered to produce monochromatic radiation, which in turn is directed towards the sample being analysed. The interaction of the incident rays with the sample causes constructive interference when Bragg's law is satisfied. The specific X-ray diffraction pattern generated in an analysis provides a unique fingerprint for the crystal being analysed. As such, XRD is used to identify, with comparison to known standards, crystal forms [5].

XRD analyses were done using a D8 powder diffractometer for graphene oxide. A CuKα radiation was used, with an Si external standard, a wavelength of 1.54051 λ and beta filter. The analyses were performed under ambient temperatures with quality = indexed. A secondary monochromator at 45 kV and 40 mA was used, and a scan range of $2\theta = 1 – 60^{o}$ with continuous scanning at a rate of 0.02 ^{o} / s.

3.3.3 Scanning electron microscopy (SEM)

The scanning electron microscope uses a focused beam of high electrons on the surface of a material to generate a signal for all solid materials. The signal is converted into an image which appears on the SEM monitor. The signals obtained from the high energy electron interactions provide information about the sample's external morphology, chemical composition, crystalline structure and orientation of materials making up the sample [6, 7].

The blends and composite morphologies were investigated using the TESCAN VEGA 3 scanning electron microscope and Oxford X – MaxN EDS. The samples were coated with carbon in order to ensure that the charge deposited on the surface of the sample by an electron beam is earthed. The examination of the samples took place at an acceleration voltage of 15 kV.

3.3.4 Surface energy evaluation system (SEES)

The surface energy evaluation system, using the sessile drop method, is used to analyse the surface energies of solids and some liquids [8]. The method works by placing a liquid of known surface energy (called the probe liquid) on the surface of the analysed solid sample. This is applicable in analysing solid samples where the contact angles can clearly be determined from the probe liquid. Then the shape of the liquid drop formed, called the contact angle, together with the known surface energy of the probe liquid become the parameters used in determining the solid's surface energy [8-10].

Contact angle measurements were performed at room temperature conditions using distilled water (H_2O) and diiodomethane (CH_2I_2) as non-polar and polar probe liquids respectively. The literature surface energies for H_2O and CH_2I_2 are: H_2O; γ^p = 34.2 mJ / m^2, CH_2I_2; γ^d = 17.8 mJ / m^2. About 10 drops of these liquids were deposited on the samples and contact angles obtained as well as surface energies as averages of at least the 10 deposited drops. Then the Owens-Wendth method was used to determine contact angles, total surface energies as well as the dispersive and polar components of the surface energies following the Equations 2.1 and 2.2

$$\gamma_s = \gamma_s^d + \gamma_s^p \qquad (2.1)$$

$$\gamma_1(1 + \mathrm{Cos}\theta) = 2\sqrt{\gamma_s^d . \gamma_l^d} + 2\sqrt{\gamma_s^p . \gamma_l^p} \qquad (2.2)$$

where θ represents the contact angle, γ is the surface energy, superscripts 'd' and 'p' are dispersive and polar components respectively and subscripts 's' and 'l' represent solid and

liquid components respectively. Then the geometric mean equation was used to calculate the interfacial tensions between the polymeric material and from contact angles as shown by Equation 2.3

$$\gamma_{12} = \gamma_1 + \gamma_2 - 2\left(\sqrt{\gamma_1^{d}.\gamma_2^{d}} + \sqrt{\gamma_1^{p}.\gamma_2^{p}}\right) \quad (2.3)$$

Where γ_{12} is the interfacial tension between component 1 and 2 in the blend, $\gamma_1{}^{d}$ and $\gamma_2{}^{d}$ are the dispersive surface energies of components 1 and 2, and $\gamma_1{}^{p}$ and $\gamma_2{}^{p}$ are the polar surface energies of components 1 and 2 in the blends and composites. Then the wetting coefficient was calculated from the interfacial tensions of PLA/EVA, PLA/GO and EVA/GO using Young's equation

$$\omega_a = \frac{\gamma_{PLA/GO} - \gamma_{EVA/GO}}{\gamma_{PLA/EVA}} \quad (2.4)$$

whereby ω_a is the wetting coefficient, $\gamma_{PLA/GO}$ is the interfacial tension between PLA and GO, $\gamma_{EVA/GO}$ is the interfacial tension between EVA and GO and $\gamma_{PLA/EVA}$ is the interfacial tension between PLA and EVA. If the value of ω_a is greater than 1, then the filler would most likely be dispersed in polymer A (PLA in this case), if it is less than -1 the dispersion is into polymer B (EVA in this case), and if it is between -1 and 1 then the filler would most probably be localised in the interface between the two polymers in the composites.

3.3.5 Melt flow index (MFI)

The melt flow index is a measure of the amount of a polymer (in grams) that flows through a die in 10 minutes. MFI measurements are performed at a specific temperature, depending on the type of polymer used, and the force required to eject the polymer through the system comes from the weight which sits on top of a ram. Then gravity takes over to push the material through the die, after which it is weighed and then the mass determined per 10 minutes. MFI is very crucial in determining the viscosities of the polymer components used. This information allows for conclusions to be drawn regarding morphology and the filler affinity [11].

The MFI analyses were performed to determine the viscosities of the polymers used. This was done using a CEAST Melt Flow Junior, and 10 samples of each polymer were analysed at 170 ℃. About 2.16 kg mass was used and the amount of polymeric material that passed through the die in 10 minutes was weighed.

3.3.6 Differential scanning calorimetry (DSC)

DSC is a thermal analysis technique that focuses on how a material's heat capacity is changed by temperature. In differential scanning calorimetry the sample and reference are subjected to a controlled temperature programme. This is followed by the measurement of the change in the heat flow rate of the sample and the reference. This allows for the detection of thermal transitions such as melts, glass transitions, phase changes and curing. The temperature programme on a DSC analysis is designed such that the sample holder temperature proportionally increases with increasing time, as such, the reference sample must be having a well-defined heat capacity for the range of temperatures scanned [12].

DSC analyses were performed in the Perkin-Elmer, Pyris 6000 Differential scanning calorimeter. Samples (~6.5 mg) were subjected to two heating cycles and one cooling in between with a temperature range from 0 to 180 ℃ for heating and 180 to 0 ℃ for cooling, at a rate of 10 ℃/min. All these were done under a nitrogen atmosphere (20 ml/min). The glass transition, melting and cold crystallization temperatures as well as the enthalpies of the samples were determined from the cooling and second heating runs. The degree of crystallinity was also calculated using Equation 2.5 below

$$X_c = \frac{\Delta H_m}{W \Delta H_m^o} \times 100 \qquad (2.5)$$

where X_c is the degree of crystallinity, ΔH_m^o is the specific enthalpy of melting for 100% crystalline pure polymers (PLA and EVA), ΔH_m is the specific melting enthalpy for a polymer and W is the weight fraction of a polymer in a blend or composite. The ΔH_m^o values used for PLA and EVA were 93.1 J/g and 277 J/g respectively.

3.3.7 Thermogravimetric analysis (TGA)

In thermogravimetric analysis, the thermal properties of a sample are analysed. It measures the weight changes of a material as a function of temperature or time under a controlled atmosphere. The thermal properties analysed include thermal stability, filler content in polymers, moisture and solvent content, and the percentage composition of components in a compound. A typical TGA analysis is performed by gradually raising the temperature of a sample in a furnace whilst its weight is measured on an analytical balance situated outside the furnace. The weight of the sample is then plotted against temperature or time in order to assess thermal transitions of the material such as: loss of solvent and plasticizers in polymers, dehydration and the decomposition of a material. This allows for the thermal degradation properties of a sample to be analysed. [13].

The thermal stability of the neat polymers, blends and composites were analysed in a Perkin-Elmer STA6000 Thermogravimetric analyser. ~23 mg samples were heated from 30 - 600 ℃ under a nitrogen atmosphere (10℃/min) and the mass loss % was recorded for each of the samples

3.3.8 Water absorption test

The water absorption test is a quantitative measurement which determines the degree to which a material absorbs water before it becomes saturated. The degree to which the samples absorbed water is determined by calculating the water absorption degree according to Equation 2.6.

$$R = \frac{W_t - W_i}{W_i} \times 100 \qquad (2.6)$$

where R is the degree of water absorption, w_t is the weight of the sample after a certain time, t, it spent in the distilled water and w_i is the initial sample mass [14].

The pressed films were cut into rectangular shapes of equal sizes and then dried in room temperature overnight to ensure that there is not any moisture absorbed by their structures. The samples were then immersed in 25 ℃ distilled water for up to 30 hours. The masses of the samples were determined prior to being immersed in distilled water and the increase in mass of the samples, i.e. the % water absorbed was determined periodically by removing the samples from the distilled water, wiping it with a paper towel and measuring the mass.

3.3.9 Atomic absorption spectroscopy (AAS)

AAS is a spectroanalytical method used to determine and/or identify chemical elements quantitatively. This is done by using the absorption of light by free atoms n their gaseous form. This technique makes use of absorption spectroscopy to determine the concentration of an analyte in solution. This requires standards having known analyte content to assess the relationship between the measured absorbance and the analyte concentration and therefore relies on the Beer-Lambert law [15].

A Flame atomic absorption spectrometer (GBC 909AA) was used for analysing the adsorption capabilities of the samples. The adsorption experiments proceeded by adding 50 ml of the metal solutions into a 100 ml beaker and then adding 4 cm x 2 cm x 0.2 cm cuts of the previously prepared composites into the solution. Then the whole mixture was stirred by a magnetic stirrer at 150 rpm (As per the stirrer settings) at room temperature for 4 hours. Then filtering took place while taking into consideration to throw away the first 5 ml of the filtrate as filter paper contains cellulose and might absorb some metal ions. Then the atomic absorption spectrophotometer was used to analyse the concentrations of metal ions present in the filtrate. The concentration of the metal ions adsorbed, C_a, was determined using Equation 2.7 which reads:

$$C_a = C_0 - C_e \tag{2.7}$$

where C_0 and C_e are initial and final concentrations (mg/L) of the heavy metals present in the metal solution before and after the adsorption for a time t. C_e is also the concentration heavy metal ions when equilibrium is reached [15], so the percentage heavy metal ions removed was obtained from Equation 2.8 below:

$$R = \frac{C_0 - C_e}{C_0} \tag{2.8}$$

Where R represents the removal efficiency of the adsorbent.

- **Preparation of Pb ion solutions**: Lead ion stock solutions were prepared by dissolving lead nitrate in deionized water as per required concentration. And then the lead aqueous solutions were prepared by dissolving the stock solution with deionized water depending on the required concentration.
- **Effect of pH**: The media of the adsorbent and the adsorbate plays a very important role in adsorption. The hydroxide and hydronium ions present in basic and acidic media respectively, can hinder or promote the process of adsorption. The effect of pH on the adsorption of lead ions was investigated by first preparing 50 µg/ml of lead ions solution. The pH of this solution was adjusted, using NaOH (1M) and HCl (1M) for acidic (pH 3) and basic (pH 12) media. Then 40 g/L of adsorbent was added, the solution agitated for 4 hours at 100 rpm. After agitation the suspension was filtered taking into note to discard the first 5 ml of the filtrate as filter paper contains cellulose which might have been mixed with the solution. Then the metal ion concentration was assessed using AAS.
- **Effect of contact time**: The contact time refers to the amount of time the adsorbate spends in contact with the adsorbent. This affects the degree to which adsorption takes place, and is crucial in adsorption studies. The optimal contact time was determined using 50 µg/ml lead ion solutions. 50 ml of these solutions were adjusted pH is accordance to the optimal pH obtained, and the dosage of adsorbent adjusted in relation to the optimal one obtained. The solutions were agitated at 100 rpm and the contact time was varied from 1 to 4 hours. Then filtering took place, after which lead ion concentration was determined using AAS.
- **Effect of initial concentration:** The initial concentration of the adsorbate can influence the degree to which adsorption takes place. This is usually adjusted to attain the optimal concentration at which adsorption occurs. The effect of initial concentration was investigated by varying the lead ion concentration from 100 to 400 ppm. This was done on the GO powder alone in order to assess the optimal concentration at which it adsorbs and use it for the effect of contact time and pH for the composites. Then agitation took place at 100 rpm, followed by filtration and then determination of lead ion concentration using AAS [15].

3.4 REFERENCES

1. F. Pendolino, N. Armata. Synthesis, characterization and models of graphene oxide. In: F. Pendolino, N. Armata. Graphene Oxide in Environment Remediation Process. Springerbriefs in Applied Science and Technology 2017; 2:5-21.
   DOI: 10.1007/978-3-319-60429-9_2
2. T. A. Makhetha, K. Mpitso, A. S. Luyt. Preparation and characterization of EVA / PLA / Sugarcane bagasse composites for water purification. Journal of Composite Materials 2016; 51:1169-1186.
   DOI: 10.1177/0021998316675399
3. B. Stuart. Infrared Spectroscopy: Fundamentals and Applications. John Wiley and Sons, Chichester (2004).
   ISBN: 9780470011140
4. A. Subramanian, J. Ahn, V. M. Balasubramaniam, L. Roudriguez-Saona. Determination of spore inactivation during thermal and pressure-assisted thermal processing using FT-IR spectroscopy. Journal of Agricultural and Food Chemistry 2006; 54:10300-10306.
   DOI: 10.1021/jf0622174
5. A. Chauhan, P. Chauhan. Powder XRD technique and its applications in science and technology. Journal of Analytical and Bioanalytical Techniques 2014; 5:1-5.
   DOI: 10.4172/2155-9872.1000212
6. C. E. Carraher Jr. Carraher's Polymer Chemistry. 8th Edition, CRC. Press Taylor & Francis Group: Boca Raton (2011).
   ISBN: 9781498737388
7. B. J. Hunt, M. I. James. Polymer characterization. Blackie Academic & Professional. London (1993).
   ISBN: 0-7514-0082-3
8. S - J. Park, M - K. Seo. Chapter 2 - solid - gas interaction. Interface Science and Technology 2011; 18:59-145.
   DOI: 10.1016/B978-0-12-375049-5.00002-5
9. V. Fernandez, M. Khayet. Evaluation of the surface free energy of plant surfaces: Towards standardizing the procedure. Frontiers in Plant Science 2015; 6:1-11.
   DOI: 10.3389/fpls 2015.00510
10. A. R. Balkenenende, H. J. A. P. van de Boogaard, M. Scholten, N. P. Willard. Evaluation of different approaches to assess the surface tension of low - energy solids by means of contact angle measurements. Langmuir 1998; 74:5907-5912.

DOI: 10.1021/la9801110

11. J. K. Fink. 17 - Rheology control. In J.K Fink, Reactive Polymers: Fundamentals and Applications. William Andrew Applied Science Publishers 2018; 3:547-562.
    DOI: 10.1016/B978-0-12-814509-8.00017-8
12. M. J. O' Neil. The analysis of a temperature-controlled scanning calorimeter. Analytical Chemistry 1964; 36:1238-1245.
    DOI: 10.1021/ac60213a020
13. R. B. Prime, H. E. Bair, S. Vyazovkin, P. K. Gallagher, A. Riga. Thermogravimetric analysis (TGA). In: J. D. Menczel, R. B. Prime. Thermal analysis of polymers fundamentals and applications. John Wiley and Sons: New York City (2009).
    ISBN 978-0-471-76917-0
14. G. Czel, T. Czicany. A study of water adsorption and mechanical properties of glass fibre/polyester composite pipes – effects of specimen geometry and preparation. Journal of Composite Materials 2008; 42:2815-2827.
    DOI: 10.1177/0021998308096668
15. N. Ariffin, M. Mustafa, A. B. Abdullah, M. R. Zaimol, M. F. Murshed, H. Zain, M. A. Faris, R. Bayuaji. Review on water adsorption of heavy metal in wastewater using geopolymer. MATEC Web of Conferences 2017; 97:1-8.
    DOI: 10.1051/matecconf/20179701023

CHAPTER 4

RESULTS AND DISCUSSION

This chapter presents findings and interpretations of this study. These follow the following chronological order: the functionalization of expandable graphite to graphene oxide, the morphology, surface energy analysis, thermal studies, water absorption and metal ion adsorption, of all the prepared samples.

4.1 FUNCTIONALIZATION OF EXPANDABLE GRAPHITE (EG) TO GRAPHENE OXIDE (GO)

4.1.1 The use of Fourier transform infrared spectroscopy (FTIR) to verify functionalization of EG to GO

Infrared spectroscopy is very crucial in terms of identifying the functional groups present in a given material, especially after chemical treatment. FTIR was used to verify the successful functionalization of EG to GO. This was done by comparing the FTIR spectra of EG (a) and GO (b) in Figure 4.1. The spectra of EG (Figure 4.1 (a)) showed three distinctive peaks. The first peak, occurring around 3060 cm^{-1}, represents the hydroxyl group (-O-H-). This broad peak is due to the moisture that might have been trapped in the EG powder. At 2075 cm^{-1}, a very sharp peak was observed. This represents the -C-H- bending in the cyclic structure of EG. The -C=C- stretching was observed at 1530 cm^{-1} for the conjugated structure of graphite. Then for GO (Figure 4.1 (b)) there were a number of newly added peaks as compared to the EG spectrum. The peak observed between 3000 and 3400 cm^{-1} is a broad peak, which corresponds to the hydroxyl (-O-H) stretching of the absorbed water molecules as well as of the present hydroxyl (-O-H) group. There was a peak registered at 2821 cm^{-1} which represents the symmetric -CH_2- stretching of GO. The stretching of -C=C- for the transition from unoxidized EG to oxidized GO is depicted by the peak at 2821 cm^{-1}. This peak also validated the aromatic ring present on the backbone of GO through the –C=C- presence. Then there were peaks registered at 1729 and 1144 cm^{-1}, which represent the -C=O and -C-OH stretching in GO respectively. This is indicative of the presence of a carboxyl group (-COOH) in GO. The successful attachment of the ester group (-C-O-C-) was validated through the peak registered at 1029 cm^{-1} that represents the stretching of the ester group. Then the peak at 869 cm^{-1} that of the C-H stretching. The observed spectrum for GO is the same as one which was obtained by

Zhong *et al* [1]. The authors concluded that it is impossible to completely remove water from GO. This was attributed to the fact that GO absorbs water from the surroundings. Therefore, this justifies the broad (-O-H) peak as well as the incompletely dry GO obtained. FTIR results were adequate to assume that GO had been successfully synthesized from EG.

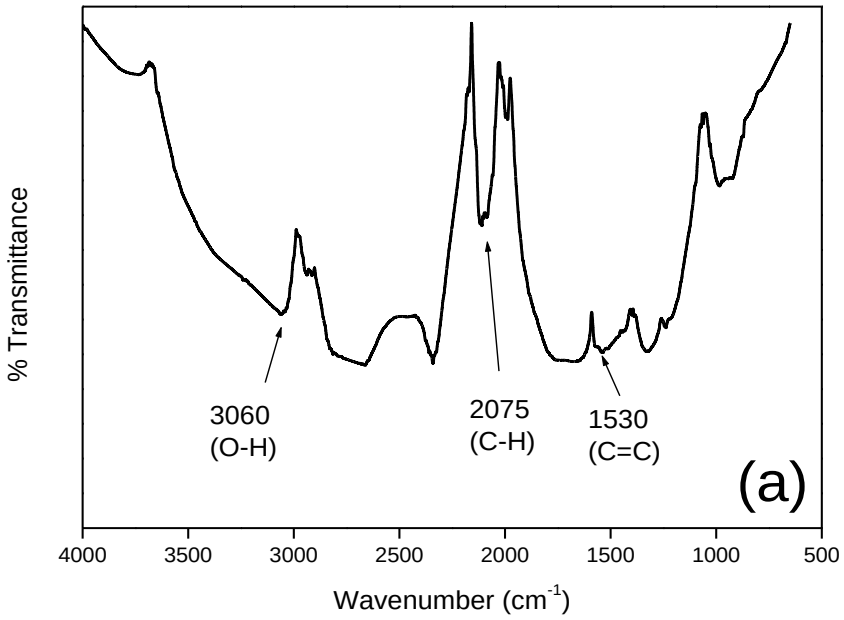

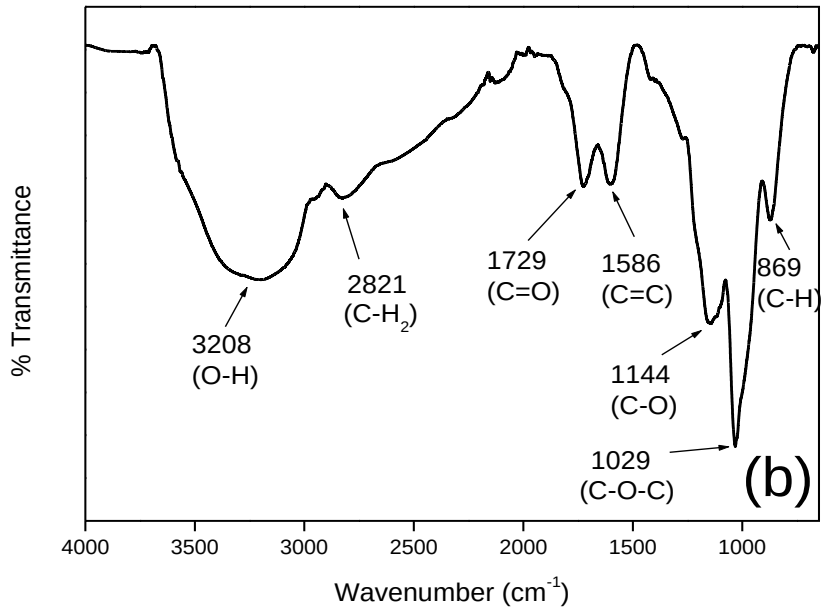

Figure 4.1: FTIR spectra of: (a) EG and (b) GO showing conversion of EG to GO.

4.1.2 X-ray diffraction (XRD) analyses to verify GO synthesis from EG

The identification of chemical components presents in a material, especially one that is crystalline, gives great insight into its chemical composition. This further helps to deduce, in case of a chemically synthesized/treated material, if the treatment was successful or not. XRD analysis was used to further characterize the prepared graphene oxide in order to verify the successful functionalization of expandable graphite to graphene oxide. In Figure 4.2, the diffractograms of expandable graphite flakes (a) as well as graphene oxide (b) are shown. The diffractogram of expandable graphite (Figure 4.2 (a)) showed a sharp peak at 25.66 º, which gave a calculated interlayer spacing (distance between two parallel atomic layers/planes, from Bragg's law) of d_{002} = 0.347 nm. This is typical for graphite and indicates a highly ordered structure. The flaky nature of the graphite used resulted in a diffractogram exhibiting a fibre-like texture with all the flakes having a c-axis orientation. This is shown by the presence of the other 004 (55.42 º) and 006 (87.07 º) peaks. Then for graphene oxide (Figure 4.2 (b)), the defining peak was observed at 7.5 º, which gave a calculated interlayer spacing of 1.18 nm. This peak was introduced with the functionalization of EG to GO as it was not present on the EG diffractogram. This newly added peak suggested the addition of oxygen containing functional groups to EG as well as the intercalation of water molecules during the functionalization. There were other peaks observed at around 25.87 º and 42.01 º for the diffractogram of GO. These were due to unoxidized graphite sections and the formation of disordered components during the chemical processing of graphite, as they were also present in the EG diffractogram. Johra *et al* [2], also observed a newly added peak for GO after functionalizing graphite powder. The authors discovered that the interlayer spacing had also increased (from 0.336 nm for graphite to 0.833 nm for GO). They went on to reiterate that the increased interlayer spacing in GO is due to the oxygen-containing functional groups being added specifically to the edges of each layer. These observations coincide with the ones obtained in this study. As such, XRD also validated the assumption that GO had been successfully synthesized from EG.

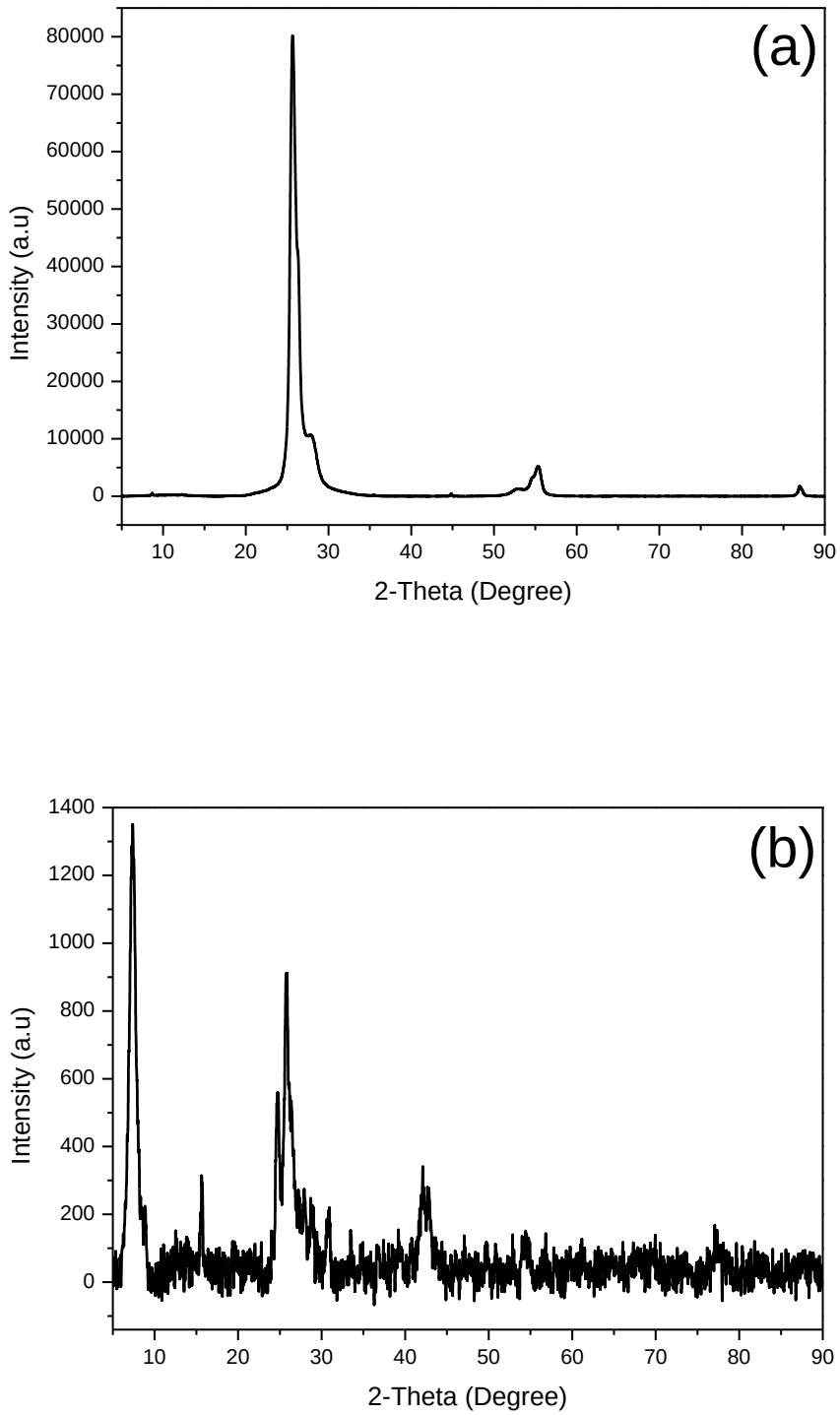

Figure 4.2: XRD patterns of (a) expandable graphite and (b) graphene oxide.

4.1.3 Scanning electron microscopy-Energy dispersive spectroscopy (SEM-EDS) analyses of EG and GO

The morphology and elemental analysis of a prepared inorganic material helps a lot in deducing the physical structure of the material, as well as its behaviour when blended with other components (polymers). Figure 4.3 shows the SEM images obtained from analysing expandable graphite at 60 × magnification (a) and graphene oxide using different magnifications ((b), (c) and (d)). The expandable graphite (a) appeared as loose flakes, which vary in size from 100 to 500 µm. The flakes appeared to have smooth surfaces and upper layers as is depicted by their shininess to some extent. The observed varying sizes of EG flakes are shown by arrow A. Then Figure 4.3 (b) is the image of graphene oxide at 60 × magnification. Here the flaky nature of graphite was still visible, however the flakes had been exfoliated, as was the intent with chemical treatment, which is shown by the rough surface of the flake on which arrow B points. The lateral sizes of the flakes for GO still had the range 100 to 500 µm, but the exfoliation seemed to have reduced their breadth and height dimensions. The flakes appeared to be less ordered than those in EG, which could still be due to the chemical treatment leading to disorder. Zooming into the GO gave a clear picture of the layered structure of GO. In Figure 4.3 (c), 500 × magnification was used and in Figure 4.3 (d), a 1000 × magnification was used. Both these images showed that GO comprises of layers, and this was expected as it was also stated in literature. The arrows C and D point to the layered arrangements of GO. These SEM images for GO are similar to those obtained by Bhawal *et al* [3], in analysing the SEM of graphite and graphene oxide. The authors also observed chemically exfoliated flakes of GO. They went on to observe that the graphite flakes seemed to be more ordered and similar sized than the disordered and unequally sized GO flakes. The disorder and agglomeration in the graphene oxide flakes was attributed to the addition of oxygen containing functional groups on the edges and surfaces of graphene oxide. SEM analysis of GO and EG validated the presence of layers in GO structure, and that chemical exfoliation takes place upon functionalizing EG to GO.

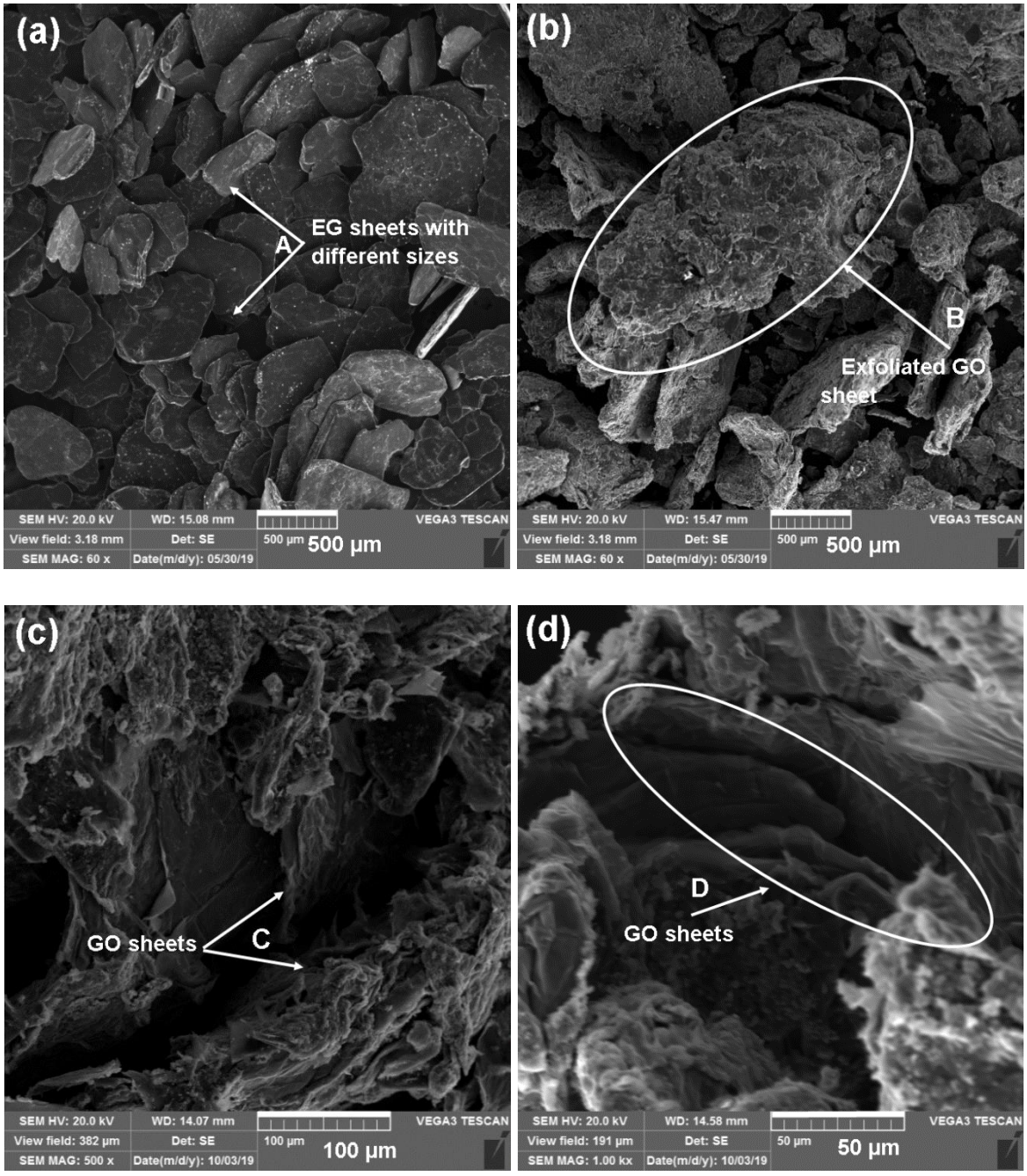

Figure 4.3: SEM images of (a) EG (60 × magnification), (b) GO (60 × Magnification), (c) GO (500 × magnification) and (d) GO (1000 × magnification).

The EDS part of SEM analysis was used, through elemental analysis, as a means of validating the successful functionalization of EG to GO. In Figure 4.4, the EDS spectra of expandable graphite (a) as well as graphene oxide (b) are shown. The spectra for EG clearly showed a very low content of oxygen (12.3%) and a very high content of carbon (83.0%). This was expected as graphite consists entirely of carbon. There were also insignificant impurities on the spectra

because of the expandable graphite grade utilized. When we compared the spectra for EG and GO, it was observed that the oxygen content from EG to GO had significantly increased from 12.3% to 39.4%. This drastic increase in oxygen content validated the successful attachment of oxygen containing functional groups to expandable graphite. SEM-EDS analysis also provided enough proof to assume that GO was successfully synthesized from EG for this study.

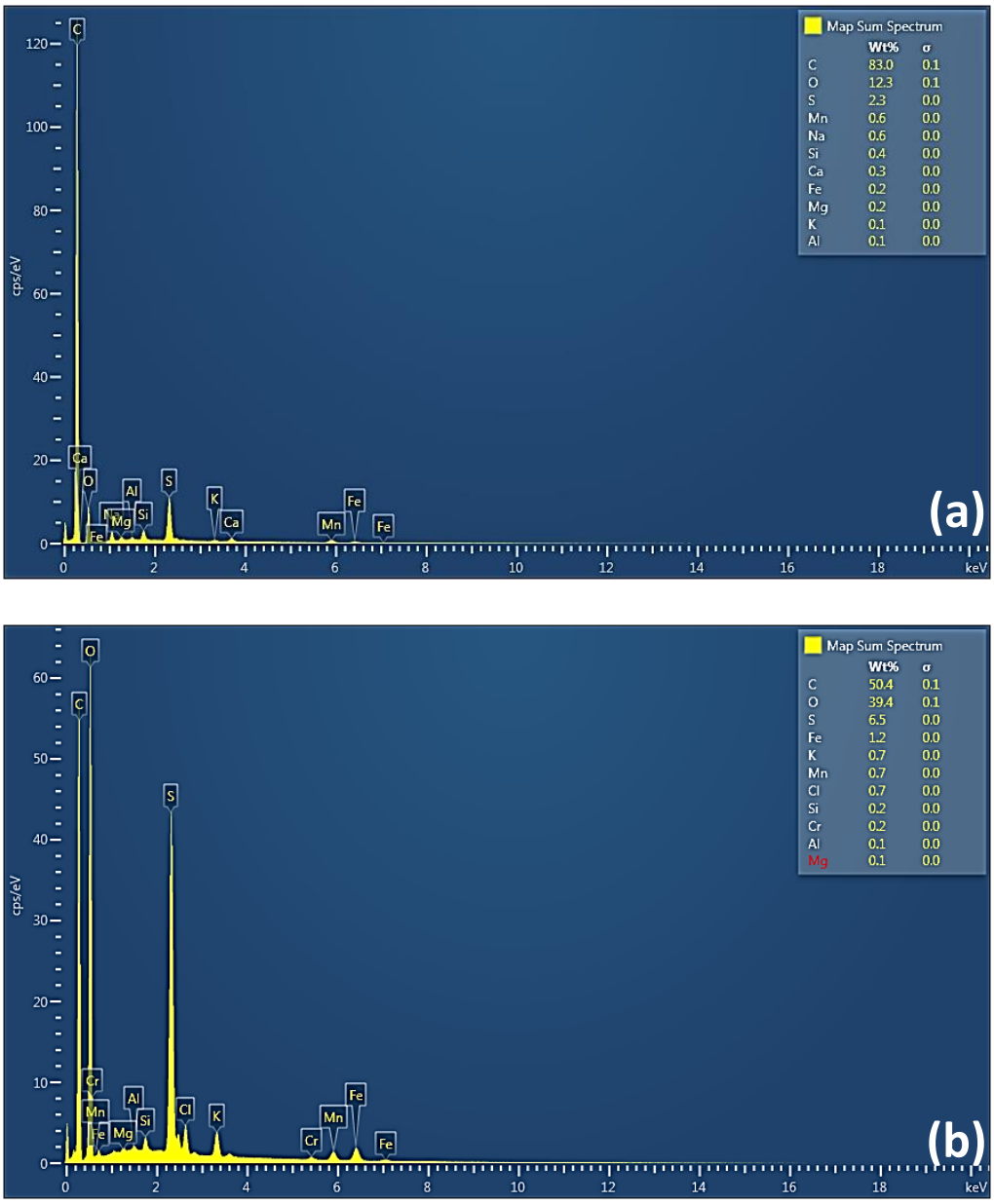

Figure 4.4: SEM-EDS spectra of (a) EG and GO (b).

4.2 MORPHOLOGY OF THE PREPARED PLA/EVA W/W BLENDS AND BLEND COMPOSITES

4.2.1 Morphology of the prepared blends and blend composites using Scanning electron microscopy (SEM)

SEM was used to study the morphology of the prepared blends and composites as well as to determine the different phases in the prepared samples and their adhesion, if any. It was also used to analyse the prepared graphene oxide's morphology as it has already been shown in the functionalization of EG to GO. The prepared blends and composites were analysed using SEM for their morphology at 200, 500 and 1000 × magnification. In Figure 4.5 the images for the blends and blend composites of ratio 70/30 w/w PLA/EVA and different loadings of GO are shown. The 70/30 w/w PLA/EVA blend (Figure 4.5 (a)) clearly shows phase separation, whereby PLA is the continuous phase and EVA is the dispersed phase. Upon adding 1 wt.% of GO to the blend (Figure 4.5(b)), it was observed that it had settled in the interface of the two polymers. Arrow A depicts the location of GO on the interface of the polymers at this composition. As the GO loading was increased (3 – 5 wt.%), it generally seemed to have dispersed within the blend and embedded into the matrices. There were also small gaps on the interfaces and cracks (arrows B and C) on the polymer phases visibly seen. Increasing GO content seems to have merged the two polymers in the blend, as phases could no longer be distinguished. This implied that GO might have had a compatibility effect on the two polymer matrices at those high loadings. Although cracks and gaps normally imply a weak interface, for water absorption and adsorption they might be of great importance. They may allow water to enter the polymeric material during absorption, as pores are one way in which water enters into a polymeric material (As shown further into the study in section 4.5).

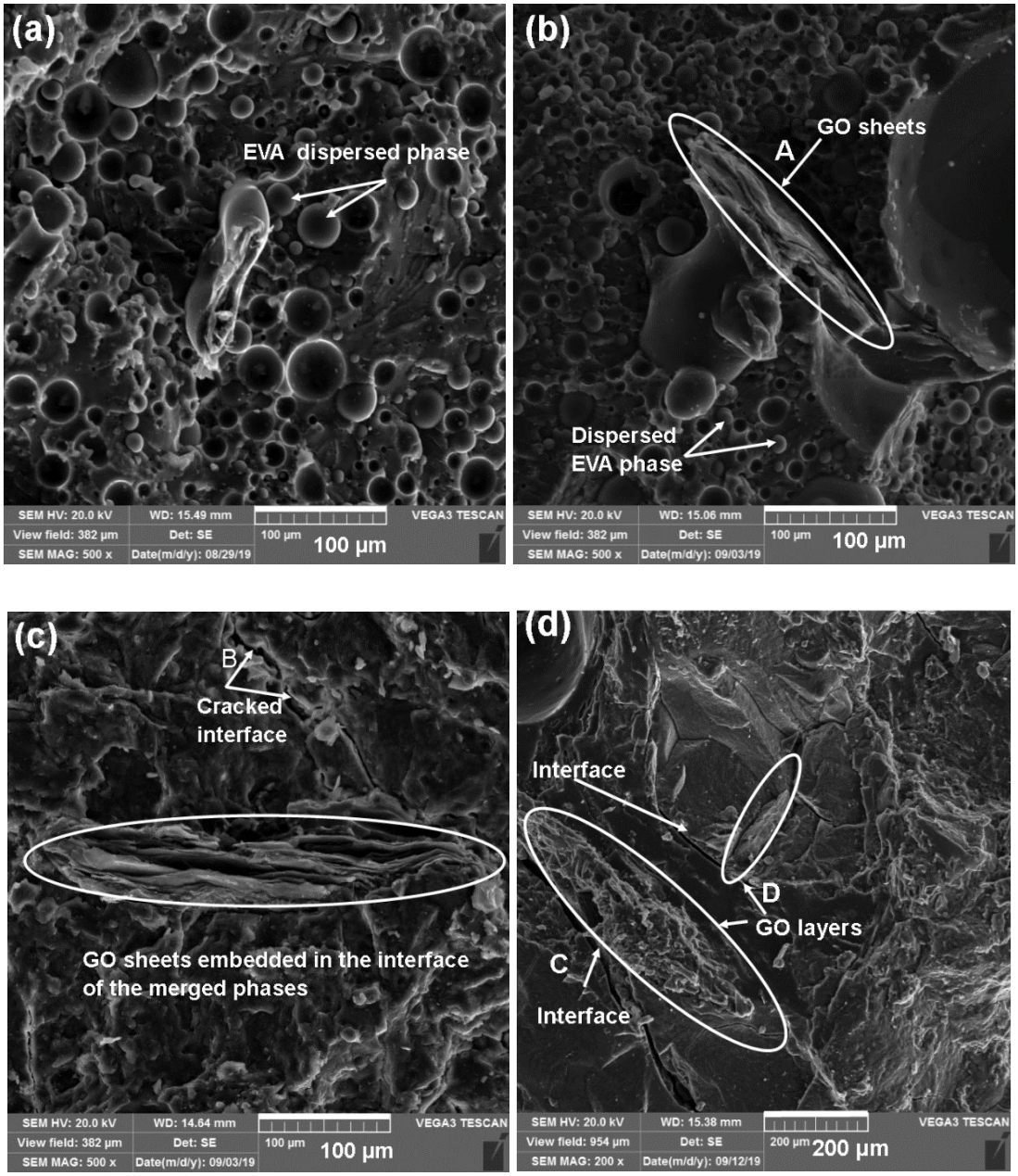
(a)
EVA dispersed phase
SEM HV: 20.0 kV
WD: 15.49 mm
VEGA3 TESCAN
View field: 382 µm
Det: SE
100 µm
SEM MAG: 500 x
Date(m/d/y): 08/29/19
100 µm
(b)
GO sheets
A
Dispersed
EVA phase
SEM HV: 20.0 kV
WD: 15.06 mm
VEGA3 TESCAN
View field: 382 µm
Det: SE
100 µm
SEM MAG: 500 x
Date(m/d/y): 09/03/19
100 µm
(c)
B
Cracked
interface
GO sheets embedded in the interface
of the merged phases
SEM HV: 20.0 kV
WD: 14.64 mm
VEGA3 TESCAN
View field: 382 µm
Det: SE
100 µm
SEM MAG: 500 x
Date(m/d/y): 09/03/19
100 µm
(d)
Interface
D
GO layers
C
Interface
SEM HV: 20.0 kV
WD: 15.38 mm
VEGA3 TESCAN
View field: 954 µm
Det: SE
200 µm
SEM MAG: 200 x
Date(m/d/y): 09/12/19
200 µm

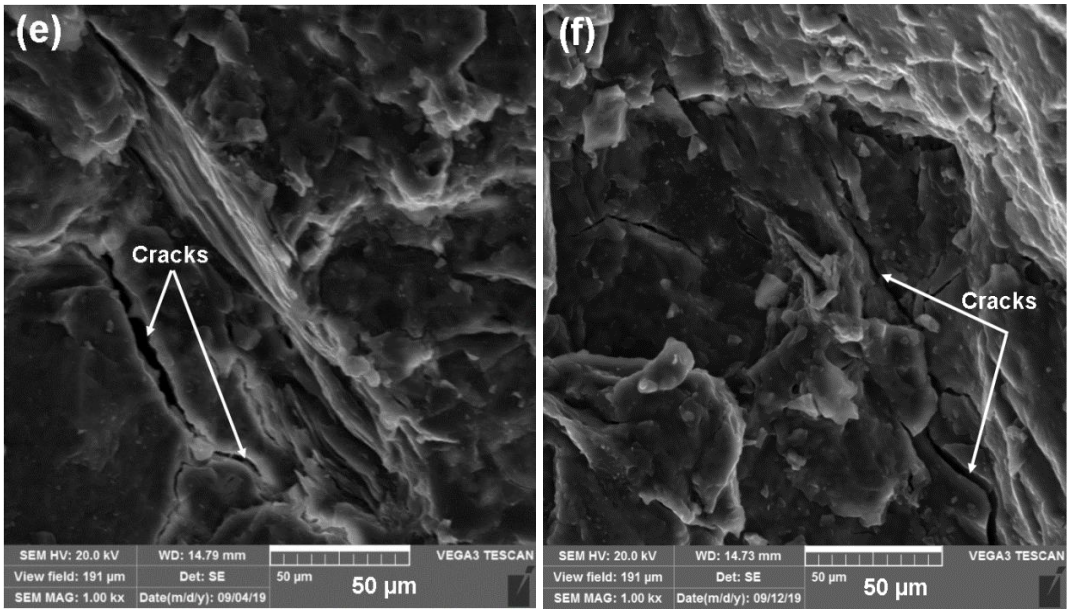

Figure 4.5: SEM images for blends and composites of rations; (a) 70/30 w/w PLA/EVA, (b) 69.3/29.7/1 w/w PLA/EVA/GO, (c) 67.9/29.1/3 w/w PLA/EVA/GO, (d) 66.5/28.5/5 w/w PLA/EVA/GO, (e) 67.9/29.1/3 w/w PLA/EVA/GO and (f) 66.5/28.5/5 w/w PLA/EVA/GO at 200, 500 and 1000 x magnifications.

Figure 4.6 shows the images for blends and composites of ration 50/50 w/w PLA/EVA with different loadings of GO (1, 3 and 5 wt.%). In the 50/50 w/w PLA/EVA blend (Figure 4.6 (a)), a co-continuous morphology was observed and it was generally hard to distinguish phases. The interface adhesion was seen to be very strong as there were no gaps between the two phases besides the breakage that might have happened during the fracturing impact. This is a sign that miscibility between the two polymers might have improved, which could have been due to the balancing of polymeric rations with complementary properties. During all GO loadings (1, 3 and 5 wt.%), it appeared to be more embedded into the polymers, with no visible cracks or gaps. These observations indicated that there was a strong interaction between GO and the polymers in the blend, although it was hard to see the exact GO localization due to co-continuity. This further confirms possible miscibility of the polymers indicated above, for the neat blend. Arrows A and B (for emphasis) show the embeddedness of GO deep into the polymer matrices for 3 and 5 wt.% GO loadings respectively, thereby illustrating a good adhesion of the components. The GO layers were clearly defined and open, indicating once more the proper functionalization of EG to GO.

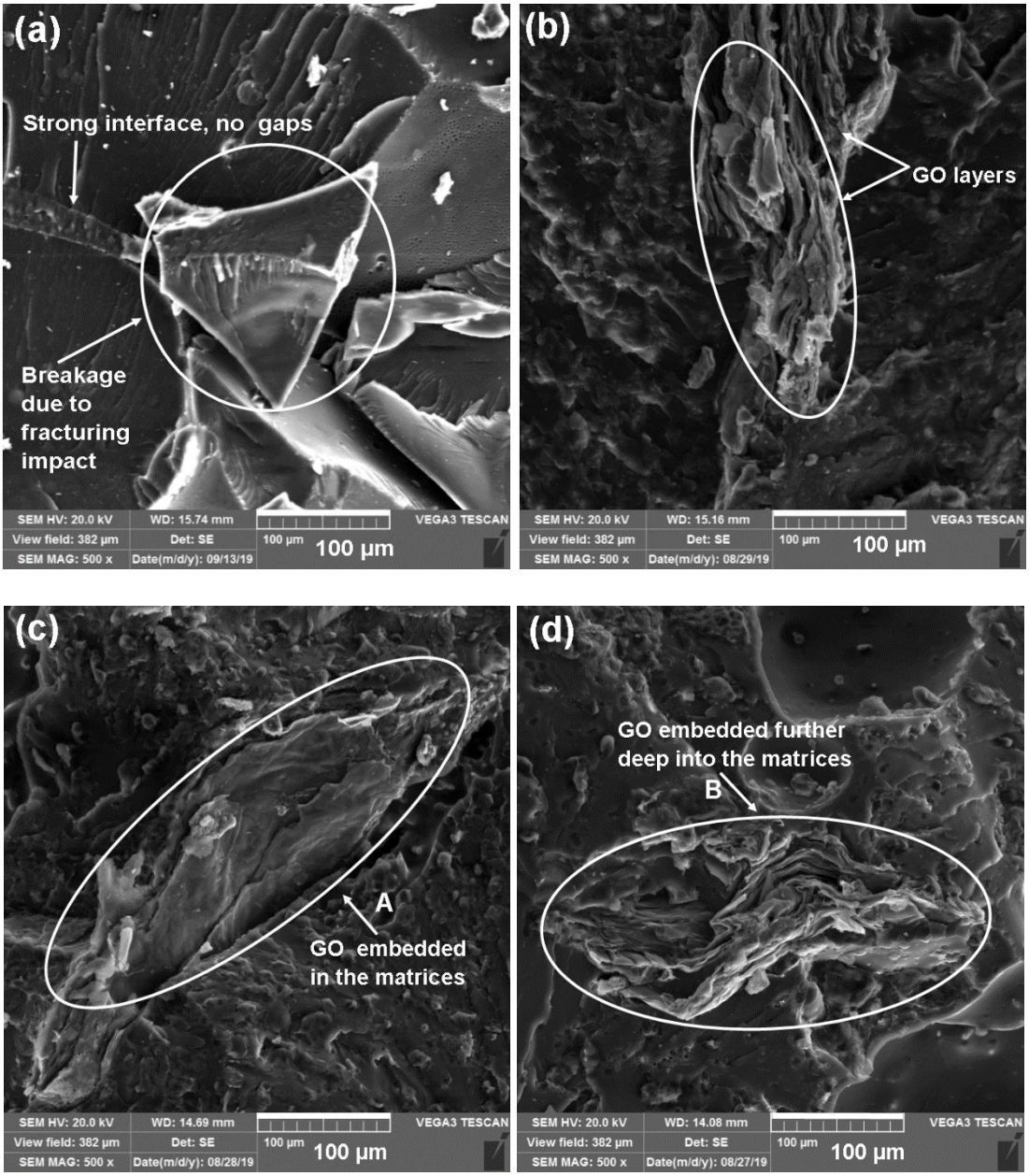

Figure 4.6: SEM images for blends and composites of rations; (a) 50/50 w/w PLA/EVA, (b) 49.5/49.5/1 w/w PLA/EVA/GO, (c) 48.5/48.5/3 w/w PLA/EVA/GO, and (d) 47.5/47.5/5 w/w PLA/EVA/GO at 500 x magnification.

Figure 4.7 displays SEM images of 30/70 w/w PLA/EVA and different GO loadings (1, 3 and 5 wt.%). This blend (Figure 4.7(a)), like the 70/30 w/w PLA/EVA above, clearly indicates phase separation. PLA was the dispersed phase with visible globules (arrows A) and EVA the continuous phase. As the GO was added (1, 3 and 5 wt.%), it seemed to have been embedded into the polymers, visible in sheeted form, and localized on the interface between the two

polymers (Figure 4.7 (b)). There were no visible gaps on the interface between the two polymers, and no cracks on the polymers as opposed to the small gaps and cracks observed on the 70/30 w/w PLA/EVA composition. This served as a confirmation that the cracks on the 70/30 w/w PLA/EVA above were as a result of the brittle PLA at a higher content (70 wt.%). Also, this suggested once more the compatibilization effect the addition of GO had on the two polymer phases. Furthermore, the embedded GO noticeably showed separated layers, which still proves the successful functionalization of EG to GO.

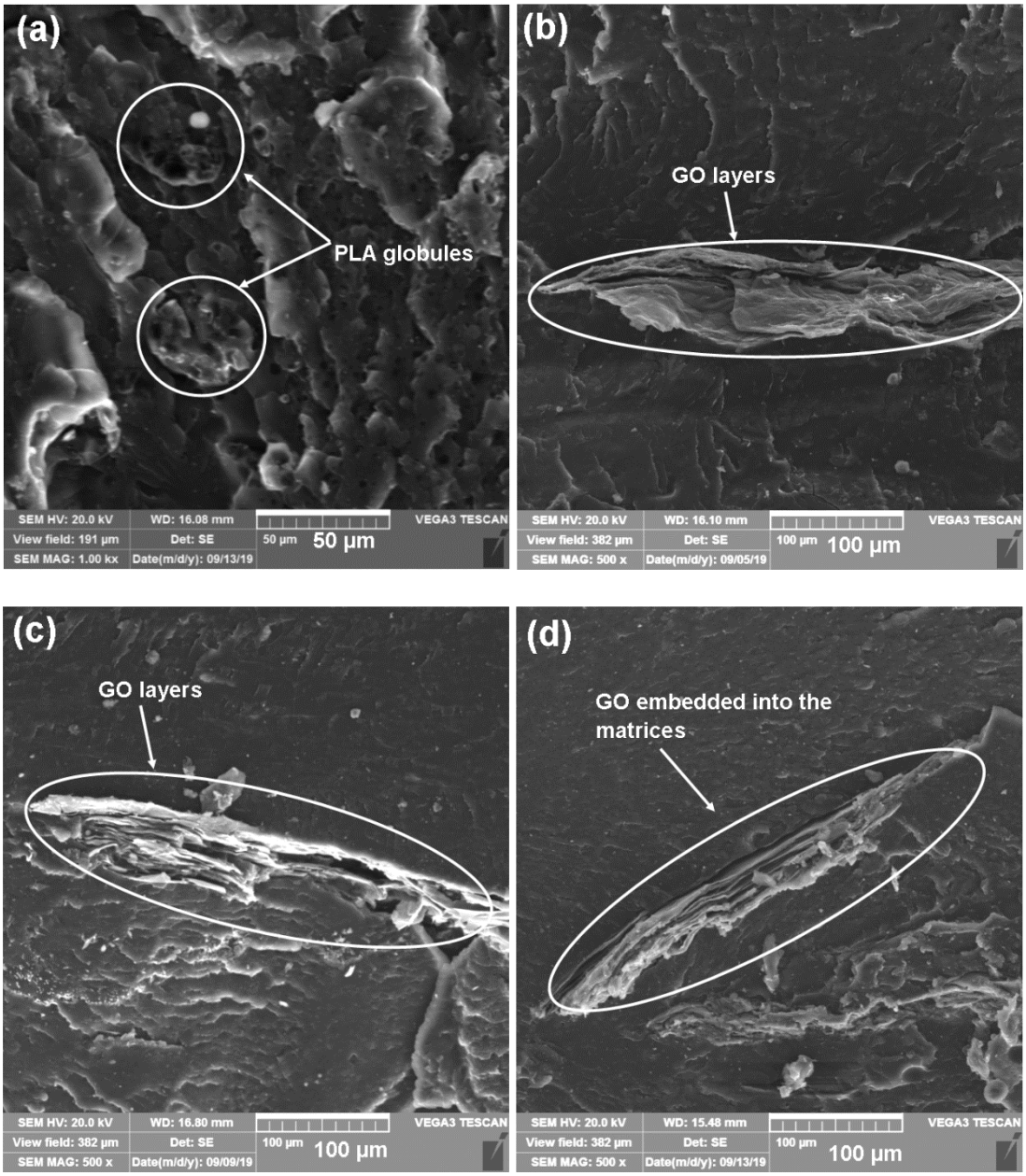

Figure 4.7: SEM images for blends and composites of rations; (a) 30/70 w/w PLA/EVA, (b) 29.7/69.3/1 w/w PLA/EVA/GO, (c) 29.1/67.9/3 w/w PLA/EVA/GO, and (d) 28.5/66.5/5 w/w PLA/EVA/GO at 500 and 1000 x magnifications.

4.3 GO LOCALIZATION IN THE POLYMER MATRICES

4.3.1 Surface energy evaluation system (SEES) and melt flow index (MFI)

The dispersion of a filler / adsorbent in a polymer matrix plays a very important role in the property control and overall morphological structure of a polymer composite system. The filler / adsorbent will selectively locate itself in a polymer system in order to attain a balanced state of flow / viscosity (melt flow index (MFI)) and thermodynamic properties (Surface properties). These two properties play a big role in assessing how the filler / adsorbent could localize in a polymer matrix. Table 4.1 depicts a summary of the melt flow indices (MFI), and surface properties (contact angles and surface energies), of the polymers used (PLA and EVA), GO and PLA/EVA/GO w/w composites with the highest GO content (5 wt.%). The contact angle values as well as surface energies for GO were obtained from literature [4]. The MFI of PLA was determined to be 2.64 g/10 min, and that one for EVA was 0.500 g/10 min. It was obvious that PLA had a higher MFI value than EVA. This clearly indicates that EVA has a higher viscosity than PLA, that is, PLA flows more easily than EVA does. These results will aid in discussing other techniques at a later stage.

The contact angles for PLA were 61.7 º ± 0.3 for H_2O and 34.9 º ± 0.4 for CH_2I_2, and the ones for EVA were 63.9 º ± 0.3 for H_2O and 36.7 º ± 0.3 for CH_2I_2. While, the ones for GO were 28.6 º for H_2O and 38.5 º for CH_2I_2. All these values were less than 90 º, implying that PLA and EVA are somewhat hydrophilic, with GO being the most hydrophilic. This was confirmed by literature, which suggests that materials having contact angles less than 90 º are generally hydrophilic [5]. Although other researchers have stated PLA to be hydrophobic, Mofokeng *et al* [6], in comparing injection moulded natural fibre reinforced composites with PP and PLA as matrices, demonstrated that PLA indeed is hydrophilic and biodegrades through hydrolysis, with temperature playing a major role. The contact angles for PLA and EVA were similar, clearly showing similar wettability properties and hydrophilicity. Going forward, the contact angles for 5 wt.% GO composites were: 30.1 º ± 1.01 for H_2O and 35.1 º ± 0.82 for CH_2I_2 for 66.5/28.5/5 w/w PLA/EVA/GO, 55.5 º ± 0.58 for H_2O and 32.3º ± 0.76 for CH_2I_2 for 47.5/47.5/5 w/w PLA/EVA/GO, and 62.4 º ± 0.47 for H_2O and 40.5 º ± 0.30 for CH_2I_2 for 28.5/66.5/5 w/w PLA/EVA/GO. For composites it was visible that all the contact angles for water were less than the ones of the pure samples (PLA, EVA and GO). This generally proposed that all these composites were somewhat more hydrophilic than the pure samples, due to the more hydrophilic GO. Amongst the composites, the one at a high content of PLA

(70 wt.%) had the lowest contact angle for water (30.1 °), while the one at a high content of EVA (70 wt.%) had a water contact angle around the one of the polymers (62.4 °). These results indicated that there is a good wettability for the 66.5/28.5/5 w/w PLA/EVA/GO composite as compared to the other composites. With all these observations, it was confirmed that there is a possibility that water could penetrate the composite easily (high water permeability). This would probably be through the cracks on the phases, and the small gaps on the interface observed in SEM results above for this blend composite. This was further validated in literature that cracks and gaps generally result in increased water permeability [7,8].

PLA, EVA, and GO had total surface energy (γ) values of 52.8, 51.1, and 43.8 mJ/m^2 respectively. The values for PLA and EVA were similar, which indicates that they both somewhat had the same surface properties, while the value for GO was lower. The dispersive surface energies ($\boldsymbol{\gamma^d}$) were: 42.1, 41.2 and 32.2 mJ/m^2, while the polar surface energies ($\boldsymbol{\gamma^p}$) were: 10.7, 9.87 and 11.6 mJ/m^2 for PLA, EVA and GO respectively. According to literature, the polar characters of surface free energies of materials play a major role in facilitating localization of the fillers and compatibility thereof. Varying polar surface free energies of the components involved in a material result in a high tension between the components and effects increased incompatibility, but similar polar surface free energies yield a reduced tension and improved compatibility of the components [9,10]. The polar surface free energies of all the components stated above showed to be similar. As such, this was an indication that the three components might interact easily, with the possibility for a low surface tension and improved compatibility.

The obtained total surface free energies (γ) for composites with 5 wt.% GO were: 69.7, 56.8 and 63.3 mJ/m^2 for 66.5/28.5/5, 47.5/47.5/5 and 28.5/66.5/5 w/w PLA/EVA/GO composites respectively. Literature suggests that an increase in the total surface free energy of a material indicates a strong interaction of the components of the material and of a material's surface with the probe liquid [11]. The total surface free energies of all the blends composites were significantly higher than those of the individual components before blending (PLA, EVA, and GO). This is an indication that the resulting blends composites have a strong interaction, which might lead to improved compatibility. This was emphasized by the assumption made above on polar surface free energy characters of the components, which suggested possible improved compatibility. Then comparing the composites, it was clearly visible that the 66.5/28.5/5 w/w PLA/EVA/GO composite had the highest total surface free energy (69.7 m.J/m^2) amongst all.

This correlates to its contact angle which was the smallest of the composites (30.1°) for water, indicating a strong interaction between the surface and the probe liquid.

The surface energies were used to calculate the interfacial tensions between PLA and EVA, PLA and GO as well as EVA and GO. The calculated interfacial tensions, as well as the wetting coefficient values are displayed in Table 4.2. From the table it can be seen that the tensions were: 0.052, 0.681 and 0.654 mJ/m^2 for the PLA/EVA, PLA/GO and EVA/GO component couples respectively. The interfacial tension between PLA and EVA was clearly the smallest (0.052 mJ/m^2). This observation suggested that the adhesive forces between PLA and EVA were strong, and thus mixing the polymers would result in a higher degree of cohesion. This would further imply that mixing the two polymers might result in their compatibility, although maybe partially miscible, as was suggested by SEM. Comparing the polymers with the adsorbent (GO), it was found that the interfacial tension between PLA and GO (0.681 mJ/m^2), and the one between EVA and GO (0.654 mJ/m^2) were practically similar, with a little variation. The percentage difference between the tension of EVA/GO and PLA/GO was 4.1%, and this is not a high margin. As such, it was safe to deduce from these values that GO had a 50/50 chance of dispersing in both the polymer phases, or even on the interface. This could account for the observed affinity of GO with both the polymer phases and their interface that was observed in SEM. The value of the wetting coefficient obtained was 0.523, which clearly lies between -1 and 1, implying that GO might have been localized on the interphase of the two polymers PLA and EVA, though interfacial tensions and SEM results suggested that it can disperse in both the polymer phases and the interface.

Table 4.1: MFI and surface properties of PLA, EVA and GO (GO values obtained from literature).

Sample	Contact angle / °		Surface energy / mJ/m^2			MFI / g/10 min
	H_2O	CH_2I_2	γ	γ^d	γ^p	
PLA	61.7 º ± 0.3	34.9 º ± 0.4	52.8	42.1	10.7	2.64
EVA	63.9 º ± 0.4	36.7 º ± 0.3	51.1	41.2	9.87	0.500
GO [4]	28.6	38.5	43.8	32.2	11.6	-
66.5/28.5/5 w/w PLA/EVA/GO	30.1 º ± 1.0	35.1 º ± 0.8	69.7	42.0	27.8	-
47.5/47.5/5 w/w PLA/EVA/GO	55.5 º ± 0.6	32.3 ±0.8	56.8	28.8	28.0	-
28.5/66.5/5 w/w PLA/EVA/GO	62.4 º ± 0.5	40.5 ± 0.3	63.3	33.0	30.3	-

γ – Total surface energy, γ^p- polar component of surface energy, γ^d- dispersive component of surface energy, MFI – melt flow index, °-Degrees

Table 4.2: Interfacial tensions and wetting coefficient of the analysed samples.

Component couple	Interfacial tension / mJ/m^2
PLA/EVA	0.052
PLA/GO	0.681
EVA/GO	0.654
ω_α	0.523

ω_α – wetting coefficient

4.4 THERMAL ANALYSIS OF NEAT POLYMERS, THEIR BLENDS AND BLEND COMPOSITES WITH GO

4.4.1 Differential scanning calorimetry (DSC)

The thermal analysis of a polymer blend system plays a very crucial role in understanding the dynamics of mixing. The transitions obtained during analysis indicate clearly the thermal properties of the materials and help in deciding where the materials will be applied. The thermal behaviour of all prepared samples was characterized using DSC. Tables 4.3 and 4.4 give a summary of peak temperature transitions, their resulting enthalpies as well as the calculated degrees of crystallinity for PLA and EVA respectively. In Figure 4.8 DSC heating curves are presented for PLA, EVA, their blends and composites with 1, 3 and 5 wt.% GO loadings of compositions: 70/30 w/w PLA/EVA (a), 50/50 w/w PLA/EVA (b) and 30/70 w/w PLA/EVA (c). Upon heating, PLA displayed three transition temperatures (Figure 4.8 (a)), which were: (i) the glass transition (T_g) at 61.7 ℃, (ii) cold crystallization (T_{cc}) at 114.3 ℃ and the melting (T_m) at 149.1 ℃. While EVA showed a side shoulder and the main melting peak at 66.3 and 97.9 ℃, respectively. The glass transition of PLA clearly indicates that PLA has amorphous fractions in it. The cold crystallization exotherm of PLA was due to its re-crystallization process during heating. That is, PLA solidifies very quickly during the cooling period, that it bypasses the crystallization process, and recrystallize during melting right after T_g, and just below T_m. PLA had a single melting peak, which was indicative of the homogenous nucleation process taking place in the neat PLA. This means that PLA had an α - crystalline arrangement, that is a uniform arrangement of crystals consisting mainly of the same size. As for the melting of EVA, the clear kink before the actual melting peak was due to the melting of the vinyl acetate group (VA), as EVA is a copolymer of vinyl acetate and polyethylene (PE). The calculated degree of crystallinity for PLA was 21.1 % (Table 4.3), and that of EVA 18.0 % (Table 4.4). This clearly meant that the two polymers do not differ that much in terms of their crystallinity and this agrees with SEES results that indicated similar surface properties for these two polymers.

Table 4.3: DSC data for PLA in the blends and blends composites.

Sample	T_g / °C	T_{cc} / °C	ΔH_{cc} / J/g	T_m / °C	ΔH_m / J/g	X_c / %	Difference ($T_{m,PLA}$-$T_{m,EVA}$) / °C
PLA	62.0 ± 0.0	114.3 ± 0.1	13.9 ± 1.3	149.1 ± 0.0	19.7 ± 0.4	21.1	-
70/30 w/w PLA/EVA	62.6 ± 0.3	-	-	152.0 ± 0.5	0.7 ± 0.1	1.1	54.1
69.3/29.7/1 w/w PLA/EVA/GO	61.0 ± 0.2	130.0 ± 0.9	-3.6 ± 0.6	151.8 ± 0.3	5.0 ± 0.9	7.7	54.7
67.9/29.1/3 w/w PLA/EVA/GO	49.9 ± 2.5	111.0 ± 1.1	-20.4 ± 2.5	144.0 ± 1.7	11.9 ± 3.1	18.8	-
66.5/28.5/5 w/w PLA/EVA/GO	46.7 ± 1.0	109.13 ± 0.4	-12.8 ± 1.9	142.2 ± 0.6	8.3 ± 7.3	13.4	-
50/50 w/w PLA/EVA	62.3 ± 0.2	-	-	151.1 ± 0.3	0.5 ± 0.2	1.2	53.0
49.5/49.5/1 w/w PLA/EVA/GO	58.3 ± 2.2	117.3 ± 0.0	-13.9 ± 1.1	152.0 ± 0.2	9.9 ± 1.4	21.4	53.4
48.5/48.5/3 w/w PLA/EVA/GO	57.9 ± 4.3	111.9 ± 0.6	-11.3 ± 0.5	150.6 ± 0.5	11.5 ± 0.2	25.4	52.2
47.5/47.5/5 w/w PLA/EVA/GO	57.4 ± 0.6	110.9 ± 0.7	-11.6 ± 2.5	150.5 ± 0.9	10.9 ± 2.5	24.6	51.7
30/70 w/w PLA/EVA	62.9 ± 0.7	-	-	-	-	-	-
29.7/69.3/1 w/w PLA/EVA/GO	59.5 ± 3.1	119.8 ± 7.1	7.6 ± 6.3	151.6 ± 1.0	4.0 ± 0.3	14.5	53
29.1/67.9/3 w/w PLA/EVA/GO	60.4 ± 2.8	115.2 ± 2.5	5.3 ± 0.5	153.6 ± 0.3	0.5 ± 0.2	1.9	54.7
28.5/66.5/5 w/w PLA/EVA/GO	59.4 ± 0.3	110.8 ± 2.8	1.1 ± 0.3	150.1 ± 0.3	4.2 ± 0.8	15.7	51.2

Tg-Glass transition temperature, T_m-Melting peak temperature, ΔH_m-Melting enthalpy T_{cc}-Cold crystallization temperature, ΔH_{cc}-Cold crystallization enthalpy, X_c-Degree of crystallinity

A closer look at the blends and blend-composites, the 70/30 w/w PLA/EVA blend (Figure 4.8 (a)), showed characteristics of both polymers, and the transitions in this blend did not change positions upon blending, indicating that they were immiscible. These were first the PLA glass transition, followed by the melting endotherms of EVA and PLA respectively. The positions of these transitions were not at all affected by blending for the 70/30 w/w PLA/EVA blend. However, the glass transition of PLA and the kink of EVA were observed to coexist as they occurred almost at the same temperature. The melting peak of EVA seemed to have lowered in intensity as compared to the neat EVA. This was expected since EVA content is the lowest (30 wt.%) in this blend. It is worth noting that the cold crystallization peak of PLA disappeared with blending for this composition. This might have been due to the presence of molten EVA chains, which might have hindered the recrystallization process of PLA. The probable explanation to this is that the chains of PLA were mobile after its glass transition. This made it easier for molten EVA to penetrate its chains, and seal into the free spaces of amorphous PLA chains, that were preparing for re-crystallization that happens between the T_g and T_m of PLA. This prevented the PLA from recrystallizing, hence the undefined or almost disappearance of its melting peak in the blend, since there were less crystals to melt. Although EVA was molten above its melting temperature, and believed that the chains would move with ease, but its high viscosity (as MFI results suggested) might have been the reason for prohibition of PLA chains to reorganize and recrystallize.

The calculated degree of crystallinity of PLA in this blend was 1.1% which was further validated by the almost undefined melting peak observed, while that of EVA (17.1%) was not significantly affected by blending. Upon the addition of GO to the blend, there were some interesting observations. The glass transition temperature of PLA and EVA kink still coexisted even though the T_g was more pronounced. This was owed to the observation that there was a stretch in the temperature transition, with EVA kink maintaining the same position, while PLA T_g went to lower temperatures. Generally, the loading of GO resulted in a decrease in PLA T_g, with a very significant change (Over 10 ℃ difference) at loadings of 3 and 5 wt.%, where the T_g decreased to 49.9 and 46.7 ℃ respectively (Table 3.3, Figure 4.8 (a)). This might have implied that GO acted as a plasticizer for the two polymers, thereby increasing the free volume on PLA chains, causing its transition to a rubbery state to be experienced earlier. The increased free volume in a polymer system has been proven to be of utmost importance for water absorption purposes [12]. Water molecules are collected into the free volume spaces and allowed free movement, so this observation might be very helpful in water studies as we go

further. Coming to the melting peak of EVA (as the next transition) in the blend, the initial loading of GO (1 wt.%) resulted in the drastic reduction of intensity and broadness (almost disappeared) of this transition, as it appeared as a small kink in place of a peak. It is worth noting that the kink was at the very same position the melting was in the neat blend (Table 4.4, Figure 4.8 (a)). For the GO loadings of 3 and 5 wt.% the EVA melting peak completely disappeared. These observations were a probable indication that GO hindered the crystallization of EVA during the cooling process, resulting in little to no crystals to melt during melting. It seems like GO had an inhibition instead of a nucleating effect in this case, due to the fact that its size was in microns and could not form nuclei sites. The layers of GO might have enveloped part of the EVA phase, or have dispersed in the polymer itself. This was also seen in SEM pictures which showed that GO was localized on the interphase between the polymers, and possibly on the polymers themselves. This led to the reappearing of the PLA T_{cc} peak, which generally shifted to lower temperatures (130.0, 111.0 and 109.3 ℃ for 1, 3 and 5 GO loadings, respectively). This suggests that the molten EVA chains were restricted by the presence of GO, inhibiting them from penetrating the free volume in the PLA amorphous chains. This process allowed the PLA chains to re-organize and re-crystalize again. With the melting peak of PLA in the blend composites, the transition generally shifted to lower temperatures and split into two peaks for 3 and 5 wt.% GO loadings. The secondary melting peaks were at 133.9 and 130.3 ℃, for 67.9/29.1/3 and 66.5/28.5/5 w/w PLA/EVA/GO respectively, while the main peaks were at 151.8, 144.4 and 142.2 ℃ for 1, 3 and 5 wt.% GO, respectively. This double melting peak observed was as an indication of the melting of different types of crystals, which might have resulted from two possible sources. The first one being the homogeneous nucleation (polymer itself) recrystallization process. The first melting peak being the melting of metastable crystals of PLA recrystallized from T_{cc} that recrystallized again and melted, and the second peak being the melting of perfect crystals. Secondly the heterogeneous nucleation due to the presence of GO, as the foreign substance which might have acted as a nucleating site for recrystallization of PLA to occur. The shifting to the lower temperatures confirms the plasticisation effect of GO as indicated above.

The degree of crystallinity of PLA in the blends composites generally increased (7.7, 18.8 and 13.4 % for 1, 3 and 5 wt.% GO loadings, respectively), as compared to the neat blend (1.1%), although it was below that of neat PLA (21.1%). While that of EVA drastically decreased from 17.1 % in the blend to 0.8 % in 1 wt.% loading of GO in the blend, to non-existent with

increased GO loading (3 and 5 wt.%). These results validate what was observed on melting of the polymers.

Moving to the 50/50 w/w PLA/EVA composition (Figure 4.8 (b)), the blend very much behaved like the 70/30 w/w PLA/EVA, where T_{cc} and T_m of PLA almost disappeared. This still validates the inhibition effect of EVA on the re-crystallization of PLA. Then in adding GO, it was firstly observed that the glass transition temperature shifted to lesser temperatures with the addition of 1 (58.26 ℃), 3 (57.29 ℃) and 5 (57.44 ℃) wt. % GO. The shift was not as significant as in the 70/30 w/w PLA/EVA composition, but was still enough to suggest that GO had a plasticization effect. The melting peak of EVA was re-defined in these blend composites, as opposed to its disappearance in the 70/30 w/w PLA/EVA blend composites. This suggests that the EVA phase at 50 wt.% content was enough to house the GO, and also allow its nucleation effect on EVA chains. The position of the peaks was maintained for both the blend and all the blend composites (98.1 for the blend, 98.6, 98.4 and 98.8 ℃ for blend composites, respectively). The PLA cold crystallization temperatures were 117.3, 111.9 and 110.9 ℃ for 1, 3 and 5 wt.% GO loadings in the 50/50 w/w PLA/EVA blend, respectively. Its melting temperature was still split into two peaks with the first peak at 143.5, 140.9 and 139.7 ℃, and the second peak at 152.0, 150.6 and 150.5 ℃, for 1, 3 and 5 wt.% GO loadings respectively. There was a general shift towards lower temperatures on both T_{cc} and T_m as the GO loading was increased. This shift still suggested the plasticization effect of GO, reduced crystallinity and somehow partial miscibility of the two polymers in its presence, on this blend. The partial miscibility is due to the reduced gap between the transitions, with PLA transitions approaching that of EVA (displayed on Table 4.3).

The neat blend showed a drastic decrease in the degree of crystallinity with respect to both EVA and PLA phases, with a very significant decrease in the degree of crystallinity of PLA in the blend (EVA from 18.0 to 11.1 % and PLA from 21.1 to 1.2 %). The GO loading had different effects on the degree of crystallinity of the polymers in the blend. The degree of crystallinity of EVA further reduced with the first two loadings, with the exception of the highest GO loading which brought the degree to almost that of the neat polymer. While the degree of crystallinity of PLA was tremendously increased from 1.2 to 25.4 %, with GO loading. This is a clear indication that GO acted as an inhibitor of crystallization in EVA, while as a nucleating agent in the chains of PLA. Hence the double melting peak which was explained to be the melting of two different types of crystal forms from heterogeneous nucleation due to the presence of solid GO and homogenous nucleation from the polymer itself.

Table 4.4: DSC data for EVA in the blends and blends composites.

Sample	T_m / ℃	ΔH_m / J/g	T_c / ℃	ΔH_c / J/g	X_c / %
EVA	97.9 ± 0.7	49.9 ± 0.8	60.0 ± 0.0	52.8 ± 2.0	18.0
70/30 w/w PLA/EVA	98.2 ± 0.3	14.2 ± 0.1	74.8 ± 2.7	22.8 ± 0.9	17.1
69.3/29.7/1 w/w PLA/EVA/GO	97.1 ± 0.7	0.6 ± 0.1	55.0 ± 0.4	45.3 ± 0.2	0.8
67.9/29.1/3 w/w PLA/EVA/GO	-	-	56.5 ± 0.9	47.9 ± 0.4	-
66.5/28.5/5 w/w PLA/EVA/GO	-	-	56.3 ± 0.7	46.3 ± 0.4	-
50/50 w/w PLA/EVA	98.1 ± 0.4	15.4 ± 2.4	69.2 ± 0.3	32.2 ± 2.1	11.1
49.5/49.5/1 w/w PLA/EVA/GO	98.6 ± 0.4	12.3 ± 1.3	78.1 ± 0.5	21.5 ± 2.5	9.0
48.5/48.5/3 w/w PLA/EVA/GO	98.4 ± 0.4	9.8 ± 0.2	79.4 ± 0.3	21.8 ± 1.4	7.3
47.5/47.5/5 w/w PLA/EVA/GO	98.8 ± 0.5	22.6 ± 7.8	78.9 ± 0.6	24.5 ± 5.4	17.2
30/70 w/w PLA/EVA	97.9 ± 0.1	16.9 ± 1.9	64.9 ± 0.1	40.1 ± 3.8	8.7
29.7/69.3/1 w/w PLA/EVA/GO	98.6 ± 0.3	19.4 ± 0.8	75.8 ± 0.8	31.8 ± 2.2	10.1
29.1/67.9/3 w/w PLA/EVA/GO	98.9 ± 0.7	14.4 ± 2.2	74.1 ± 0.6	33.3 ± 3.1	7.6
28.5/66.5/5 w/w PLA/EVA/GO	98.9 ± 0.5	10.8 ± 1.0	78.4 ± 0.3	29.5 ± 3.1	5.9

T_m-Melting peak temperature, ΔH_m -Melting enthalpy T_c - Crystallization temperature, ΔH_c - Crystallization enthalpy, X_c - Degree of crystallinity.

Lastly, the heating of the 30/70 w/w PLA/EVA composition (Figure 4.8 (c)) did not show any significant deviation in the glass transition of PLA, and the VA melting in the blend. The two transitions seemed to be very close to each other, and almost merged. The melting temperature of EVA main chain also did not change at all. The presence of PLA did not seem to have any effect on the melting transition of EVA for this blend. Like in the other presented blends above, there was no registration of the cold crystallization and melting temperatures of PLA (Table 4.3, Figure 4.8 (c)). This was very much expected as the PLA content was the lowest in this blend, and also considering the effect EVA has on the PLA chains, as explained in the blends above. Then with the addition of GO, there were slight changes in all the transitions in the blend composites, but not so significant to thoroughly emphasize on. The trend was the same with 50/50 w/w PLA/EVA blend composites, where T_g of PLA slightly shifted to lower temperatures, while the melting temperature of EVA, the T_{cc} and Tm of PLA slightly shifted to higher temperatures.

As the blend did not show any melting peak for PLA, it was obvious that there would not be any degree of crystallinity, which showed that PLA was completely amorphous in the blend. As for EVA, the blend registered a very low degree of crystallinity (8.7%). It was assumed that PLA had already solidified during the crystallization of EVA. Its chains might have penetrated those of molten EVA, causing its crystallization to occur earlier and the degree of crystallinity to be reduced, since PLA is amorphous at that stage. The addition of GO to the blend resulted in the recurrence of the melting peak of PLA, whereby it was possible to calculate the maximum degree of crystallinity of 15.7 %, as opposed to its non-existence in the blend. The one for EVA in the blend composites dropped even further as compared to the blend and pure EVA (8.7 % in the blend and 5.9 % in the blend composites). These observations reiterate that GO had an inhibition effect on the crystallization of EVA, and a nucleating effect on the chains of PLA, as was the case with the 50/50 w/w PLA/EVA ration.

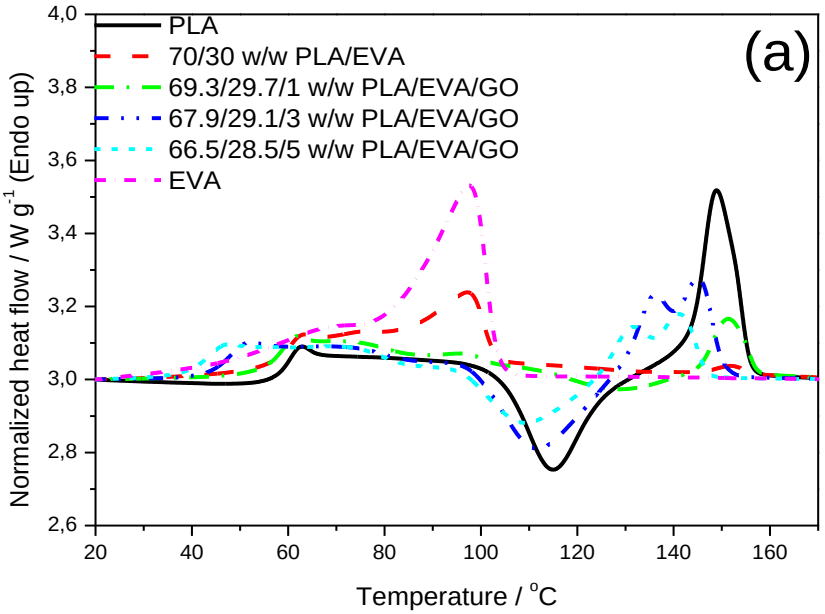
(a)
PLA
70/30 w/w PLA/EVA
69.3/29.7/1 w/w PLA/EVA/GO
67.9/29.1/3 w/w PLA/EVA/GO
66.5/28.5/5 w/w PLA/EVA/GO
EVA
Normalized heat flow / W g-1 (Endo up)
Temperature / °C
4,0
3,8
3,6
3,4
3,2
3,0
2,8
2,6
20
40
60
80
100
120
140
160

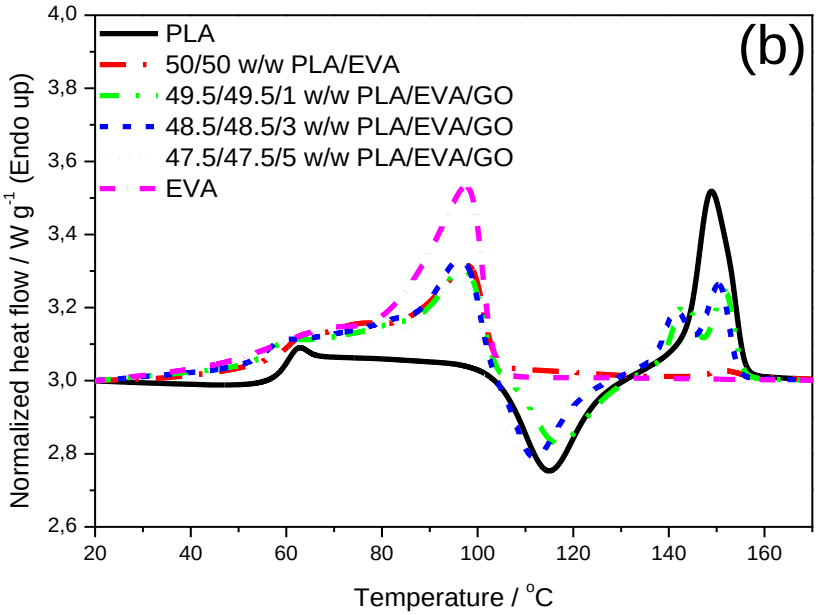
(b)
PLA
50/50 w/w PLA/EVA
49.5/49.5/1 w/w PLA/EVA/GO
48.5/48.5/3 w/w PLA/EVA/GO
47.5/47.5/5 w/w PLA/EVA/GO
EVA
Normalized heat flow / W g-1 (Endo up)
Temperature / °C
4,0
3,8
3,6
3,4
3,2
3,0
2,8
2,6
20
40
60
80
100
120
140
160

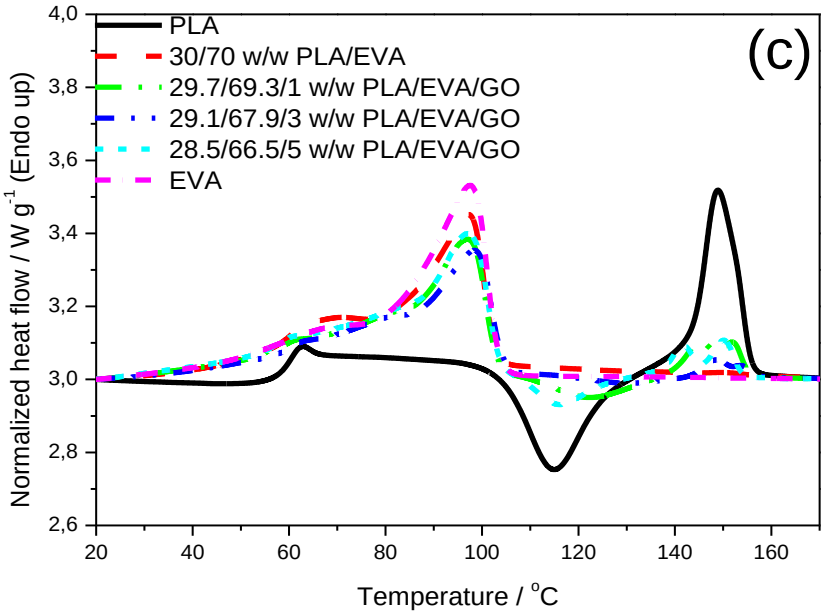

Figure 4.8: DSC heating curves for neat PLA and EVA, blends and composites of compositions: (a) 70/30 w/w PLA/EVA (b) 50/50 w/w PLA/EVA, and (c) 30/70 w/w PLA/EVA all with different GO loadings (1. 3 and 5 wt.%).

Figure 4.9 presents the cooling curves for neat PLA and EVA, 70/30 (a), 50/50 (b) and 30/70 (c) w/w PLA/EVA blends and composites with 1, 3 and 5 wt.% GO loadings. It can clearly be seen that PLA did not crystalize upon cooling, and that EVA showed a single crystallization temperature at 60 ℃ (Table 4.4), without a VA kink. PLA, instead showed a kink at 55 ℃ which represents the glass transition temperature. The reason why PLA could not crystallize upon cooling was probably due to the rapid rate at which it naturally solidifies. It does not allow enough time for perfect crystals to form. It solidifies while the chains are still amorphous, then bypasses the crystallization process to re-crystallize just after its glass transition and before melting, during the re-heating process. In blending PLA and EVA (Figure 4.9 (a)), the crystallization temperature of EVA came earlier at 74.8 ℃, with a VA kink right after the main crystallization peak. The glass transition of PLA was not necessarily visible, but it could have merged with the VA transition, as they normally occur at almost the same temperature. The early crystallization of EVA could be due to the PLA chains catalysing the crystallization process of EVA, but not necessarily acting as nuclei sites. Then upon adding GO to the 70/30

w/w PLA/EVA blend, there was a tremendous decrease (19.8 ℃) in the crystallization temperature of EVA from 74.8 to 55 ℃. The intensities of these peaks for all the blend composites were extremely reduced. This meant that GO acted as a plasticizer and an inhibitor, thereby hindering the crystallization process of EVA, hence the disappearance of the melting peak of EVA during the re-heating.

The 50/50 w/w PLA/EVA blend behaved similar to the 70/30 w/w PLA/EVA, where the crystallization temperature of EVA occurred earlier (69.2 ℃) due to the presence of PLA chains, and PLA T_g still occurred around 55 ℃. Adding 1, 3 and 5 wt.% GO, it was generally observed that the EVA crystallization peaks for all blend composites occurred at even earlier temperatures, around 79 ℃. In this blend GO acted as a nucleating agent, whereby it formed nuclei sites where the crystallization of EVA emanated. Also, it still proves that at this ratio EVA was enough to house the GO and showcase its capability to nucleate. The T_g of PLA was still clearly visible in all the blend composites, and still maintained its position around 55 ℃.

The 49.5/49.5/1, 48.5/48.5/3 and 47.5/47.5/5 w/w PLA/EVA/GO composites had crystallization peaks at 78.8, 78.1 and 79.4 ℃ (Table 3.4) respectively for EVA. This clearly indicated that the presence, and increased addition of GO brought partial miscibility to these composites. This was done by catalysing the crystallization process, that is the presence of GO resulted in the ordering of the crystals to occur faster. The intensity of these peaks was the same, and similar to the one for pure EVA and 50/50 w/w blend, which showed that EVA was not hindered from crystalizing. The same behaviour was observed in the 30/70 w/w PLA/EVA blend as well as its blend composites

DSC analyses for the three rations of PLA/EVA/GO used in this study provided insight into the thermal transitions of these polymers individually, when blended and with different GO loadings. This helped to further make the assumption that the adsorbent, GO, had a compatibilization effect on the PLA/EVA matrices upon its increased addition. This was achieved by selectively localizing in either the EVA or PLA phase, or even the interface. The GO seemed to have an auto-catalytic effect on the crystallization of the blends, depending on the ratios. In the 70/30 w/w PLA/EVA ratio it acted as an inhibitor, while in 50/50 and 30/70 w/w PLA/EVA ration it acted as a nucleating agent.

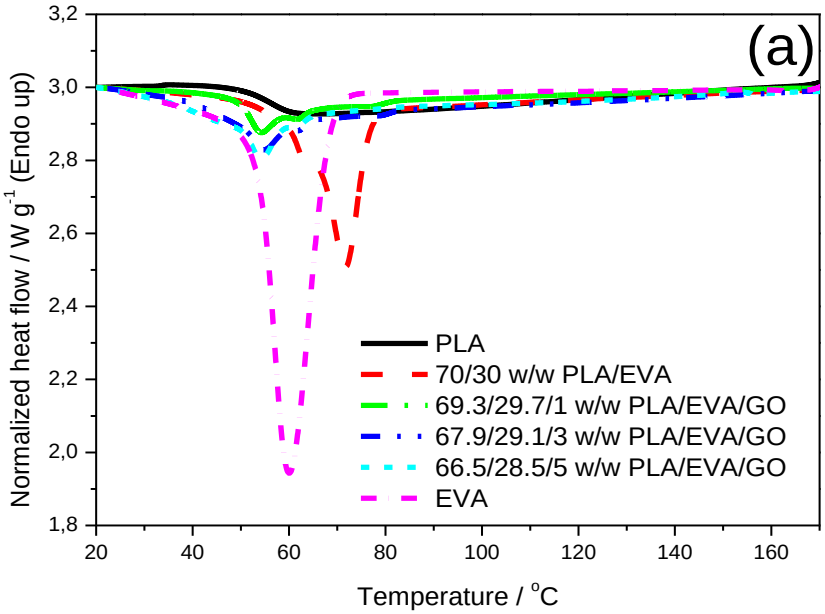
(a)
Normalized heat flow / W g-1 (Endo up)
Temperature / °C
PLA
70/30 w/w PLA/EVA
69.3/29.7/1 w/w PLA/EVA/GO
67.9/29.1/3 w/w PLA/EVA/GO
66.5/28.5/5 w/w PLA/EVA/GO
EVA

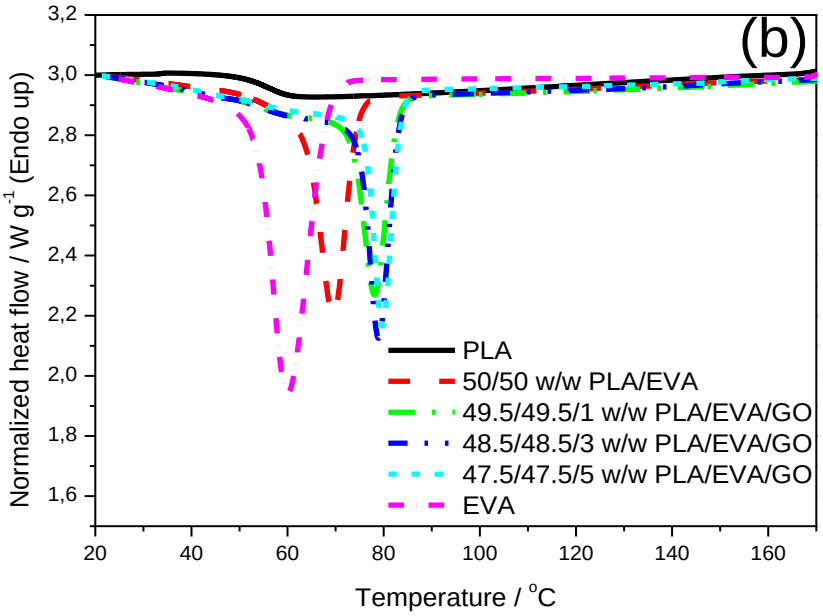
(b)
Normalized heat flow / W g-1 (Endo up)
Temperature / °C
PLA
50/50 w/w PLA/EVA
49.5/49.5/1 w/w PLA/EVA/GO
48.5/48.5/3 w/w PLA/EVA/GO
47.5/47.5/5 w/w PLA/EVA/GO
EVA

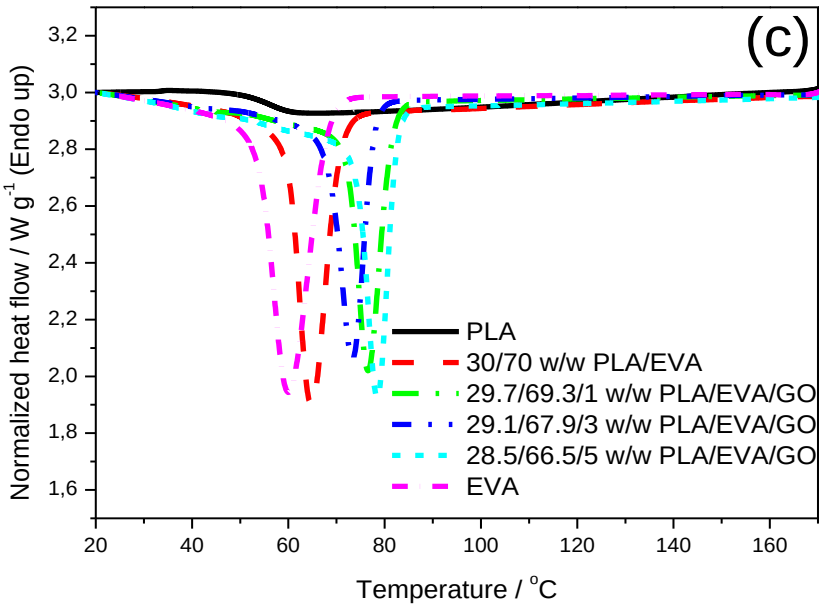

Figure 4.9: DSC cooling curves for neat PLA and EVA, blends and composites of compositions: (a) 70/30 w/w PLA/EVA, (b) 50/50 w/w PLA/EVA, and (c) 30/70 w/w PLA/EVA all with different GO loadings (1. 3 and 5 wt %).

4.4.2 Thermogravimetric analysis (TGA)

The thermal degradation behaviour of a polymer system assists in making conclusions on the thermal stability of the components involved, as well as their influence on one another. The successful masking of a certain component in the polymer system is usually observed through an improved thermal stability of that component. TGA was used to assess the thermal degradation of the neat components (GO, PLA and EVA) as well the blends and blend composites with GO, to determine their thermal stabilities. Figure 4.10 shows the TGA (Figure 4.10 (a)) and TGA derivative (Figure 4.10 (b) curves obtained from analysing the neat polymers (PLA and EVA) and the prepared GO. The degradation of PLA occurred following a single step, which started at 282.5 ℃ on the TGA curve (Figure 4.10 (a)), and had a maximum degradation at 300 ℃ shown on the derivative TGA curve (Figure 4.10 (b). The degradation of PLA occurs via hydrolysis, lactide reformation, oxidative main chain scission and inter or intramolecular trans-esterification reactions [13]. Then the TGA curve for EVA clearly showed that the polymer followed a two-step degradation process. The first step happened at a mass

loss of 18%, at an onset of 321.1 ℃ and a maximum degradation at 348 ℃. This step was due to the deacetylation (removal of acetic acid) in the EVA chain, and the 18% mass loss indicates clearly that the EVA used had 18% vinyl acetate content. Then, the second step was observed at an onset of 444.9 ℃ and a maximum of 462 ℃. This degradation step was owed to the main chain decomposition of EVA. The thermal degradation of EVA proceeds via the elimination of acetic acid under heat, which forms a polyalkane that degrades by chain scissions to form a variety of volatile hydrocarbons [14]. From analysing The TGA and derivative TGA curves for these two polymers, it was clearly visible that EVA was more thermally stable than PLA. This was because in EVA, apart from having had two degradation steps, the first one occurred at 321.1 ℃, which is higher than that of PLA (282.5 ℃). The thermal degradation of GO followed three distinct steps. The first one occurred at a temperature range of 48.5-148.7 ℃, and was attributed to the removal of previously absorbed water in the layers of GO. This step accounted for about 14% mass loss, and was linked to the second step, which occurred at a temperature range of 148.7-225.6 ℃. This step accounted for the major mass loss (about 22%) of GO, and represents the decomposition of hydroxyl, carboxylic and lactone groups. This degradation step results in the releasing of water from the hydroxyl groups, carbon dioxide from the carboxylic acid groups, and carbon monoxide from lactone groups [15]. The third degradation step followed, with a temperature of 225.6-350.0 ℃, and accounted for about 12% mass loss. The step was owed to the decomposition of quinone and ketone groups present in GO. Literature suggests that there is a covalently linked organosulfate group on the structure of GO, which is as a result of the usage of sulphuric acid in modifying EG to GO [15,16]. The organosulfate group also degrades in this third step, releasing sulphur dioxide in the process [15,16]. Moreover, it has been alleged that although many researchers do not talk about the presence of this group on GO, it bears a great significance in that it helps enhance the reactivity of graphene oxide [15,16]. From here there was no significant weight loss observed as the graphite backbone remained, which consists of carbon only. A char of 28.5 mass% remained after the run, which was as a result of the inorganic nature of GO which does not degrade in the temperature range used, as well as the inert atmosphere. The TGA analysis of GO served as validity, once more, that GO was successfully synthesized.

Table 4.5: TGA results for all the analysed samples.

Sample	$T_{1, onset}$ / °C	$T_{1, max}$ / °C	$T_{2, onset}$ / °C	$T_{2, max}$ / °C	Char / Mass %
PLA	282.5	297.1	-	-	1.7
GO	48.5	92.6	148.7	159.8	28.5
70/30 w/w PLA/EVA	258.4	271.7	454.4	478.5	2.9
69.3/29.7/1 w/w PLA/EVA/GO	282.6	296.4	440.7	466.0	1.0
67.9/29.1/3 w/w PLA/EVA/GO	266.6	283.2	437.1	465.6	1.3
66.5/28.5/5 w/w PLA/EVE/GO	264.6	281.3	435.8	465.8	1.7
50/50 w/w PLA/EVA	275.2	285.5	451.8	475.1	0
49.5/49.5/1 w/w PLA/EVA/GO	256.9	275.1	447.9	475.5	2.0
48.5/48.5/3 w/w PLA/EVA/GO	241.0	267.9	446.8	474.4	3.0
47.5/47.5/5 w/w PLA/EVA/GO	244.0	288.8	448.0	475.5	4.6
30/70 w/w PLA/EVA	243.8	283.7	457.7	484.1	2.7
29.7/69.3/1 w/w PLA/EVA/GO	235.6	259.2	458.5	480.6	2.2
29.1/67.9/3 w/w PLA/EVA/GO	234.8	262.3	456.3	482.6	3.6
28.5/66.5/5 w/w PLA/EVA/GO	240.5	275.1	453.3	480.4	4.1
EVA	321.1	348.2	444.9	461.8	0

$T_{1,onset}$ and $T_{2, onset}$ represent onset degradation temperatures for the first and second peak respectively, in the TGA curves, while $T_{1, max}$ and $T_{2, max}$ represent the peak maxima temperatures of the first and second peak in derivative TGA curve

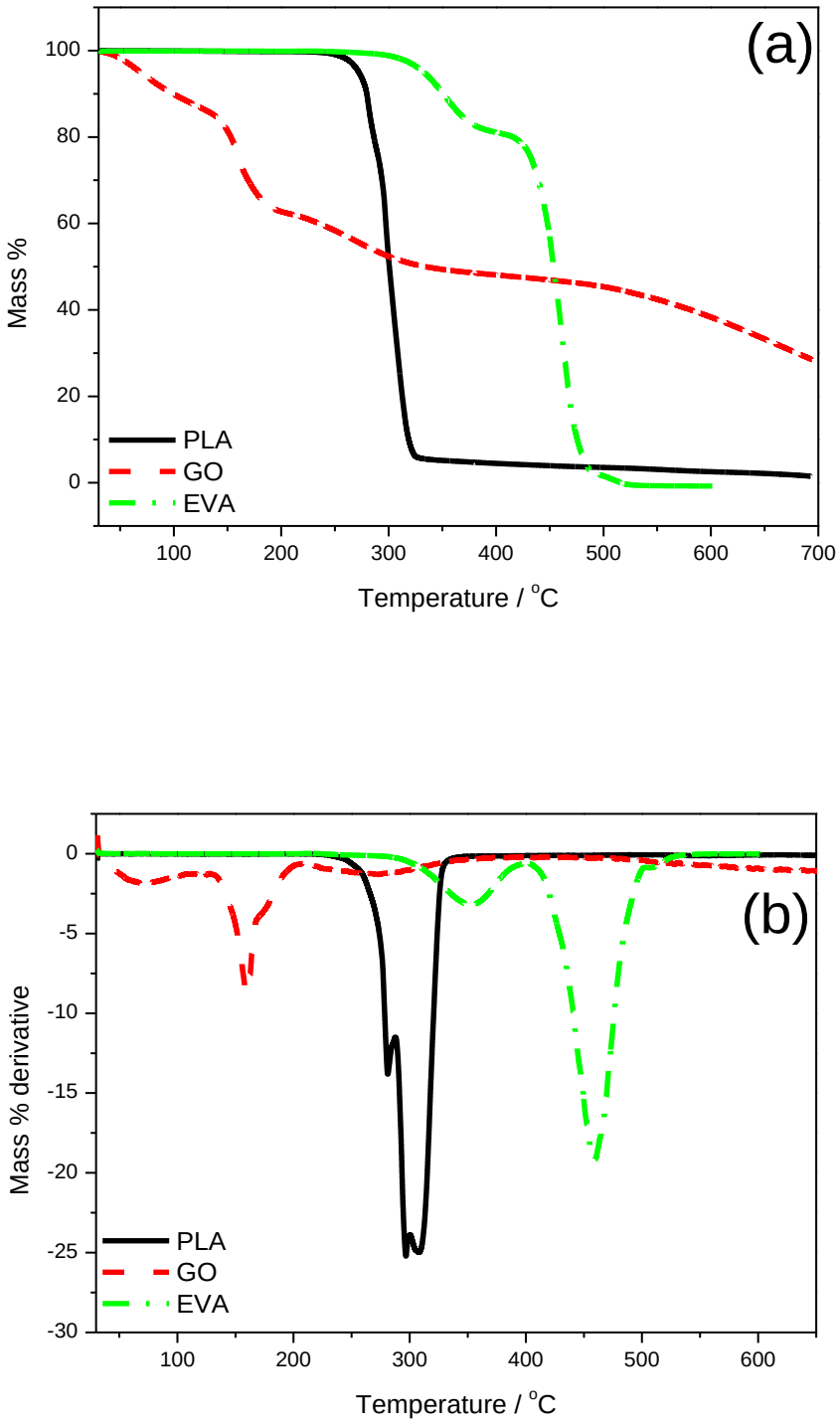

Figure 4.10: TGA (a) and derivate TGA curves (b) for PLA, EVA and GO.

Figures 4.11 and 4.12 show the TGA and derivative TGA curves, respectively, of the neat blends and blends composites that were analysed. Then the Table 4.5 shows the onset, maximum degradation temperatures, as well as the char values for the neat polymers, their blends and blends composites of this study. In the 70/30 w/w PLA/EVA blend (Figure 4.11 (a), Figure 4.12(a)), two degradation steps were observed with onsets 258.4 and 454.4 ℃, which clearly indicated that the two polymers degraded separately in the blend. This proves the immiscibility character of PLA and EVA that was seen on SEM and DSC results, with the first step belonging to PLA and the second step to EVA. Their maximum degradations on the TGA derivative curves were at 271.7 ℃ and 478.5 ℃, respectively. The first step was due to the main chain decomposition of PLA, and this step coexisted with the deacetylation step of EVA (first degradation step of EVA). This was a shift to lower values as compared to the initial and maximum degradation temperatures of PLA (282.5 and 297 ℃), which might have been due to the release of VA in the first degradation step of this blend. The degradation of VA releases acetic acid as already stated previously, this acetic acid contains the hydroxyl group as one of its components, which might be released as water/moisture. It is well known that the presence of moisture/water in biodegradable polymers induces early degradation [17]. Therefore the decreased thermal degradation temperatures of PLA in the blend might have been due this moisture during the release of VA. Then the second step for this blend, with the calculated onset of 358.8 ℃ and a maximum degradation at 478.5 ℃, represented the main chain degradation of EVA. This step had a higher onset and maximum degradation temperatures than that of neat EVA. This furthering apart of PLA and EVA transitions during degradation, implied that apart from being immiscible, the two polymers were also incompatible to some extent. This is further validated by the inhibition of PLA re-crystallization and almost disappearance of its melting peak, which was observed in DSC analysis above. Upon adding GO (1, 3 and 5 wt. %) to the 70/30 w/w PLA/EVA blend, the two main degradation steps were still observed (from PLA and EVA), with an additional but not so significant step between them. The degradation temperatures generally seemed to approach each other in this blend composites, as the PLA degradation step increased to higher temperatures (from 258.4 of neat blend to 282.6 ℃ in composites) as compared to PLA in the neat blend. While that of EVA decreased to lower temperatures (from 454.4 of neat blend to 435.8 ℃ in composites). This approaching of transitions meant that the presence of GO might have brought partial miscibility to the polymers in the blend, thereby giving the average thermal degradation temperature. The additional degradation step between the transitions could have resulted from a number of factors. Firstly, this step might have been due to the probable degradation of VA content during

the degradation of PLA. Secondly, this step could have represented the presence of GO showing pyrolysis of oxygen containing functional groups at that temperature. Lastly, a layer of combined PLA, EVA and GO in one phase.

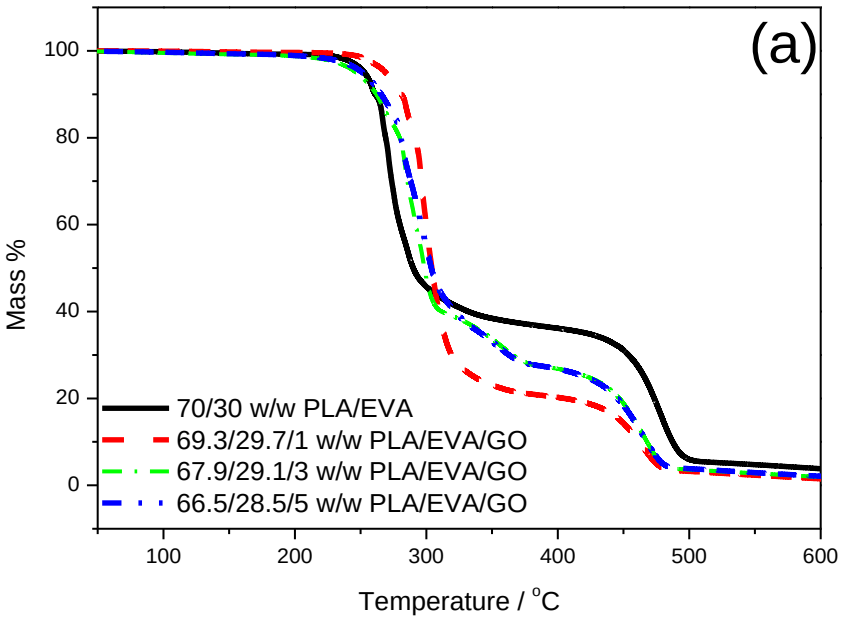

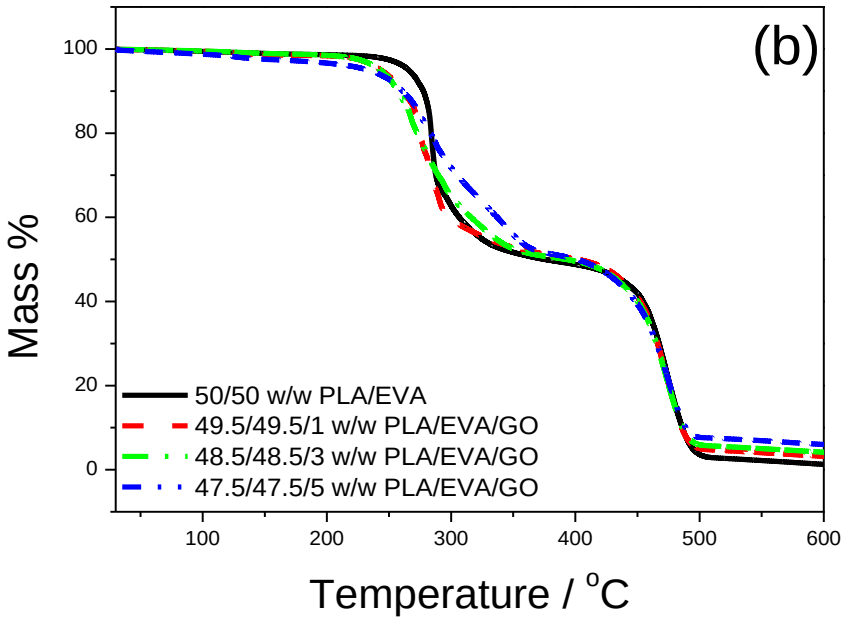

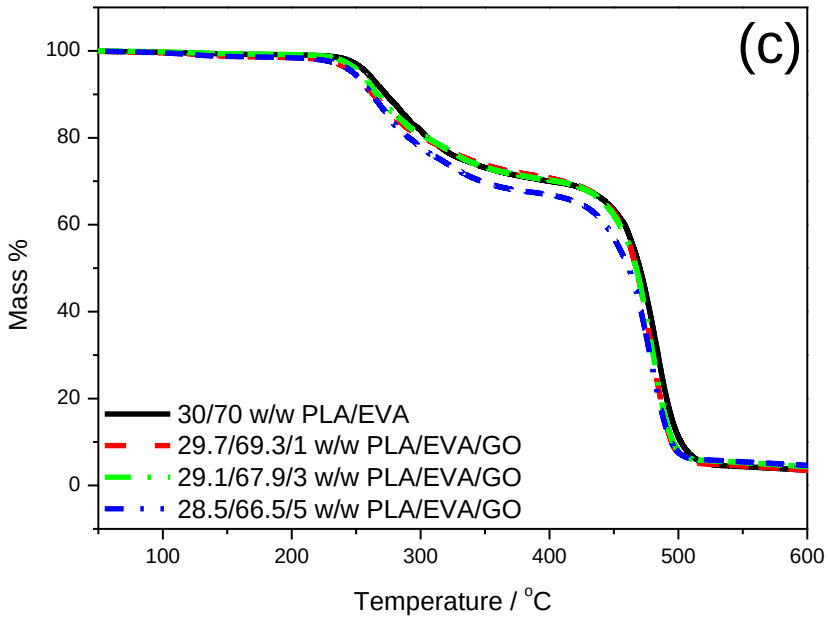

Figure 4.11: TGA curves for the 70/30 (a), 50/50 (b), 30/70 (c) w/w PLA/EVA blends as well as composites at different GO loadings (1, 3 and 5 wt.%).

With the 50/50 w/w PLA/EVA ration (Figure 4.11 (b), Figure 4.12 (b)), the blend still had two degradation steps. The first step was found at an onset of 275.2 ℃ and a maximum degradation at 285.5 ℃. While the second degradation step had an onset of 451.8 ℃ and a maximum of 475.1 ℃. Although it was clear from these observations that the first degradation step was lower than that of neat PLA, but it has improved tremendously from the 70/30 w/w PLA/EVA blend (258.4 ºC). On the other hand, the second step moved slightly to lower temperatures as compared to the 70/30 w/w PLA/EVA blend (454.4 ºC), though still above that of neat EVA. Although polymers were still immiscible in the blend, but the approaching of these degradation steps towards each other implied an improvement in compatibility as opposed to the previous blend (70/30). This suggested compatibility was even observed by SEM and DSC results above, together with SEES measurements. The blend composites in this ration still showed two main degradation steps. The previously observed minor step between them was only seen on 1 wt.% loading on the TGA curves, but as the loading was increased it seemed to have merged into the two main degradation steps. This made it hard to distinguish the end of the first step and the beginning of the second step. However, this step was more pronounced on the

derivative TGA curves as GO loading was increased. This phenomenon alone might have implied that GO had improved the mixing of the two polymers even further in this ratio. The onset temperatures of the first/PLA (From 275.2 of the neat blend to 241.2 ℃ in composites) and second/EVA (From 451.8 of the neat blend to 446.8 ℃ in the composites) degradation steps moved to lower temperatures with increased GO loading. As previously stated, the decrease in transition temperatures in the presence of GO might be as a result of GO releasing moisture/water, therefore deteriorates the degradation of PLA.

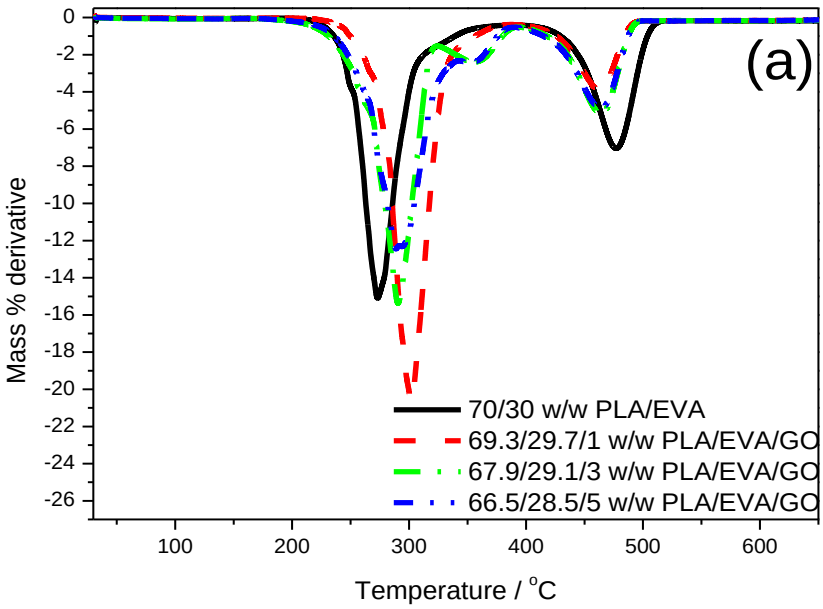

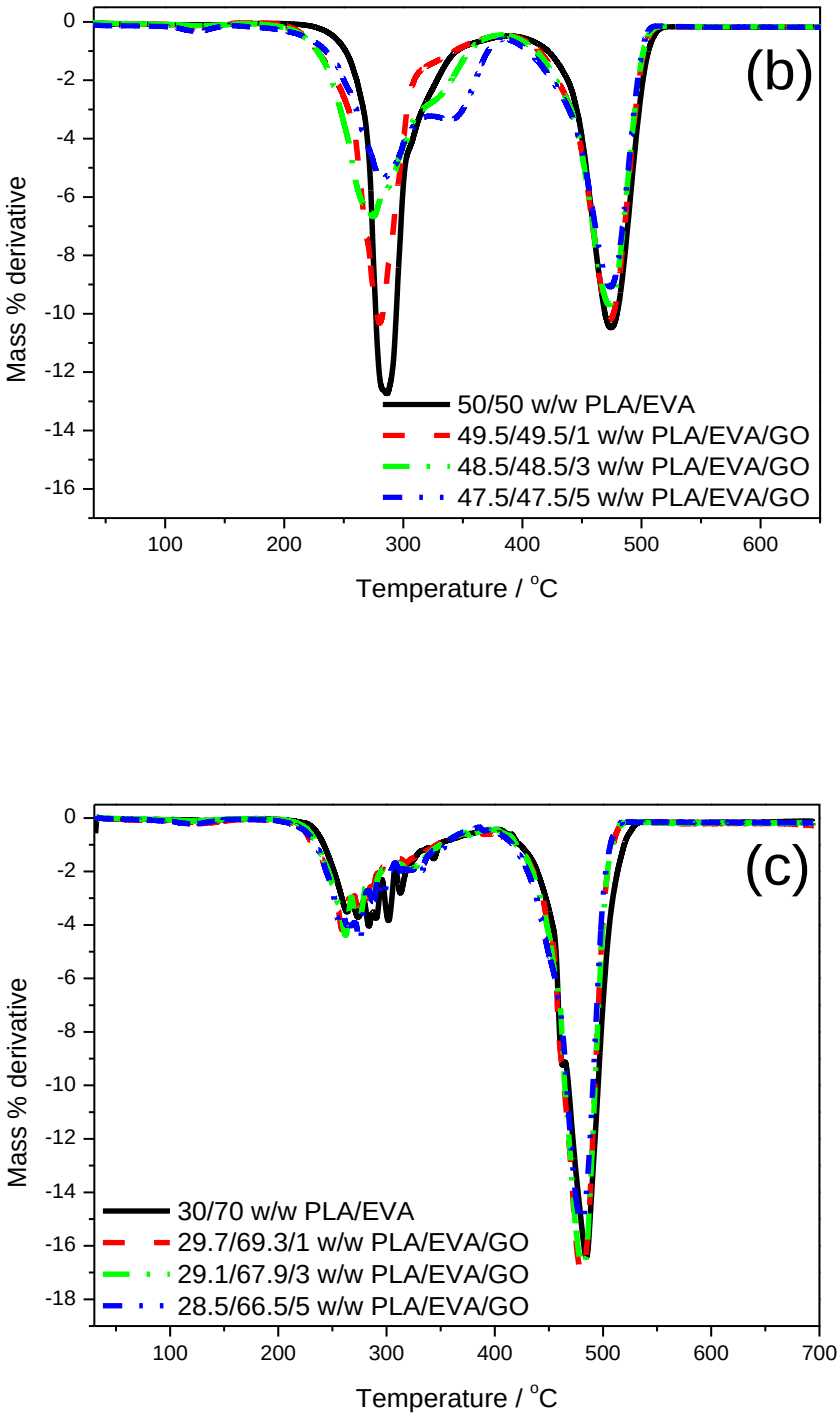

Figure 4.12: TGA derivative curves for the 70/30 (a), 50/50 (b), 30/70 (c) w/w PLA/EVA blends as well as composites at different GO loadings (1, 3 and 5 wt.%).

Coming to the 30/70 w/w PLA/EVA ration (Figure 4.11 (c), Figure 4.12 (c)), the blend still showed two degradation steps. A drastic reduction in the onset temperature of the first degradation step (243 ℃) was observed, in comparison to other blends and neat PLA. As there is less PLA content in this blend, the VA degradation step might have been dominant and therefore significantly shifted this first step to lower temperatures due to the release of high VA, as the EVA content is higher in this blend (70 wt.%). The second degradation step seemed to move a bit to a higher onset temperature (457.7 ℃). The behaviour in this blend is similar to the one observed in the 70/30 w/w blend, whereby the transitions were furthering apart, indicating less compatibility of the polymers. With the blend composites, the behaviour with respect to the onset of thermal degradation of the first/PLA (From 243 of the neat blend to 234.6 ℃ in composites) and the second/EVA step (From 457.7 of the neat blend, to 453.3 ℃) was the same as in the other composites above. The trend showed a further decrease in degradation temperatures, which still verifies that the degradation components from VA and GO caused premature degradation in PLA, resulting in the reduction of degradation temperatures in the entire composites. The minor step was also visible on derivative curves only as was observed on the 50/50 ratio.

It was clear that the neat GO lost 71.5 % of its original mass during the entire temperature range on TGA analysis (30 to 700 ºC), and the char remained was 28.5% . The char expected on each loading should not exceed 28.5 % of the original mass, of which was the char left on the neat GO analysis. Looking at all blend composites, the char content that remained for all samples was almost 100% of the original GO content. This indicated that after each analysis there was a presence of both polymer (PLA or EVA, or both) and GO, since the percentage char exceeded the expected 28.5 % of the original GO mass used. This finding suggested that the GO improved the thermal stability of the polymers, as SEM and SEES results indicated that GO could settle in either of the two polymer phases, or even the interface. This showed that GO had an autocatalytic effect on the thermal degradation of the polymers. It speeded the initial degradation of the blends, but insulated the polymers that they form part of the char at higher temperatures. Interchangeably, the TGA results also confirmed the masking of GO by the polymers, even at high temperature.

4.5 WATER ABSORPTION STUDIES OF THE PREPARED BLENDS AND BLEND COMPOSITES

Water absorption studies are generally used to assess the hydrophilicity of a material. This analysis can also help a great deal in identifying possible materials that can be used for metal adsorption from solution, as the material first has to be water permeable before it can attach heavy metals on it. The water intake analysis of the prepared blends and blend composites was done in order to check the degree to which the blends and blend composites absorbed water, or rather, their water intake efficiency. Figure 4.13 shows the resultant water absorption curves for blends and blend composites of (a) 70/30, (b) 50/50 and (c) 30/70 w/w PLA/EVA with different loadings of GO (1, 3 and 5 wt.%). Table 4.6 presents the water absorbed after chosen time intervals, as well as the maximum water absorbed (%) for these blends and blend composites. It should be noted that researchers have found out that water can penetrate polymeric material in mainly three ways; firstly, through the diffusion of water molecules into the free volume spaces of the composites, secondly through micro-cracks/voids in between the phases and lastly through the capillary transport [14-16]. The most probable mode of penetration for this analysis was through diffusion and micro cracks, which was owed to hydrophilicity to some extent of the polymeric material proven by SEES (which encourages diffusion). Furthermore, the general immiscibility of the polymers, observed in DSC might have encouraged water intake through spaces on the interface. It should be noted that the water intake generally increased with an increase in time, until a certain maximum absorption point where the absorption was constant, for all analysed samples.

Table 4.6: The water intake percentages for all the blends and blend composites.

Sample	Water absorbed at 50 hours / %	Water absorbed at 250 hours / %	Water absorbed at 450 hours / %	Maximum water absorbed / %
70/30 w/w PLA/EVA	4.0	9.3	9.7	10.0
69.3/29.7/1 w/w PLA/EVA/GO	1.0	2.3	3.2	3.2
67.9/29.1/3 w/w PLA/EVA/GO	3.7	5.0	5.4	5.5
66.5/28.5/5 w/w PLA/EVE/GO	5.2	10.1	10.7	10.7
50/50 w/w PLA/EVA	3.3	8.1	9.1	9.1
49.5/49.5/1 w/w PLA/EVA/GO	13.3	21.4	22.9	23.0
48.5/48.5/3 w/w PLA/EVA/GO	5.3	12.5	13.9	13.9
47.5/47.5/5 w/w PLA/EVA/GO	1.0	2.1	2.4	2.5
30/70 w/w PLA/EVA	1.1	2.1	2.9	3.1
29.7/69.3/1 w/w PLA/EVA/GO	2.8	6.0	7.3	7.3
29.1/67.9/3 w/w PLA/EVA/GO	2.5	6.1	7.3	7.5
28.5/66.5/5 w/w PLA/EVA/GO	2.3	4.9	6.3	6.5

In the 70/30 w/w PLA/EVA ration (Figure 4.13 (a)), the blend had a maximum water intake of 10.0 %. When GO was added, the maximum water intake generally dropped significantly. The maximum values were 3.2, 5.5 and 10.7 % (Table 4.6), for 1, 3 and 5 wt.% GO loadings, respectively. The initial loading of GO (1 wt.%) seemed to have shocked the system, sealed into the interfaces (as SEM results showed) and closed up the spaces, thereby closing the pathways for water absorption. Increasing the GO content (3 and 5 wt.%), the samples began to regain their water intake capabilities to the maximum intake value above that of the neat blend (10.7 % for 5 wt.% GO loading). This might have been due to the morphology observed in SEM for these composites. It was clearly shown that the addition of GO to these matrices resulted in a very poor surface, visible as cracks on the interface and spaces on the interfaces. These cracks and spaces could aid the penetration of water into the composites, thereby increasing the water intake degrees of the composites with increasing GO content, hence the increase in water uptake. Apart from GO decreasing the intake of water in the blend, but the maximum water intake of the composites was directly proportional to the GO loading.

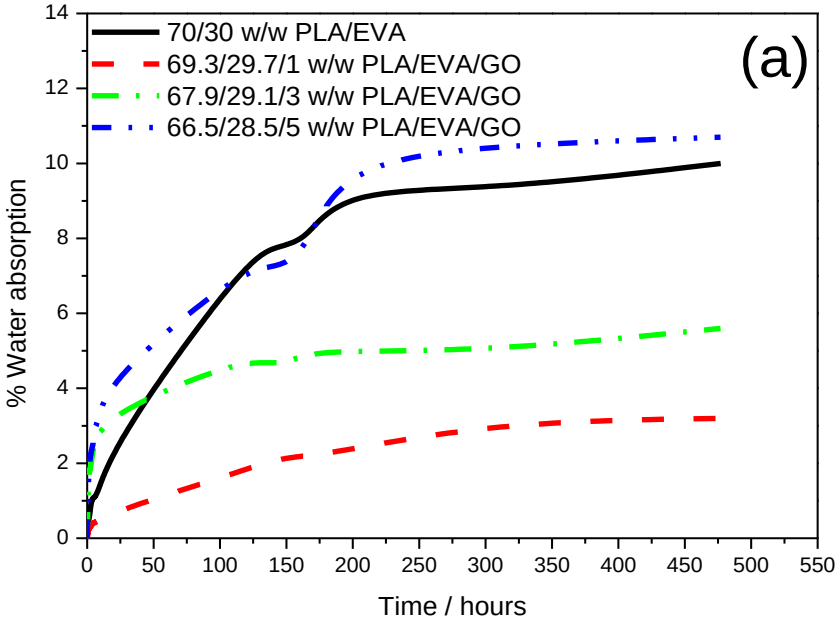

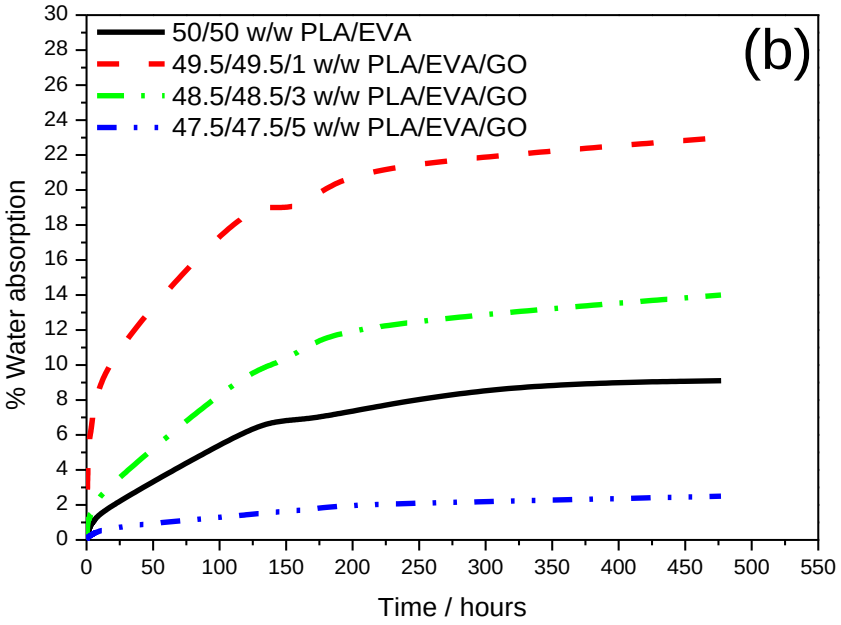

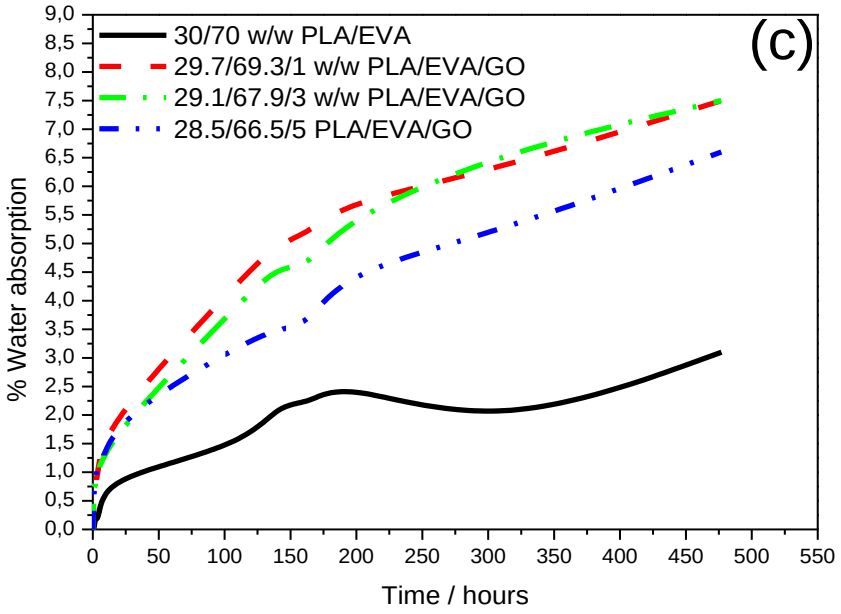

Figure 4.13: Water absorption curves for blends and composites of (a) 70/30, (b) 50/50 and (c) 30/70 w/w PLA/EVA blends and composites with 1, 3 and 5 wt.% GO loadings.

In the 50/50 w/w PLA/EVA ration, the blend had a maximum water absorption of 9.1 %. This was a bit below the maximum absorption observed for the 70/30 w/w PLA blend. Then in adding GO to this ration, there was a general increase in the maximum water intake of the blend composites, although an inverse proportion in relation to GO was observed, as opposed to the direct proportion observed in the 70/30 ratio. The resultant maximum absorption degrees were: 23.0 %, 13.9 % and 2.5 % (Table 4.6) for 1, 3 and 5 GO loadings, respectively. This behaviour could have been due to that there is a balance of polymeric material (co-continuity) in this ration. SEM images suggested that the localization might have happened in both the polymers and the interface since there was no distinguishable phase, and the interaction was very strong. The strong interaction might have closed the water pathways, the high intake of water might have been due to the open layers of GO, which allowed passage of water. This further shows that GO on its own has the ability of absorbing water.

Then for the 30/70 w/w ration (Figure 4.13 (c)), the blend had a maximum water absorbed of 3.1 %. This had clearly been the least absorbing amongst the blends, and was attributed to the higher content of EVA. DSC demonstrated that EVA might have sealed up the free volume in the amorphous chains of PLA, thereby disturbing the crystallization and closing all air pathways for water to pass through. As GO was loaded on the 30/70 w/w PLA/EVA blend, the maximum water intake increased from 3.1 in the blend, to around 7 % in the composites . This behaviour of the GO confirms that it has the ability to absorb water through its layers, as the blend interaction in this ratio was found to be also strong.

In generally comparing the three ratios used (70/30, 50/50 and 30/70 w/w PLA/EVA), the highest maximum water intakes were found to be 23.0, 13.9 and 10.7 %, which belonged to 49.5/49.5/1, 48.5/48.5/3 and 69.3/29.7/5 blend composites, respectively. Water intake analysis was helpful in identifying these blend composites, which would further be used for metal adsorption.

4.6 ADSORPTION OF Pb(II) HEAVY METAL IONS USING ATOMIC ABSORPTION SPECTROSCOPY (AAS)

Assessing the metal (Pb(II) in this case) adsorption of a material is very important as heavy metals continue to pose dire health consequences when consumed. Identification of an efficient heavy metal removing material (materials) could benefit the health sector a lot, as these would be used industrially to alleviate the contamination of water by heavy metals crisis. AAS was

used to analyse the adsorption efficiency of GO as well its composites. However, it was done for the sample compositions that had a higher water absorption capacity, namely: 66.5/28.5/5, 49.5/49.5/1, and 48.5/48.5/3 w/w PLA/EVA/GO composites. An extra 47.5/47.5/5 PLA/EVA/GO composite, with the lowest water intake was also analysed as a control. Three different conditions were studied, which were the effect of initial concentration, pH and contact time. The effect of initial concentration was analysed using only the synthesized GO powder. This was in order to investigate the concentration of lead ions at which GO adsorbs the most and use it for contact time and pH. Table 4.7 presents the obtained adsorbed concentrations of lead ions when 100, 200, 300 and 400 ppm lead (Pb(II)) solutions were used. The percentage amounts adsorbed were 85.5, 94.1, 95.3 and 95.7 % for the above Pb(II) solutions, respectively. From these results, a clear direct proportion between the content of lead in solution and the degree of adsorption was observed. This was shown by the increasing percentage adsorption as the initial lead concentration increased on neat GO. This was also validated by Figure 4.14, wherein a clear logarithmic growth function was obtained for the increasing initial concentration versus percentage adsorption. From this it was determined that the solution containing 400 ppm lead ions was adsorbed the most by GO. This trend observed could be due to the fact that with increasing lead content there was an increase in the adsorbate to be adsorbed, and that at high adsorbate concentration both chemical and physical adsorption would effectively occur. The prepared GO powder on its own (without polymers) proved very effective in adsorbing lead ions from solution. The 400 ppm lead solution was taken as the optimal concentration and used for pH and contact time analysis.

Table 4.7: AAS results of GO at different contact times.

Sample	Initial Pb concentration / ppm	Adsorbent sample mass (w) / g	Concentration Pb adsorbed (C_a) /ppm	% Adsorbed
GO	100	0.7079	85.5	85.5
GO	200	0.7033	188.2	94.1
GO	300	0.7016	286.0	95.3
GO	400	0.7052	382.9	95.7

At different initial concentrations, pH 7 and 4 hours contact time were used

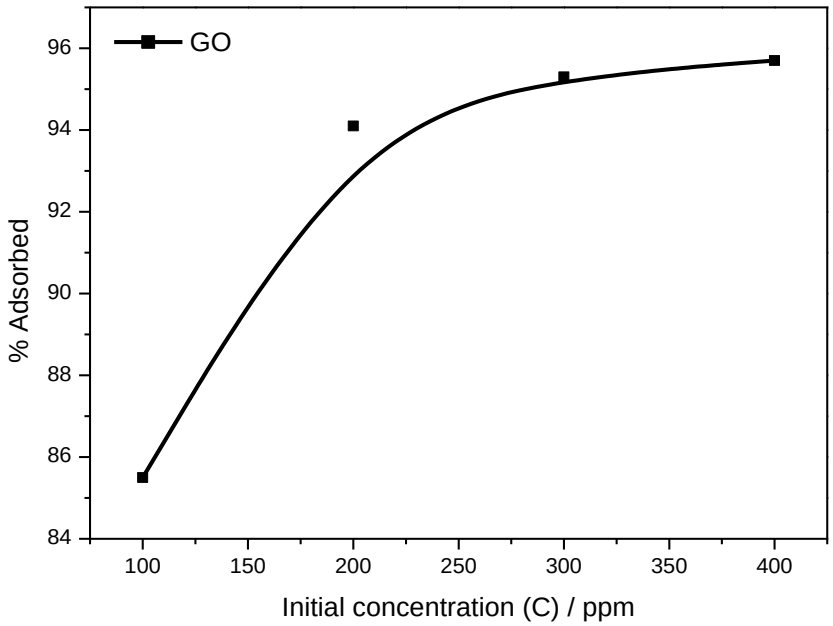

Figure 4.14: A graph showing the percentage lead ions adsorbed by the prepared GO against the initial lead solution concentration.

Table 4.8 shows the AAS results obtained under acidic (pH 3) and basic (pH 12) media. From these observations, it was clear that the adsorption of lead ions did not depend on GO only. The polymer matrices contributed a great deal to the adsorption of lead ions, and this was shown by considerably higher adsorption concentrations as well as percentages for the composites than the GO powder on its own. This could be attributed to that when filtering the powder sample in GO alone, the physically adsorbed lead ions might have gone back to the lead solution as there were no settling sites in the powder. The results in Table 4.8 also outline the adsorption degrees of the 66.5/28.5/5, 49.5/49.5/1, 48.5/48.5/3 and 47.5/47.5/5 w/w PLA/EVA/GO composites at pH 3 and 12 media. The 66.5/28.5/5 w/w PLA/EVA/GO composite showed a higher adsorption at a pH of 12 (97.5%) than at a pH of 3 (94.9 %). This was also the case for the 49.5/49.5/1 w/w PLA/EVA/GO composite (96.6 % for pH 12, 92.6 % for pH 3), 48.5/48.5/3 w/w PLA/EVA/GO composite (96.9 % for pH 12, 93.1 % for pH 3) and the 47.5/47.5/5 w/w PLA/EVA/GO composite (96.9 % for pH 12, 93.5 % for pH 3). Surprisingly, the control sample that had the lowest water intake capacity on the section above also showed amongst the highest adsorbed samples (96.9 % for pH 12, 93.5 % for pH 3). This

is an indication that not only the absorption ability is the driving force in the metal intake, but several factors were involved. These factors might have been: the oxygen containing functional groups on GO and polymers themselves, the size of the adsorbate, concentration of adsorbent, pH, and contact time amongst others. This meant that for every composition a higher adsorption concentration and percentage was found where the lead containing solution was basic. This may be because in basic media there is an abundance of hydroxide ions (OH^-) which would encourage adsorption of Pb(II) ions to themselves. In addition, the Pb(II) ions would have sufficient adsorption sites in order to be complexed into the oxygen containing functional groups of the adsorbent. In the acidic media, there is an abundance of hydronium ions, and these might protonate the highly nucleophilic oxygen containing functional groups of adsorbents, and compete with lead ions for adsorption sites. In comparing all the analysed samples here, it was clear that the 66.5/28.5/5 w/w PLA/EVA/GO composite generally showed a higher adsorption capacity (97.5 %). This might be due to the high content of GO in the composite mainly, as it has numerous oxygen containing functional groups. Also, this composite together with the 67.9/29.1/3 w/w PLA/EVA/GO composite were the only ones showing cracks and voids in SEM, although all the samples were fractured. These cracks might have acted as physical adsorption sites for Pb(II) ions. Moreover, the weak interaction of GO and the polymer matrix observed in SEM for the 66.5/28.5/5 w/w PLA/EVA/GO composite implied that the GO is exposed in the composite because of the weak adhesion. This, even though bad for morphology, could work to also increase the adsorption capacity as the GO is not hindered.

Table 4.8: AAS results for composites at two different pH levels.

Sample	pH	Adsorbent sample mass / g	Concentration Pb Adsorbed (C_a) / ppm	% Adsorbed
49.5/49.5/1 w/w PLA/EVA/GO	3	0.6027	370.4	92.6
49.5/49.5/1 w/w PLA/EVA/GO	12	0.6936	386.4	96.6
48.5/48.5/3 w/w PLA/EVA/GO	3	0.6636	372.4	93.1
48.5/48.5/3 w/w PLA/EVA/GO	12	0.6101	387.6	96.9
47.5/47.5/5 w/w PLA/EVA/GO	3	0.6616	374	93.5
47.5/47.5/5 w/w PLA/EVA/GO	12	0.6902	387.6	96.9
66.5/28.5/5 w/w PLA/EVA/GO	3	0.8462	379.6	94.9
66.5/28.5/5 w/w PLA/EVA/GO	12	0.8741	390	97.5

At two different pH levels (3 and 12), 400 ppm initial concentration and 4 hours contact time were used

The effect of contact time is shown in Table 4.9 as well as Figure 4.15. Here the general trend was that an increase in contact time resulted in an increase in the amount of lead ions adsorbed. In Table 4.9, it is portrayed that the rate of adsorption was the highest between 0 and 180 minutes. Then from 180 to 240 minutes the rate slowed down, and equilibrium was approached and reached. This observation could have been due to the adsorbent samples approaching saturation as time went on, and thus reducing the rate at which adsorption occurred. The maximum adsorption was found at 240 minutes for all samples as was expected, because as the duration is increased there is continuous adsorption until saturation. The 66.5/28.5/5 w/w PLA/EVA/GO composite proved to have had adsorbed a higher percentage and concentration of lead ions (97.5 %) for the given time. However, its overall adsorption capacity was the lowest (Figure 4.15). This might have been due to saturation being reached at a faster rate for this composition. Generally, the contact time did not have much of an influence on the degree to which lead ions were adsorbed from solution, it had a great impact on the rate at which the metal ions were adsorbed. All three investigated parameters (contact time, pH and initial concentration) yielded a considerably high efficiency of the investigated samples to remove heavy metals from solution.

Table 4.9: AAS results for composites at different contact times.

Sample w/w PLA/EVA/GO	Contact time / min	Adsorbent sample mass (w) / g	Concentration Pb Adsorbed (C_a) / ppm	% Adsorbed
66.5/28.5/5 w/w PLA/EVA/GO	60	0.8743	292.1	73.0
66.5/28.5/5 w/w PLA/EVA/GO	120	0.8752	301.2	75.3
66.5/28.5/5 w/w PLA/EVA/GO	180	0.8788	385.2	96.3
66.5/28.5/5 w/w PLA/EVA/GO	240	0.8801	390.0	97.5
49.5/49.5/1 w/w PLA/EVA/GO	60	0.6029	250.3	62.6
49.5/49.5/1 w/w PLA/EVA/GO	120	0.6035	292.1	73.0
49.5/49.5/1 w/w PLA/EVA/GO	180	0.6011	377.6	94.4
49.5/49.5/1 w/w PLA/EVA/GO	240	0.6025	386.4	96.6
48.5/48.5/3 w/w PLA/EVA/GO	60	0.6078	255.5	63.9
48.5/48.5/3 w/w PLA/EVA/GO	120	0.6092	295.3	73.8
48.5/48.5/3 w/w PLA/EVA/GO	180	0.6072	377.6	94.4
48.5/48.5/3 w/w PLA/EVA/GO	240	0.6005	387.6	96.9
47.5/47.5/5 w/w PLA/EVA/GO	60	0.6911	257.8	64.5
47.5/47.5/5 w/w PLA/EVA/GO	120	0.6802	295.7	73.9
47.5/47.5/5 w/w PLA/EVA/GO	180	0.6911	379.6	94.9
47.5/47.5/5 w/w PLA/EVA/GO	240	0.6922	387.6	96.9

At different contact times, pH 12 and 400 ppm initial concentration were used

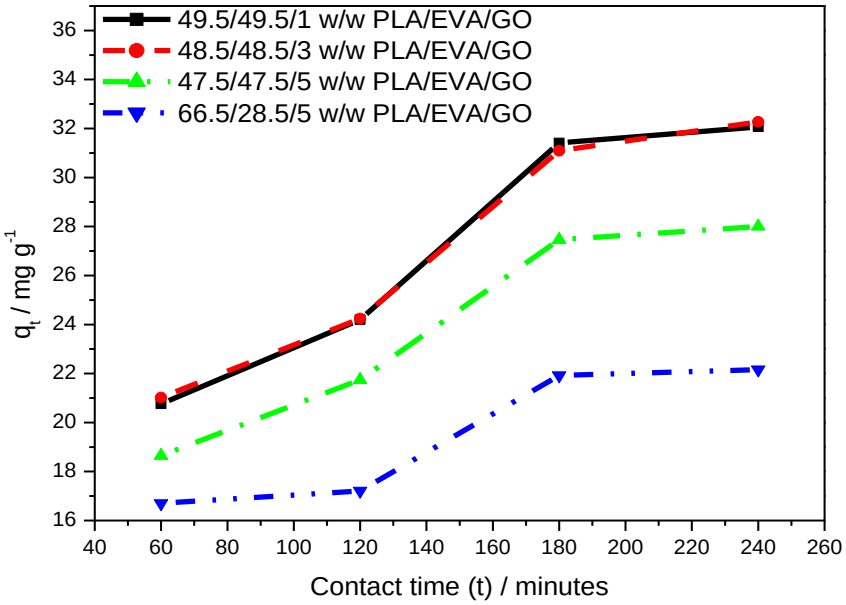

Figure 4.15: Adsorption capacity against contact time for different samples.

4.5.1 Adsorption isotherms

Isotherm modelling provides a way to express, through isotherms, the interaction of adsorbates with adsorbents at relatively low concentrations and fluid media.

4.5.1.1 Freundlich isotherm

Figure 3.16 shows a Freundlich plot for GO alone under different initial concentrations. The Freundlich constants together with their correlation coefficient are shown on Table 4.10. The plot is clearly well fitted with a high correlation effect (Figure 4.16). The values of n (1.760) and 1/n (0.5683) in Table 4.10 clearly suggest a favourable adsorption for this model. This means the Freundlich model fits this analysis, implying that adsorption might have occurred on a heterogeneous surface with different binding sites for adsorbates.

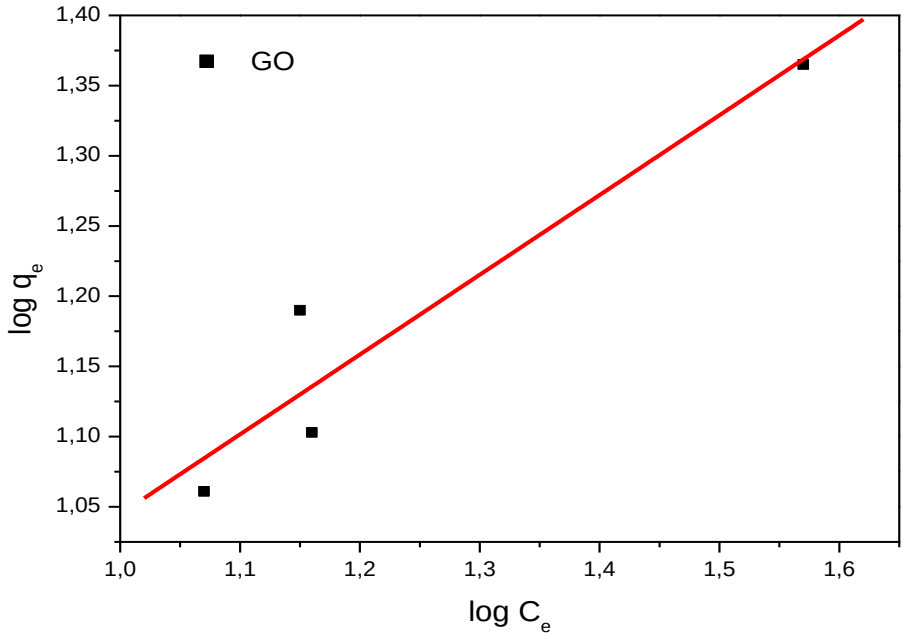

Figure 4.16: Freundlich plot for GO adsorption of Pb(II) ions at different initial concentrations.

Table 4.10: Freundlich isotherm constants for adsorption of Pb(II) ions from solution by GO.

Sample	**K_F**	**n**	**$\frac{1}{n}$**	**R^2**
GO	2.996	1.760	0.5683	0.95062

4.5.1.2 Langmuir isotherm

Figure 4.17 shows the Langmuir plot for GO under different initial concentrations of Pb(II), and the Langmuir isotherm constants with the correlation coefficient are listed in Table 4.11. It was clearly observed that the Langmuir isotherm provided a better linear fit than the Freundlich isotherm. This is also validated by the correlation coefficient of the Langmuir isotherm (0.9958) being closer to one than that of the Freundlich isotherm (0.9506). The R_L value (0.1089) also suggests that adsorption was favourable on a monolayer and homogenous basis.

Although both models gave a favourable outcome, it is important to note that the Langmuir isotherm proved more applicable to this study. This implies that the adsorption of Pb(II) ions onto GO mostly took place on a homogenous surface, whereby there was a single dominant adsorption site even though there were areas of heterogeneity here and there. This was further explained by the fact that GO generally preferred the interphase between PLA and EVA. This might have been where adsorption took place the most, with areas of heterogeneity here and there, that is where GO had preferred either of the two phases instead of the interphase.

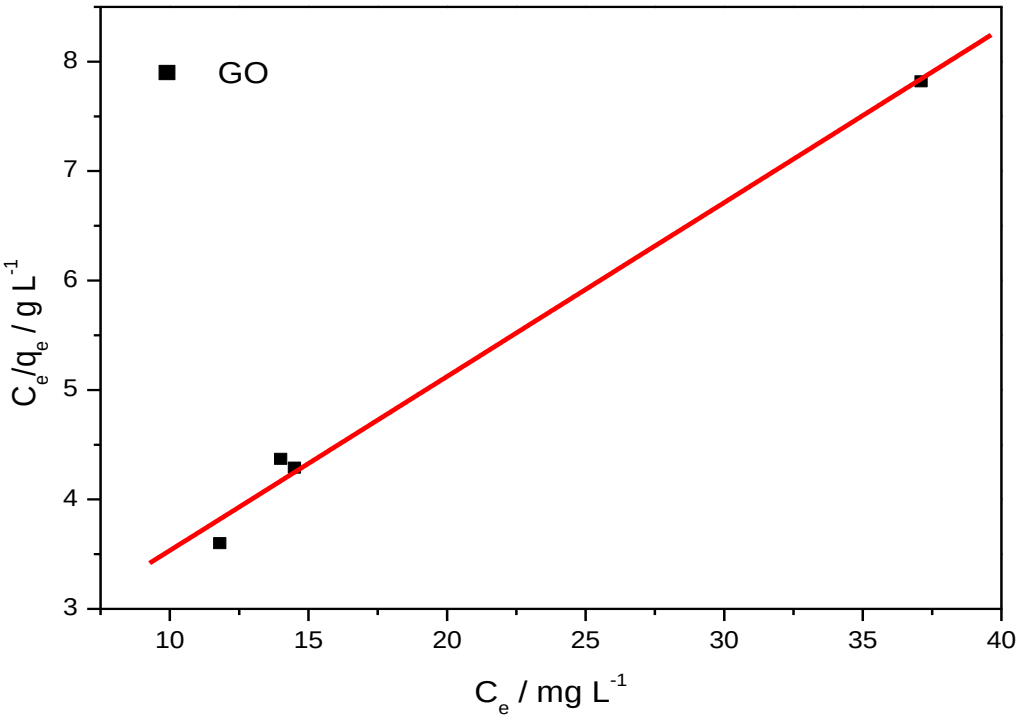

Figure 4.17: Langmuir plot for GO adsorption of Pb(II) ions at different initial concentrations.

Table 4.11: Langmuir isotherm constants for adsorption of Pb(II) ions from solution by GO.

Sample	q_m	B	R_L	R^2
GO	6.290	0.08179	0.1089	0.9958

4.7 REFERENCES

1. L. Zhong, K. Yun. Graphene oxide-modified ZnO particles: Synthesis, characterization, and antibacterial properties. International Journal of Nanomedicine 2015; 10:79-92. DOI: 10.2147/IJN.588319
2. F. T. Johra, J-W. Lee, W-G. Juang. Facile and safe graphene preparation on solution based platform. Journal of Industrial and Engineering Chemistry 2014; 20:2883-2887. DOI: 10.1016/j.jiec.2013.11.022
3. P. Bhawal, S. Ganguly, T. Chaki, N. Nas. Synthesis and characterization of graphene oxide filled ethylene methyl acrylate hybrid nanocomposites. Royal Society of Chemistry 2016; 6:20781-20790. DOI: 10.1039/C5RA24914G
4. B. Chen, N. Ma, X. Ba, H. Zhang. Effects of graphene oxide on surface energy, mechanical, damping and thermal properties of ethylene-propylene-diene rubber/petroleum resin blends. Royal Society of Chemistry 2012; 2:4683-4689. DOI: 10.1039/C2RA01212J
5. P. A. Tran, T. J Webster. Understanding the wetting properties of nanostructured selenium coatings: the role of nanostructured surface roughness and air-pocket formation. International Journal of Nanomedicine 2013; 8:2001-2009. DOI: 10.2147/IJN.S42970
6. J. P. Mofokeng, A.S Luyt, T. Tabi, J. Kovacs. Comparison of injection moulded, natural fibre-reinforced composites with PP and PLA as matrices. Journal of Thermoplastic Composite Materials 2011; 25:927-948. DOI: 10.1177/0892705711423291
7. S. Sreeremya. Adsorption-Review. International Journal of Advance Research and Development 2017; 2:15-18.

8. N. Venkateshwaran, A. Elayaperumal, A. Alavudeen, M. Thiruchitrambalam. Mechanical and water absorption behaviour of banana/sisal reinforced hybrid composites. Materials and Design 2011; 32:4017-4021.
DOI: 10.1016/j.matdes.2011.03.002
9. B. Natarajan, Y. Li, H. Deng, L. Brinson, L. Schadler. Effect of interfacial energetics on dispersion and glass transition temperature in polymer nanocomposites. Macromolecules 2013; 46:2833-2841.
DOI: 10.1021/ma302281b1
10. V. Khoshkava, M. Kamal. Effect of surface energy on dispersion and mechanical properties of polymer/nanocrystalline cellulose nanocomposites. Biomicromolecules 2013; 9:3155-3163.
DOI: 10.1021/bm400784j
11. D. E. Phackham. Surface energy, surface topography and adhesion. International Journal of Adhesion and Adhesives 2003; 23:437-448.
DOI: 10.1016/S0143-7496(03)00068-X
12. H. Ardebili, E. Wong, M. Pecht. Hygroscopic swelling and sorption characteristics of epoxy molding compounds used in electronic packaging. IEEE Transactions on Components and Packaging Technologies 2003; 26:206-214.
DOI: 10.1109/TCAPT.2002.806172
13. V. H. Sangeetha, R. Valapa, S. K. Nayak, T. O. Varghese. Super toughened renewable poly (lactic acid) based ternary blends system: effect of degree of hydrolysis of ethylene vinyl acetate on impact and thermal properties. Royal Society of Chemistry Advances 2016; 6:72681-72691.
DOI: 10.1039/C6RA13366E
14. K. Wang, Q. Deng. The thermal and mechanical properties of poly (ethylene-co-vinyl acetate) random copolymers (PEVA) and its covalently crosslinked analogues (cPEVA). Polymers 2019; 11:1-18.
DOI: 10.3390/polym11061055
15. E. Aliyev, V. Filiz, M. Khan, Y. Lee, C. Abetz, V. Abetz. Structural characterization of graphene oxide: surface functional groups and fractionated oxidative debris. Nanomaterials 2019; 9:1-15.
DOI: 10.3390/nano9081180
16. S. Eigler, C. Dotzer, F. Hof, W. Bauer, A. Hirsch. Sulfur species in graphene oxide. Chemistry: A European Journal 2013; 19:9490-9496.

DOI: 10.1002/chem.201300387

17. Y. Fan, H. Nishida, Y. Shirai, T. Endo. Thermal stability of poly (L-lactide): influence of end protection by acetyl group. Polymer Degradation and Stability 2004; 84:143-149. DOI: 10.1016/j.polymdegradstab.2003.10.004
18. M. S. Mat-Shayuti, M. Z. Abdullah, P. S. M. Megat – Yusoff. Water absorption properties and morphology of polypropylene / polycarbonate / polypropylene-graft-maleic anhydride blends. Asian Journal of Scientific Research 2013; 6:167-176. DOI: 10.3923/ajsr.2013.167176
19. E. Gaudichet-Maurin, F. Thominette, J. Verdu. Water sorption characterisitics in moderately hydrophilic polymers, part 1: effect of polar group's concentration and temperature in water sorption in aromatic polysulfones. Applied Polymer Science 2008; 109:3279-3285. DOI: 10.1002/app24873
20. A. Espert, F. Vilaplana, S. Karlsson. Comparison of water absorption in natural cellulosic fibers from wood and one year crops in polypropylene composites and its influence on their mechanical properties. Composites: Part A 2004; 35:1267-1276. DOI: 10.1016/j.compositesa.2004.04.004

CHAPTER 5

CONCLUSIONS

The section below gives an outline of the conclusions derived from the analysis and interpretation of results. It also gives recommendations for future work, in order to improve on the study and optimize the findings.

The main aim of this study was to prepare the adsorbent graphene oxide, functionalized from expandable graphite using the modified Hummer's method, and mask it with polymers (PLA and EVA) to extend its life expectancy in water purification applications. GO was successfully synthesized from graphite powder. This was validated by: (i) XRD which displayed a peak implying the attachment of oxygen containing functional groups to expandable graphite, (ii) FTIR spectra which displayed numerous peaks that are as a result of the successful attachment of various oxygen containing functional groups, and (iii) SEM - EDS whereby the images of GO portrayed successful exfoliation of graphite, and the EDS showed the amount of oxygen content to have increased for the synthesized GO.

The other aim was to prepare environmentally friendly PLA / EVA / GO polymer composites and subject them to various characterizations to assess the possibility of other applications, including water purification. The preparation was successfully achieved by melt mixing. Morphology studies revealed that the two polymers were immiscible in all the blends, with the 50/50 w/w PLA/EVA blend showing optimal properties. The blend demonstrated exceptional interaction, without cracks on the polymers and no spaces/gaps on the interface. This suggested an improved compatibility, although the polymers were immiscible. With the composites, GO was generally seen to be on the interphase of the two polymers, even though it favoured both the polymer phases equally. The consensus was that the presence of GO brought compatibility between the polymers in all the blend systems. The GO seemed to have been embedded in the polymers on the interface and some of the polymer material enveloped into the GO layers. The addition of GO also merged the two polymer phases, and on the 50/50 w/w ration an intact co-continuous morphology was observed, thereby proving its compatibilization effect. The 70/30 w/w PLA/EVA ration showed cracks on the polymer phases and gaps on the interfaces with 3 and 5 wt.% GO loadings. These cracks and spaces later aided in water absorption as well as metal ion adsorption, even though these processes did not depend entirely on their existence.

In SEES results, contact angle measurements showed PLA and EVA to be somewhat hydrophilic, while GO was more hydrophilic than the two. The polar surface energies for all three components (PLA, EVA and GO) were similar, and this indicated that all these components would mix with ease. The calculated interfacial tensions between PLA and GO and EVA and GO were equivalent, which suggested a 50/50 chance of GO settling into either one of the polymers, or even the interphase. This resulted in an obtained wetting coefficient value of 0.523 mJ/m^2, which suggested that GO was situated mostly on the interface between PLA and EVA.

In DSC results, PLA and EVA were proven to be immiscible as was seen from their individual melting peaks in the blends. The cold crystallization and melting peaks of PLA disappeared in the presence of EVA, in the blends. The conclusion drawn was that the presence of molten EVA inhibited the process of re-crystallization of PLA by filling into the free spaces of its chains before the re-crystallization process. The crystallization of EVA was observed earlier than that of neat EVA, for all the blends. As such, it was deduced that the presence of PLA catalysed the crystallization process of EVA, even though it did not improve its degree of crystallinity, showing that PLA acted as obstacles in EVA aligning its chains. These two polymers seemed to have influenced each other negatively, as none improved another's thermal properties. Then adding GO, the glass transition of PLA was generally shifted to lower temperatures, which brought the idea that GO had a plasticisation effect on the polymer matrices. It also seemed to have a nucleating effect on PLA chains and an inhibition effect on EVA crystallization. This was based on the observations that the cold crystallization peak of PLA was re-defined, it's melting peak split into two and the degree of crystallinity generally increased. While the degree of crystallinity of EVA was generally significantly reduced for the blend composites.

Thermal degradation studies also brought some interesting observations. In the blends, two main degradation steps were observed, which indicated that the two polymers (PLA and EVA) degraded separately and validated the immiscibility observed in SEM and DSC results. The first degradation step (PLA) was seen to move to lower temperatures in all blends, which was attributed to the degradation of vinyl acetate which releases water as one of its thermal degradation volatiles. Furthermore, the degradation steps seemed to move apart in the 70/30 w/w and 30/70 w/w PLA/EVA blends, as compared to the neat polymers, and this showed that the two polymers were not only immiscible, but also incompatible. It was only the 50/50 w/w PLA/EVA blend which showed degradation steps that were trying to approach one another,

and this portrayed compatibility to some extent, as was also seen in SEM images for this blend. With the blend composites, GO was observed to have an auto-catalytic effect on the thermal stability of the polymers. Initially it caused the degradation of the polymers to occur earlier as it released its organic thermal degradation volatiles. Mostly water, as it is detrimental to the thermal degradation of biodegradable polymers as they undergo hydrolytic degradation, hence the early degradation in PLA (first step). While after the removal of organics, at higher temperatures, it insulates the polymers. This was seen by the second degradation step (EVA) moving to higher temperatures, and the presence of char amounting to the total remaining of the GO inorganics as well as the polymers. All these observations brought the general conclusion that the polymers were successful in masking GO, and concurrently the GO improved their thermal stability to some extent.

In water purification studies, the first part, water absorption, resulted in the 50/50 w/w (1, 3 and 5 wt.% GO) composites and the 66.5/28.5/5 w/w composite generally having a higher degree of absorption. This was attributed to the exposed GO layers in SEM images of the 50/50 w/w samples, and the cracks on the polymers and spaces on the interface for the 66.5/28.5/5 w/w PLA/EVA/GO composite. The second part, AAS, resulted in every analysed sample adsorbing a considerably large amount of lead ions. The effect of concentration done on GO showed it to have a very high metal intake on its own, and the optimal Pb(II) concentration was 400 ppm. This high metal intake proves the effectiveness of the oxygen containing functional groups present on GO, in trapping metal ions. The blend composites proved to adsorb more lead ions than the individual GO, and this validated the efficiency of the polymers used also in adsorbing heavy metals from solution. The blend composites were proven to adsorb more lead ions in basic than acidic media, which was owed to successful complexation and enough binding sites in this media. In terms of contact time, it was established that the optimal time for rate of adsorption was between 180 and 240 minutes. This means that in using these blend composites commercially (should the need arise), care should be taken that before and after the mentioned time frame the metal ion intake would be the slowest. The 66.5/28.5/5 composite, although having showed poor properties everywhere else, had the highest adsorption degree of lead ions, and this was due to the cracks observed in SEM which provided ease access and settling of the lead ions by both physical and chemical adsorption. Mathematical modeling of GO metal ion intake revealed that there was a homogenous adsorption site, as the Langmuir isotherm gave a better linear fit. This means that the adsorption of Pb(II) to GO was most effective probably where GO was on the interface, than when it was on either of the polymer

phases. With all the findings, it was concluded that all the aims and objectives of this study were successfully achieved, even beyond water purification the composites can be used in packaging, interior automotive designs, with further studies in mechanical properties.

Recommendations for future work:

- Performing mechanical analysis on the prepared samples to test their endurance if they were to be used commercially (Preferably impact testing)
- Analyse the effect of initial concentration on the adsorption of composites to be able to do adsorption isotherms.
- Do a desorption study on the samples in order to assess the possibilities of their re-usage
- Including a compatibilizer in sample preparation to assess its impact on properties and thus adsorption
- Using a blowing agent that would form pores on the samples, thereby allowing the metal ions easy access to the filler.

ACKNOWLEDGEMENTS

This journey has not been an easy one at all. It is by prayer and God that I developed the drive to keep pushing, as such before anything my greatest appreciation goes to God.

I would like to specially acknowledge my supervisor Mr. Khotso Mpitso as well as my co – supervisor Dr. Puseletso Mofokeng. They tolerated me throughout whilst providing academic as well as personal support.

I am eternally grateful to my family; Mr. Monakoe Mokoena (Uncle), Mrs. Alice Mokoena (Aunt), and their wonderful children, who are my siblings. I would not have been where I am if it was not for you.

I would also like to thank Dr. Mfiso Mngumezulu, Mrs. Cheryll-Ann Konig and Mr. Tsietsi Tsotetsi for always being available for consultation.

The whole chemistry department has been like family to me, and I am very grateful for having them as family and knowing I could count on them.

I am grateful and thankful to the following people: Miss Ntsoaki Mokoena, Miss Moleboheng Mosikili, Miss Nomangaliso Xaba, Miss Chido Molotsane, Miss Zamambo Dlamini, Mr. Paseka Mokoena, Mr. Sello Mbambo, Prof. Richard Ocaya, Prof. Lehlohonolo Koao, and Mr. Thabang Mofube. The emotional support has been of great significance.

An acknowledgement also goes to Dr. Remy Bucher (Ithemba L*A*BS) and Dr. Patrick Komane (University of Johannesburg) for assisting with XRD and AAS respectively.

Lastly, I am very grateful for having received financial support from the National Research Foundation (NRF) as well as the Sasol Inzalo Foundation (SAIF), South Africa. All of these would not have been possible had it not been for these sponsors.

APPENDIX

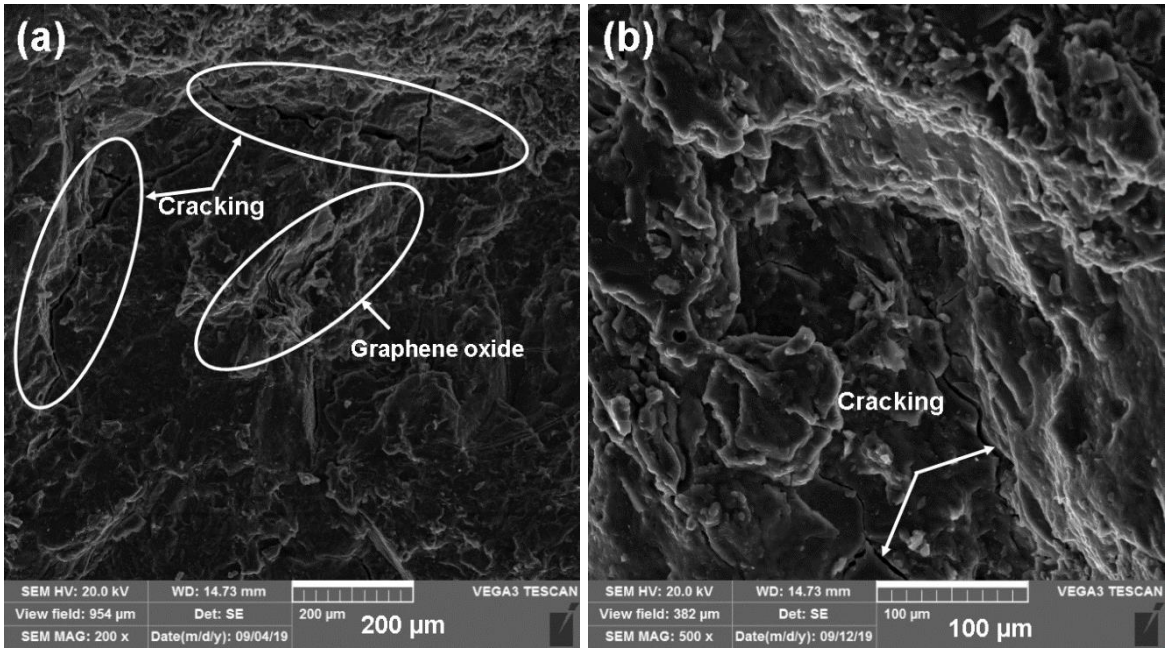

Figure A1: SEM images for (a) 67.9/29.1/3 and (b) 66.5/28.5/5 w/w PLA/EVA blend composites at 200 and 500 x magnifications, respectively.

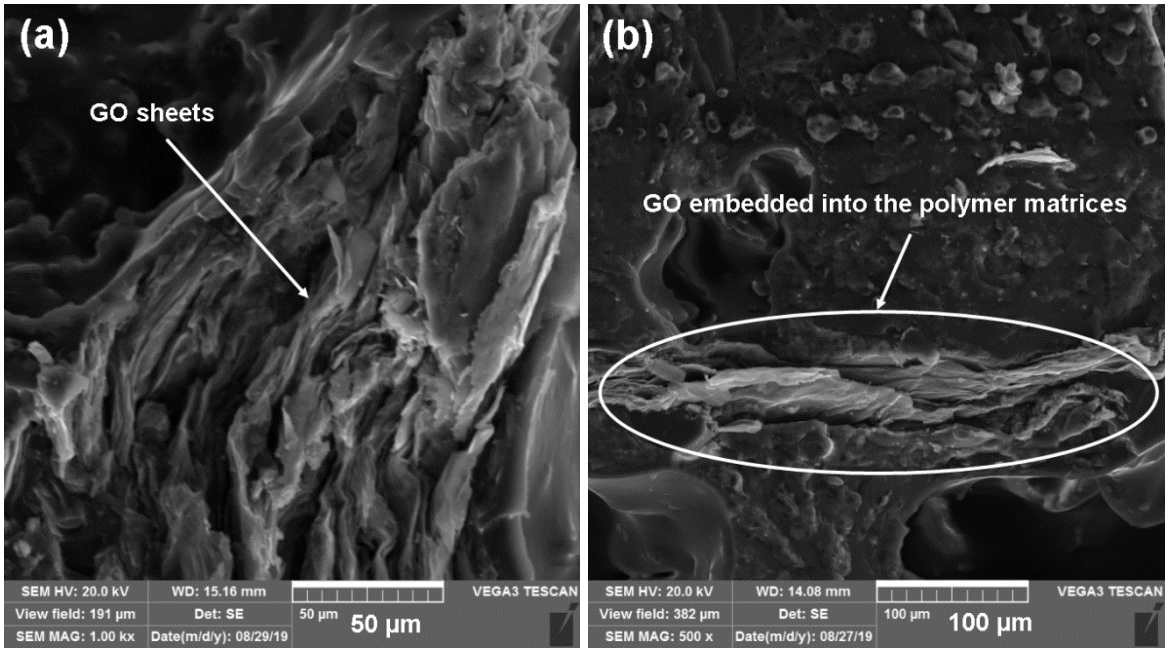

Figure A2: SEM images for (a) 49.5/49.5/1 and (b) 47.5/47.5/5 w/w PLA/EVA blend composites at 1.0k and 500 x magnifications, respectively.

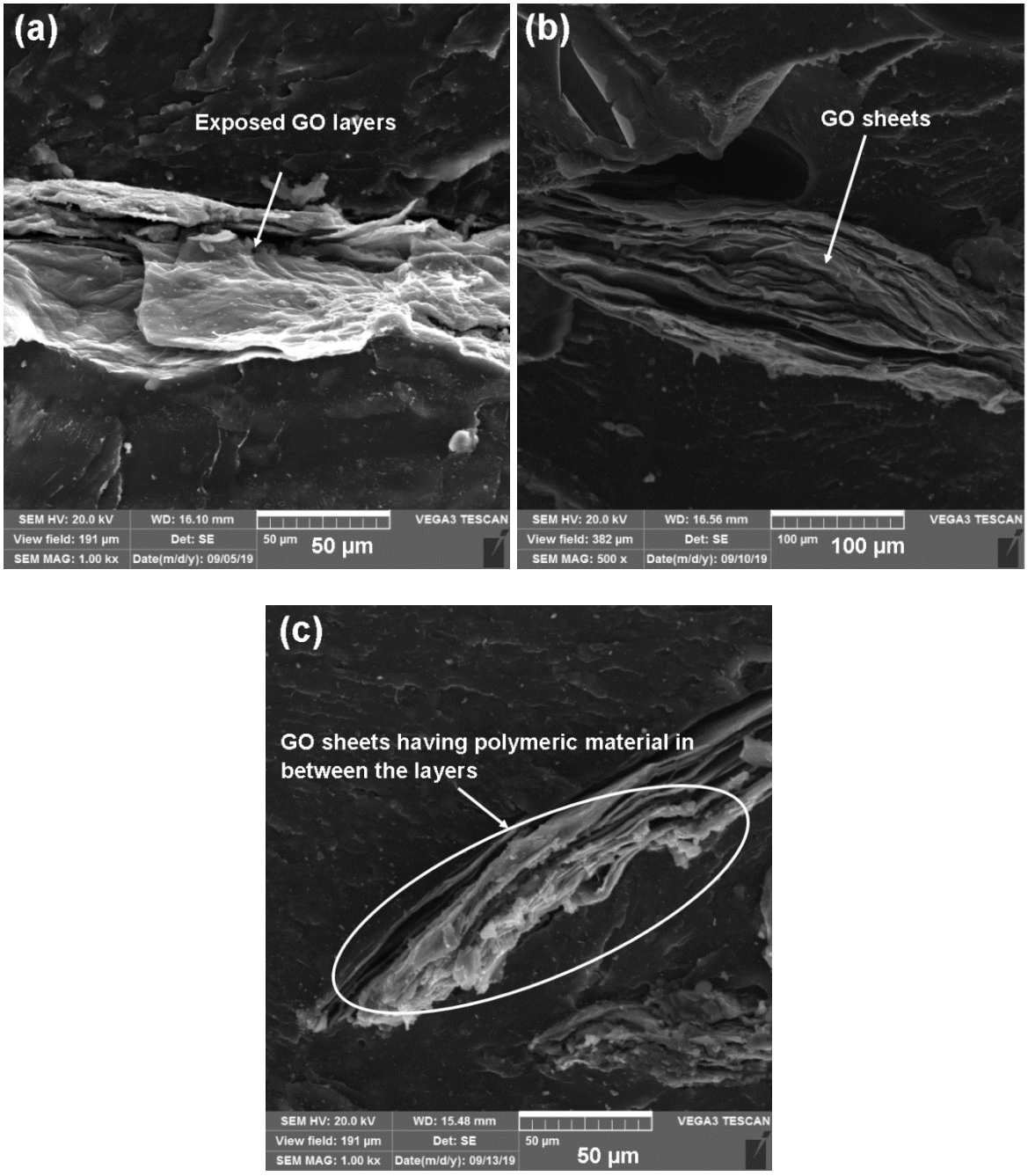

Figure A3: SEM images for (a) 29.7/69.3/1, (b) 29.1/67.9/3 and (c) 28.5/66.5/5 w/w PLA/EVA blend composites at 1.0k, 500 and 1.0k x magnifications, respectively.